The lactate receptor HCAR1 in the regulation of neurogenesis and angiogenesis during stroke

Kimberly Dungdung Phan

Dissertation for the degree Master of Pharmacy

45 credits

Section for Pharmacology and Pharmaceutical Biosciences

Department of Pharmacy

The Faculty of Mathematics and Natural Sciences

UNIVERSITY OF OSLO

May 2020

The lactate receptor HCAR1 in the regulation of neurogenesis and angiogenesis during stroke

Kimberly Dungdung Phan

Main supervisor
Postdoctoral fellow Samuel Geiseler

Co-supervisor
Associate professor Cecilie Morland

Department of Pharmacy

The Faculty of Mathematics and Natural Sciences

UNIVERSITY OF OSLO

May 2020

2020

The lactate receptor HCAR1 in the regulation of neurogenesis and angiogenesis during stroke

Kimberly Dungdung Phan

http://www.duo.uio.no/

Print: University Print Centre, University of Oslo

Acknowledgements

The work presented in this dissertation was performed in the Neurobiology and Toxicology group at the Section for Pharmacology and Pharmaceutical Biosciences, Department of Pharmacy, from the Faculty of Mathematics and Natural Sciences at the University of Oslo.

As much as I know it sounds cliché, it is also no less true that this thesis would not have been completed without the endless support of so many colleagues, friends and family.

First and foremost, I would like to acknowledge the entire Neurobiology and Toxicology group, particularly my supervisors, postdoctoral fellow Samuel Geiseler and associate professor Cecilie Morland, for their guidance and availability throughout this project. My last year has been filled with so much erudition and experience, and has granted me the possibility to work on my personal development in various aspects.

Special thanks go to my two fellow classmates, Camilla Brox and Teresa Dang Nguyen, who shared parts of the master project with me; thanks for an exceptional collaboration. It has been an honour to work by their sides ever since day one. Without them, the semester would not have been as pleasant; filled with laughter, joy and motivation.

I am also particularly grateful and indebted to my friends, family, and partner. Thanks for the unconditional, unequivocal and loving support that have helped me accomplish what I have up till now, and taught me to never give up in spite of obstacles and rough times.

Last but not least, I would like to thank myself. As much as the people surrounding me have supported and motivated me through these past five years, all this work up till now would not have come through without my own willpower. In a modern time where expectations and achievements set high standards, self-awareness have become just as important. I am therefore grateful for being the purposeful, stubborn and persistent person I've always been. And after handing in my dissertation, I can finally say to myself "you finally made it, thank you".

Kimberly Dungdung Phan

Oslo, May 2020

Abstract

Millions of people suffer from stroke every year, being a leading cause of morbidity and mortality worldwide. The current pharmacological and endovascular therapies in stroke aim to restore cerebral blood flow, but are not suitable for many stroke patients due to a number of risk factors. With the limited post-stroke rehabilitation treatments available, prevention of stroke will continue to be an area of research with a large impact. One of the best preventive strategies in stroke is exercise, which has shown to reduce risk factors and improve brain function through direct effects in the brain. Trophic growth factors are elevated after exercise which enhances neurogenesis and angiogenesis, and have been suggested to exert the neuroprotective effects in the ischaemic brain.

The lactate receptor (HCAR1) has recently shown to be highly enriched in fibroblasts in the meninges, particularly the pia mater. Furthermore, activation of these receptors by lactate injections or high-intensity exercise, enhance cerebral vascular endothelial growth factor A (VEGF-A) levels and angiogenesis, and perhaps also directly enhance neurogenesis. Since HCAR1 can be stimulated by circulating lactate arriving from the blood as a result of exercise, this may explain the underlying beneficial effects of exercise in stroke.

The present study aimed to examine the HCAR1-induced vascularization and neurogenesis in response to exercise in the neuroprotection of stroke. Wild-type mice and HCAR1 knockout mice were subjected to high-intensity exercise (at levels known to significantly increase blood-lactate levels), medium-intensity exercise, or intraperitoneal injections of lactate or saline (control) daily for 5 consecutive days a week for 7 weeks in total. Following the treatments, focal ischaemia was induced by permanent coagulation of the distal middle cerebral artery, and the mice were allowed a 3-weeks recovery phase before being sacrificed by perfusion fixation to collect the brains. Whole cresyl violet-stained sections were analysed for comparison of infarct volume. Interestingly, no significant differences between the treatment groups or genotypes were found. Possible reasons for the lack of observed effects are presented. In conclusion, preventive and prolonged exercise preconditioning or lactate injections do not protect against ischaemia-induced cell death 3 weeks after stroke. Moreover, the outcome was independent of HCAR1-mediated effects. Overall, these findings provide new insights of the long-lasting effects (3 weeks after stroke induction) on the stroke outcome of exercise preconditioning and lactate treatment, through the lactate receptor HCAR1.

Abbreviations

3,5-DHBA	3,5- dihydroxybenzoic acid
ACA	Anterior cerebral artery
AHA	American Heart Association
AMPA	α-amino-3-hydroxy-5-methyl-4-isoxazolepropionic acid
ANLS	Astrocyte-neuron lactate shuttle
ANOVA	One-way analysis of variance
ARRB2	Arrestin beta 2
ASA	American Stroke Association
ASICs	Acid-sensing ion channels
ATP	Adenosine triphosphate
BBB	Blood brain barrier
BDNF	Brain-derived neurotrophic factor
BSA	Bovine serum albumin
cAMP	Cyclic adenosine monophosphate
CBF	Cerebral blood flow
CNS	Central nervous system
CV	Cresyl violet
DAPI	4′,6-diamidino-2-phenylindole
DCX	Doublecortin
DG	Dentate gyrus
DGCs	Dentate granule cells
dMCAO	Distal middle cerebral artery occlusion
DNA	Deoxyribonucleic acid
ECs	Endothelial cells
FELASA	Federation of Laboratory Animal Science Association
FGF	Fibroblast growth factor
FNDC5	Fibronectin type III domain-containing protein 5
HCAR1	Hydroxy carboxylic acid receptor 1
HE	Hematoxylin-eosin
I.p.	Intraperitoneal
I.v.	Intravenous

ICA	Internal carotid artery
ICH	Intracerebral haemorrhage
Ig	Immunoglobulin
IGF	Insulin-like growth factor
IHC	Immunohistochemistry
IL	Interleukin
Ki67	MKI67 protein
KO	Knockout
LDH	Lactate dehydrogenase
MAPK	Mitogen-activated protein kinase
MCA	Middle cerebral artery
MCAO	Middle cerebral artery occlusion
MCTs	Monocarboxylate transporters
NaPi	Sodium phosphate
NeuN	Neuron-specific nuclear protein
NF-κB	Nuclear factor kappa B
NSCs	Neuronal stem cells
NMDA	N-methyl-D-aspartate
NO	Nitric oxide
NOS	Nitric oxide synthase
NPs	Neural progenitors
PBS	Phosphate-buffered saline
PCA	Posterior cerebral artery
PcomA	Posterior communicating artery
PCR	Polymerase chain reaction
PFA	Paraformaldehyde
PGC1α	Peroxisome proliferator-activated receptor γ coactivator 1α
RGLs	Radial glia-like cells
PI3K	Phosphoinositide 3-kinase
ROI	Region of interest
ROS	Reactive oxygen species
SAH	Subarachnoid haemorrhage
SD	Standard deviation

SGZ	Subgranular zone
SIRT1	Silent information regulator 1
S_{max}	Maximum running speed
SVZ	Subventricular zone
TCA	Tricarboxylic acid cycle
TLR	Toll-like receptor
TNF	Tumour necrosis factor
tPA	Tissue plasminogen activator
TRKB	Tropomyosin receptor kinase B
TTC	Triphenyltetrazolium chloride
TWS	Trainable Weka Segmentation
VEGF	Vascular endothelial growth factor
VEGFR	Vascular endothelial growth factor receptor
VO_{2max}	Maximal oxygen consumption
WT	Wild-type

Table of contents

1 Introduction

1.1 Cerebral stroke

1.1.1 Definition and classification

Stroke is defined as a neurological deficit attributed to an acute focal injury of the central nervous system (CNS) by cerebrovascular aetiology. The term “stroke” is broadly used , and can roughly be divided into two main types: ischaemic and haemorrhagic (Fisher, 2010; Lopez et al., 2012; Ntaios, 2019; Parmar, 2018; Sacco et al., 2013). Ischaemic stroke is caused by the formation of a blood clot or another obstruction in a blood vessel in the brain, whereas haemorrhagic stroke occurs due to a rupture of a blood vessel or an abnormal vascular structure, leading to bleeding in the brain (Lopez et al., 2012; Parmar, 2018). Both hinder adequate blood supply to the stroke area. For haemorrhagic stroke, it is common to distinguish between intracerebral haemorrhage (ICH) and subarachnoid haemorrhage (SAH). ICH may be defined as a focal collection of blood within the brain parenchyma or ventricular system that is not caused by trauma, whereas SAH as bleeding into the subarachnoid space (Sacco et al., 2013).

These vascular causes of stroke are major causes of disability and death worldwide (Sacco et al., 2013). This dissertation deals mainly with ischaemic stroke.

1.1.2 Epidemiology and aetiology

Every year, millions of individuals suffer from stroke, making it a leading cause of morbidity and mortality worldwide. When considered separately from other cardiovascular diseases, stroke ranks as the fifth leading cause of death in the United States, behind diseases of the heart, cancer, chronic respiratory disease and unintentional injuries/accidents. Each year approximately 795 000 Americans experience a new or recurrent stroke, in which ischaemic stroke remains the most common type of stroke caused by vascular occlusion. 87% of all strokes are ischaemic and 10% are ICH strokes, whereas 3% are SAH strokes. The prevalence is estimated to be 7.2 million Americans above 20 years of age, and increases with advancing age in both males and females (Benjamin et al., 2019; Ntaios, 2019). In Norway there are about 12 000 new cases of strokes annually, equivalent to 30-40 new stroke cases every day. Among these, three out of four patients are above 70 years (Thomassen, 2019).

The aetiology of ischaemic stroke is either due to a transient or permanent thrombotic or embolic event that causes a critical reduction in cerebral blood flow (CBF) to the brain (Hui et al., 2019; Ntaios, 2019). In a thrombotic event, an obstruction within the blood vessel due to dysfunction within the vessel itself is the cause, often accompanied by and secondary to another disease such as atherosclerotic disease or inflammatory condition. In an embolic event, blood flow is obstructed due to debris from elsewhere in the body through which settles in the affected vessel in the brain (Hui et al., 2019). Within hours of the stroke, the central zone of the ischaemic area consists of irreversibly damaged and necrotic tissue which constitutes the infarct core. The surrounding zone, the penumbra, consists of damaged tissue which may recover and retain structural integrity by restoration of CBF. Restoration of CBF can either be due to removal of the clot by pharmacological or endovascular therapy, or by collateral blood flow from neighbouring capillaries that may buffer the loss of blood supply during a stroke attack (Gilberto González et al., 2006; Meschia & Brott, 2018).

1.1.3 Pathophysiology

Restriction of CBF during an ischaemic stroke results in depletion of oxygen and glucose supply to the brain, and failure to support cellular homeostasis. This disturbance elicits a complex interplay of multiple interdependent molecular processes (the ischaemic cascade) that for instance include excitotoxicity, acidotoxicity, ionic imbalance, oxidative stress, inflammation, and apoptosis (Doyle et al., 2008; Gilberto González et al., 2006; Quillinan et al., 2016).

Ionic imbalance, excitotoxicity and acidotoxicity

Despite the fact that the human brain compromise only 2% of the body weight, it requires 20% of total oxygen consumption (Edvinsson & Krause, 2001). Large amount of oxygen is required to generate sufficient adenosine triphosphate (ATP) by oxidative phosphorylation to maintain and restore ionic gradients (Doyle et al., 2008). The first consequence of reduced CBF is depletion of substrates for energy-generation, particularly oxygen and glucose. While ATP consumption continues despite insufficient synthesis, ATP levels will be exhausted, and lactate accumulates via anaerobic glycolysis. Accumulation of lactate causes acidosis with concomitant loss of ionic homeostasis, and enhancement of free-radical formation (Huang & McNamara, 2004; Mergenthaler et al., 2004; Xing, Arai, et al., 2012).

Energy failure as a result of ATP depletion leads to perturbation of the Na^+/K^+-ATPase (Phan et al., 2002). This ion pump maintains high intracellular:extracellular K^+-ratio necessary for the

propagation of action potentials. Impairment of this pump causes neuronal plasma membrane depolarization, and subsequently release of potassium into the extracellular matrix and entry of sodium into the cells (Caplan, 2009). Energy failure also prevents the plasma membrane Ca^{2+}-ATPase from maintaining low calcium concentrations within the cells (Doyle et al., 2008). The ion imbalance, due to elevated intracellular Na^+, Ca^{2+}, Cl^- and extracellular K^+ levels, triggers additional release of Ca^{2+} from organelles and excitatory processes (Durukan & Tatlisumak, 2007).

With energy depletion and loss of membrane potential, excitotoxity may occur. Accumulation of Na^+ inside the cells causes reversal of amino acid transporters, particularly glutamate transporters, and release of glutamate into the extracellular compartment in large amounts (Dirnagl et al., 1999; Doyle et al., 2008). The excitatory neurotransmitter causes direct neurotoxicity on neurons, via the activation of glutamate receptors. The ionotropic glutamate receptors are ligand-gated ion channels, and overactivation of these receptors exacerbates excitotoxicity. The N-methyl-D-aspartate (NMDA) receptor is permeable for Ca^{2+} and overactivation leads to further increase of intracellular Ca^{2+} load and membrane depolarization, whereas overactivation of the α-amino-3-hydroxy-5-methyl-4-isoxazolepropionic acid (AMPA) receptor causes Na^+-influx which results in activation of NMDA, by removal of Mg^+-blockade, and thus indirectly exacerbates excitotoxicity (Dirnagl et al., 1999; Quillinan et al., 2016). As a result of glutamate-mediated overactivation, Na^+ and Cl^- enters the neurons through monovalent ion channels while water passively follows, and causes cytotoxic oedema (Dirnagl et al., 1999). Overactivation of NMDA and AMPA receptors also activates catabolic enzymes such as proteases, lipases and DNases, triggering a cascade of events leading to apoptosis and/or necrosis (Doyle et al., 2008; Quillinan et al., 2016). In contrast to ionotropic receptors, the metabotropic glutamate receptors show a more complex role in brain injury; however, most evidences indicate a neuroprotective role through antiapoptotic signalling and decreased excitability (Bruno et al., 2001; Quillinan et al., 2016).

As mentioned earlier, metabolic acidosis can occur due to lactate accumulation, which may further exacerbate calcium overload. The following reduction in pH and increased dissociated protons, activates sodium-selective acid-sensing ion channels (ASICs) which are permeable to calcium, allowing further influx of Ca^{2+} into the cell and contributing to neuronal cell death (Doyle et al., 2008; Quillinan et al., 2016).

Oxidative stress

When the oxygen supply is limited, the electron transport chain in mitochondria becomes highly reduced and cytochrome c will no longer be able to reduce oxygen to water (Chan, 1996; Traystman et al., 1991). The result is the production of reactive oxygen species (ROS), which contributes to further aggravating of the mitochondrial dysfunction. During the reperfusion phase, in addition to the focal cerebral ischaemia itself, oxygen radicals are produced by enzymatic conversions, such as from the cyclooxygenase-dependent conversion of arachidonic acid to prostanoids (Lo et al., 2003). The surge in production of these radicals plays an important role in the reperfusion-induced injury of stroke. These radicals can activate matrix metalloproteases, which degrade collagen and laminins in the basal lamina, leading to disrupted integrity of the vascular wall and increases blood brain barrier (BBB) permeability (Crack & Taylor, 2005).

Several oxygen radical species can be produced in response to ischaemia, including superoxide and hydrogen peroxide. (Quillinan et al., 2016). Ischaemia also activates nitric oxide synthase (NOS), leading to increased generation of nitric oxide (NO), which combines with superoxide to produce peroxynitrite, a potent oxidant (Gilberto González et al., 2006). These ROS, especially peroxynitrite and superoxide, can bind irreversibly and directly to cellular constituents such as proteins, double bounds of phospholipids, and nuclear deoxyribonucleic acid (DNA), changing the structure of the target molecules and causing cell injury. They also serve as important signalling molecules that trigger inflammation and apoptosis (Dirnagl et al., 1999; Quillinan et al., 2016).

Neuroinflammation

Inflammation plays an important role in the pathogenesis of ischaemic brain injury (Durukan & Tatlisumak, 2007; Iadecola & Alexander, 2001; Tobin et al., 2014). The inflammatory response can be divided into an acute and prolonged inflammatory process, characterized by rapid activation of resident immune cells (microglia), production of proinflammatory mediators and infiltration of various types of inflammatory cells, such as neutrophils, different types of T cells, macrophages, and other cells across the disrupted BBB (R. Jin et al., 2010). Although the acute inflammatory response may further amplify and cause secondary injuries, a more delayed inflammatory response may be reparative (Quillinan et al., 2016).

The Ca^{2+}-related activation of intracellular second-messenger systems, the increase in oxygen free radicals, and hypoxia itself, all triggers the expression of proinflammatory genes by

inducing synthesis of transcription factors, such as nuclear factor kappa B (NF-κB) (O'Neill & Kaltschmidt, 1997), hypoxia inducible factor 1 (Ruscher et al., 1998) and interferon regulatory factor 1 (Iadecola et al., 1999). Thus, inflammatory mediators are produced, such as tumour necrosis factor (TNF) α, interleukin (IL) 1β , and platelet-activating factor (Rothwell & Hopkins, 1995). In addition, microglial cells, the resident macrophages of the brain, are activated rapidly (within minutes) in response to brain injury and produce a plethora of proinflammatory mediators. Activated microglia also precedes macrophage infiltration (Schilling et al., 2003), and have the potential to produce neurotoxins, such as NO, ROS and toxic prostanoids. In addition, neutrophils, followed by macrophages and monocytes, adhere to the endothelium and migrate from the blood into the brain parenchyma through adhesion molecules on the vascular endothelial cell surface, and contribute to the inflammatory process by production of toxic mediators (Durukan & Tatlisumak, 2007). These inflammatory cells exacerbate tissue damage, but may also be protective against ischaemic and excitotoxic injury, as they also participate in tissue remodelling and reconstruction following injury (Dirnagl et al., 1999; R. Jin et al., 2010).

Apoptosis

Excitotoxicity, ionic imbalance, oxygen free radicals, inflammation, mitochondrial and DNA damage, and cytochrome c release are all triggers of apoptosis (Durukan & Tatlisumak, 2007; Quillinan et al., 2016). Apoptosis is a genetically controlled mechanism of cell suicide, particularly seen in cells within the penumbra and associated with milder injury, whereas necrosis is the predominant mechanism that follows acute, permanent vascular occlusion (Dirnagl et al., 1999; Moskowitz & Lo, 2003). Caspases are aspartate-specific cysteine proteases (Dirnagl et al., 1999). Following ischaemia, caspase activation occurs in response to pro-apoptotic signals, and these protein-cleaving enzymes cleaves more than 30 proteins, which are essential for nucleus and cell integrity. The apoptotic cells become oedematous and lose their cellular architecture by cytoskeletal breakdown, leading to cell death and rapid removal by phagocytosis without eliciting an inflammatory reaction (Durukan & Tatlisumak, 2007; Love, 2003). Apoptosis is an energy-consuming process, so reperfusion could potentiate apoptosis (as opposed to necrosis) by restoring cellular energy (B. Schaller & Graf, 2004).

There are two major pathways of apoptosis which promotes caspase activation: the extrinsic (receptor-driven) and the intrinsic pathways (non-receptor-driven). The extrinsic pathway is triggered by death receptors (e.g. Fas and TNF), whereas the intrinsic pathway is triggered by

cytochrome c release from mitochondria due to apoptotic stimuli. Eventually, both pathways cause caspase-3 activation, resulting in the protein degradation and apoptosis (Dirnagl et al., 1999; Quillinan et al., 2016).

1.1.4 Treatment of ischaemic stroke

The treatment goals of acute ischaemic stroke are to restore CBF, support the energy metabolism in ischaemic tissue, treat the complications of stroke-related oedema, and prevent common acute medical complications (such as haemorrhagic transformation and orolingual oedema) (Ntaios, 2019). To date, the only successful acute treatments available to improve stroke outcome is revascularization (restoration of CBF) either mechanically with the use of a stent retriever or pharmacologically with tissue plasminogen activator (tPA) (National Institute of Neurological Disorders and Stroke rt-PA Stroke Study Group, 1995; Saver et al., 2015).

The American Heart Association/American Stroke Association (AHA/ASA) recommends intravenous (i.v.) alteplase (0.9 mg/kg, maximum dose 90 mg over 60 minutes with initial 10% of dose given as bolus over 1 minute) as treatment for patients within 3 hours of symptom onset. The same regimen may also be given within 3 to 4.5 hours to selected patients (W. J. Powers et al., 2018). Alteplase is a recombinant tPA which promotes fibrinolysis (thrombolysis) by activating plasminogen (Ntaios, 2019). Plasminogen activators are serine proteases which diffuse into the thrombus and cleave plasminogen to release plasmin locally. Plasminogen is normally in the plasma, partially bound to histidine-rich glycoprotein which immobilize the glycoprotein. The resulting product, plasmin, is a trypsin-like protease that digests fibrin, as well as fibrinogen, factors II, V and VII, and many other proteins. Eventually, the thrombolysis is terminated by its main physiological inhibitor α_2-antiplasmin and the general protease inhibitor α_2-macroglobulin (Henderson et al., 2016; J. Schaller & Gerber, 2011).

Endovascular therapy, by mechanically thrombectomy, is an option for those who can’t receive or respond fully to tPA, and should also be given to those eligible to fibrinolytic therapy. The AHA/ASA guidelines recommends stent retrievers as the preferred devices to achieve highest rates of recanalization (Hui et al., 2019; Meschia & Brott, 2018; W. J. Powers et al., 2018). The treatment, in addition to i.v. tPA, can remove large proximal clots rapidly, increases reperfusion rates and may improve long-term function outcome than i.v. tPA alone (Saver et al., 2015).

Despite successful acute treatments available, multiple constraints limits these options, such as strict inclusion-, exclusion- and diagnostic criteria, side effects and narrow time window for administration. Thrombolytic therapy may for instance only be used for patients over 18 years within 3 hours (sometimes up to 4.5 hours) with severe stroke symptoms or mild but disabling stroke symptoms. Onset of symptoms >4.5 hours, acute intracranial haemorrhage, gastrointestinal malignancy or recent bleeding, major surgery or serious trauma, and certain medications (e.g. antiplatelet and anticoagulation) are among the many contraindications (W. J. Powers et al., 2018). In addition, not all patients undergo substantial or complete reperfusion, and side effects and complications follow. There is a risk of orolingual angioedema as a side effect of i.v. alteplase, and worsening of the brain injury may occur due to delayed reperfusion and increase the risk of brain haemorrhage, making treatment suboptimal (Hui et al., 2019; Miller et al., 2011; Saver et al., 2015).

1.1.5 Prevention

Primary prevention of stroke includes physical activity, avoidance of obesity, good nutrition, treatment of hypertension, dyslipidaemia and diabetes mellitus, as well as abstinence from smoking and/or heavy drinking. Physical activity is associated with reduced risk of stroke, and the AHA/ASA recommends at least moderate- to vigorous-intensity aerobic physical activity at least 40 min/day 3 to 4 days/week for healthy adults. The treatments of the risk factors can be implemented with either lifestyle modifications or pharmacological therapy (Kernan et al., 2014; Meschia et al., 2014). Antihypertensive and antidiabetic treatment are recommended to target, respectively, blood pressure of <140/90 mmHg (Meschia et al., 2014) and fasting blood glucose level of <126 mg/dl (Moghissi et al., 2009). In addition, recommendations for the secondary prevention of ischaemic stroke have been published, which for instance include anticoagulation treatment, antiplatelet drug therapy, carotid endarterectomy and more (Kernan et al., 2014; Ntaios, 2019).

With the limited post-stroke treatment options available, prevention of stroke will continue to be the area of study with the greatest impact. In the following sections we will focus on exercise as preventive strategy.

1.2 Modelling stroke in mice

As there are no *in vitro* models that can properly reflect the complexity of the pathological mechanisms during stroke, experimental rodent models serve as an essential tool to investigate the mechanisms of ischaemic cerebral injury, and to develop novel therapeutic strategies (Durukan & Tatlisumak, 2007; Llovera et al., 2014). Although mimicking all aspects of human strokes in one animal model is not possible, the different models serve as excellent tools to expand our understanding of the events in ischaemic and reperfused brain (Durukan & Tatlisumak, 2007).

Most models use a permanent or transient occlusion of the middle cerebral artery (MCA) to induce stroke in rodents (Engel et al., 2011). The MCA is one of the major arteries supplying blood to the brain, and the artery and its branches are common cerebral vessels affected in human ischaemic stroke, accounting for approximately 70% of the infarcts (Bogousslavsky et al., 1988). The MCA arises from the internal carotid artery (ICA), and runs into the lateral sulcus where it branches to the cerebral cortex, including the primary motor and sensory cortex. The right and left MCA are connected to the anterior cerebral arteries (ACA), and the posterior cerebral arteries (PCA) which is connected to the posterior communicating arteries (PcomA). Together, these arteries constitute the Circle of Willis (figure 1.1).

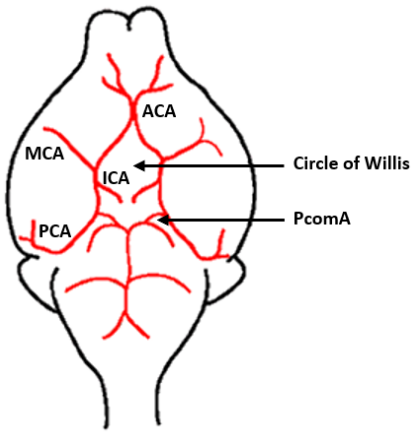

Figure 1.1. Schematic illustration of the Circle of Willis. Blood vessels supplying blood to the brain form a circle-like arterial structure called the Circle of Willis. The Circle of Willis is formed by the middle cerebral arteries (MCA) and the anterior cerebral arteries (ACA), which are branches of the internal carotid arteries (ICA), and also by the posterior cerebral arteries (PCA) which is connected to the posterior communicating arteries (PComA).

MAO occlusion (MCAO) can be conducted in several ways, either transiently or permanently, and at proximal or distal parts of the MCA (McBride & Zhang, 2017). The “filament model”

or “intraluminal suture model” is one of the most commonly used MCAO models. In this model, a suture filament is transiently introduced into the ICA, and advanced forward into the Circle of Willis until the tip interrupts the blood supply and occludes the origin of the MCA (Engel et al., 2011; Longa et al., 1989). The cessation of blood supply to the MCA halts the blood flow proximal to the lenticulostriate arteries, which supply the basal ganglia. The result is brain infarction affecting subcortical regions, particularly the striatum, in addition to a major part of the neocortex. This approach mimics one of the most common types of ischaemic stroke in humans with different grades of damage, and offers the advantage of inducing reproducible transient or permanent ischaemia (Engel et al., 2011). Another MCAO model, induces permanent occlusion distal to the lenticulostriate arteries by transcranial electrocoagulation using diathermic forceps, the so-called “coagulation model”. This approach predominantly affects the cortex, and spares the striatum. Infarcts modelled by the permanent distal MCAO (dMCAO) model encompass about 10-15% of the hemisphere, thereby mimicking the majority of human stroke lesions located in the cortical MCA territory (Carmichael, 2005; Howells et al., 2010; Llovera et al., 2014). MCAO may also be performed using microsphere/macrosphere injections or thrombotic clot embolization, representing embolic MCA occlusion (Carmichael, 2005). The macrosphere technique involves administration of large spheres (300–400 μm diameter) into the ICA and further to the MCA, producing an infarct of similar size and location as the permanent “suture model” (Gerriets et al., 2003). The microsphere technique utilises smaller spheres (50 μm diameter), giving smaller, multifocal lesions, and mimicking distal and diffuse embolism (Mayzel-Oreg et al., 2004; Miyake et al., 1993). Embolic MCAO by thrombotic clots may be performed using autologous blood or thrombin administered into the MCA, which forms spontaneous or thrombin-induced clots. This approach models clot-induced stroke in humans (Z. Zhang et al., 1997).

In addition, other models of ischaemic strokes are published, including models based on photothrombosis, endothelin-1 and other craniectomy methods (e.g. by microaneurysm clips, ligatures or hooks used to lift the MCA from the brain surface to interrupt blood flow), which will not be presented here (for review, see Carmichael, 2005 and Fluri et al., 2015).

1.3 Effects of exercise on the brain

Physical activity and exercise are among the best preventive strategies in stroke. Physical activity can be defined as “any bodily movement produced by skeletal muscles that results in

energy expenditure", and exercise as "a subset of physical activity that is planned, structured, and repetitive and has as a final or an intermediate objective to improve and maintain the physical fitness" (Caspersen et al., 1985). Physical activity and exercise are associated with improved risk factors and may reduce stroke risk itself (Lee et al., 2003; J. Li & Siegrist, 2012; Willey et al., 2011). Although the beneficial effects of exercise are well-documented, no consensus has been reached regarding the optimal exercise regime. The relationship between the amount or intensity of exercise and stroke risk remains unsettled (Meschia et al., 2014).

The protective effects of physical exercise may partly be mediated through reduced blood pressure (Whelton et al., 2002) and insulin resistance (Dylewicz et al., 1999), improved endothelial function (Endres et al., 2003) and lipid metabolism (Schenk & Horowitz, 2007), and reduced excess body weight (Goodpaster et al., 2010). In addition, physical activity has been shown to improve brain function and plasticity by affecting neurogenesis and the neural system (e.g. synaptic strength, neurotransmission and long-term potentiation) involved in learning and memory, particularly in later life. Exercise may therefore also reduce symptoms in neurodegenerative and mental diseases such as Alzheimer's disease, depression and anxiety (Cotman & Berchtold, 2002; Hillman et al., 2008; van Praag et al., 2005).

Neurogenesis and angiogenesis appear to be tightly co-regulated after stroke and trauma, especially during the recovery phase post-injury (Thored et al., 2007). The underlying molecular mediators of neurogenesis and angiogenesis overlap, and promoting neurogenesis has shown to augment angiogenesis, and *vice versa* (Carmeliet & Tessier-Lavigne, 2005; Ohab et al., 2006). Trophic growth factors, such as brain-derived neurotrophic factor (BDNF) (Cotman & Berchtold, 2002), vascular endothelial growth factor (VEGF), insulin-like growth factor (IGF) 1 (Lopez-Lopez et al., 2004) and fibroblast growth factor (FGF) 2 (Cotman & Berchtold, 2002), are elevated after exercise which enhances neurogenesis and angiogenesis (Ferrara, 2000; van Praag et al., 2005). These may exert the neuroprotective effects in the ischaemic brain.

1.3.1 Exercise and neurogenesis

Exercise has been shown to enhance hippocampal neurogenesis (Fabel et al., 2003; Farmer et al., 2004; van Praag, Christie, et al., 1999), and increase synaptic plasticity, neurotransmission and growth factor gene expression in the hippocampus of physically active rats and mice (Cotman & Berchtold, 2002; Farmer et al., 2004; van Praag, Christie, et al., 1999). Increased

levels of BDNF and FGF-2 and brain uptake of circulating IGF-1, as a result of exercise, affects the neural system in several ways. BDNF promotes survival of newly differentiated neurons (Arsenijevic & Weiss, 1998), IGF-1 promotes neuronal differentiation of neural progenitors (NPs) (Aberg et al., 2000; Arsenijevic & Weiss, 1998), and increased FGF-2 in hippocampal astrocytes stimulates proliferation and differentiation of hippocampal NPs (Yoshimura et al., 2001). For decades, it was proclaimed that adult mammalian brains did not grow new neurons, until the discovery that adult brains in rodents had niches of ongoing neurogenesis, particularly in the subventricular zone (SVZ) next to the lateral ventricles and the subgranular zone (SGZ) in the dentate gyrus (DG) of the hippocampus (Ohab et al., 2006). The elevated levels of trophic factors released in response to exercise may regulate the downstream processes leading to increased number of new neurons in adult animals (van Praag, Kempermann, et al., 1999).

Adult hippocampal neurogenesis is a process involving generation of new functional dentate granule cells (DGCs) from adult neuronal stem cells (NSCs), through amplification of intermediate NPs and neuroblasts, which thereafter integrate into the existing neuronal circuits. Adult hippocampal NSCs, also known as radial glia-like cells (RGLs), exists in the SGZ of the DG (Toda et al., 2019). Various environmental factors activate the neurovascular niche for neurogenesis, including exercise and stroke (Ohab et al., 2006; van Praag, Kempermann, et al., 1999), which stimulate quiescent RGLs and facilitate their proliferation. Active RGLs self-renew and generate intermediate NPs that subsequently divide and differentiate into neuroblasts, finally giving rise to DGCs (Esposito et al., 2005; Toda et al., 2019). After proper integration of new DGCs, adult-born DGCs are functionally connected to the hippocampal circuit within a time period from four to six weeks after birth (Toda et al., 2019). In the SVZ, neuroblasts migrate in chains anteriorly through the rostral migratory stream to the olfactory bulb, in which they differentiate into interneurons (Doetsch & Alvarez-Buylla, 1996; Kornack & Rakic, 2001; Lois et al., 1996; Pencea et al., 2001) and subsequently integrate with the existing circuitry (Carleton et al., 2003).

It is well known that adult NSCs in the SVZ and SGZ can be activated after stroke, thereby proliferating and differentiating to neuroblasts. These neuroblasts migrate into the infarcted area (e.g. the striatum and cerebral cortex), and contribute to repair of the brain and formation of glial scar tissue (Arvidsson et al., 2002; Jin et al., 2001; Parent et al., 2002; R. L. Zhang et al., 2001). However, a long-distance migration of newly born immature neurons occurs (Jin et al., 2003) and the number and capacity of NSCs decrease with age. Post-stroke neurogenesis is

therefore not able to replace all lost or damaged neural cells, or fully recover the damaged brain (Encinas et al., 2011; Koh & Park, 2017). Many growth factors have been found to protect the NSCs (Koh & Park, 2017), and elevated levels of these in response to exercise may therefore enhance neurogenesis and protect the brain following stroke.

1.3.2 Exercise and angiogenesis

Alongside with neurogenesis, exercise has also shown to increase endothelial cell proliferation, vascular growth factor levels (Fabel et al., 2003; Lopez-Lopez et al., 2004) and angiogenesis in young adult animals (Morland et al., 2017; Swain et al., 2003). Angiogenesis is associated with neurogenesis in the SVZ and SGZ (Alvarez-Buylla & Lim, 2004; Leventhal et al., 1999; Wurmser et al., 2004), and the effect of exercise on the vasculature may also be important for enhancing neurogenesis (van Praag et al., 2005). Induced angiogenesis in response to exercise is associated with overexpression of angiogenic factors, such as VEGF-A. These factors are believed to play a key role in new vessel formation (Ding et al., 2006).

Angiogenesis is the formation of new blood vessels, and the process can be divided into two categories: capillary growth by sprouting of capillaries from pre-existing mature endothelial cells (ECs) (vessels), and blood vessel remodelling with growth (enlargement) of the newly sprouted and existing vessels, primarily arterioles (Bloor, 2005; Folkman & Shing, 1992). During sprouting, activated ECs branch out from existing capillaries, extend through the surroundings and re-enter the capillary bed by joining with other capillaries or venules, before they become functional. For angiogenesis to take place, the extracellular matrix must be degraded to permit ECs to disengage and migrate. During the process of disengaging, the BBB integrity may be perturbed (Egginton et al., 2001; Haas et al., 2000; Hansen-Smith et al., 1996; Xing, Hayakawa, et al., 2012). In addition to be a potent angiogenic factor, VEGF-A also increases vascular permeability, which may lead to oedema and extensive tissue injury in the penumbra (Bates et al., 2002; Weis & Cheresh, 2005). The control of VEGF-A production, through changes in its mRNA stability and rate of transcription, regulates the blood vessel growth. Several subtypes of the VEGF receptor (VEGFR) exist, namely VEGFR-1, VEGFR-2 and VEGFR-3. VEGF-A regulates angiogenesis through the actions of VEGFR-1 and VEGFR-2, activation of the latter increases angiogenesis, whereas activation of the former decreases it (Geiseler & Morland, 2018). Binding of VEGF-A to VEGFR-2 activates phosphoinositide 3-kinase (PI3K) (Ruan & Kazlauskas, 2012), which further activates kinase B (Akt) (Koch &

Claesson-Welsh, 2012) and promotes the migration of ECs of the BBB (Kureishi et al., 2000; Morales-Ruiz et al., 2000; Radisavljevic et al., 2000; Wu et al., 2011).

The ECs of cerebral capillaries are linked by complex tight junctions to form the BBB, and the abluminal side is covered by astrocyte end-feet, microglial cells and pericytes (Correale & Villa, 2009), which further contribute to the regulated penetrance of substances between brain and blood. Under physiological conditions, the cerebral ECs are relatively quiescent, but traumatic brain injury induces angiogenesis at an early stage after the injury and leads to proliferation and migration of ECs (Y. Zhang et al., 2014). Studies with transient and permanent MCAO in rats have shown increased expression of VEGF-A in the ischaemic brain, suggesting that post-stroke angiogenesis may be induced by VEGF-A (Hayashi et al., 1997; Kovacs et al., 1996; Lennmyr et al., 1998). Consistent with these findings, late (24 and 48 hours) administration of VEGF-A has shown to enhance angiogenesis in the ischaemic brain, improving neurological recovery (Z. G. Zhang et al., 2000). However, angiogenesis is generally delayed or impaired by aging, with decreased EC proliferation in the adult brain (Edelberg & Reed, 2003; Reed & Edelberg, 2004). Stroke patients with a higher density of blood vessels appear to have reduced morbidity and survive longer (Krupinski et al., 1994). This may be explained by the formation of new blood vessels, which results in a more efficient network of collaterals. The increased collateral formation may bypass the occluded vessel, reduce the extent of perfusion-loss in stroke and thereby rescue the penumbra (Clayton et al., 2008; Geiseler & Morland, 2018). Physical exercise may therefore maintain the angiogenic response with aging and serve as a preventive strategy in stroke.

1.3.3 Exercise and lactate

The benefits of physical exercise have long been established, through elevated levels of growth factors to enhance neurogenesis and angiogenesis. Although the effects are well known, the initial signals from muscle to brain are unknown and the molecular pathways responsible for the induction of growth factors remain to be elucidated. One molecule that has been proposed as a potential signal for the exercise-mediated effects is the endogenous metabolite lactate.

During exercise lactate is released by the active skeletal muscles, accumulates in the blood, and crosses the BBB via endothelial monocarboxylate transporters (MCTs) (E et al., 2013; Pierre & Pellerin, 2005). Studies have shown that lactate produced during exercise induces BDNF expression and tropomyosin receptor kinase B (TRKB) signalling in the hippocampus, through

the induction of silent information regulator 1 (SIRT1) of the peroxisome proliferator-activated receptor γ coactivator 1α (PGC1α) and fibronectin type III domain-containing protein 5 (FNDC5) pathway. SIRT1 increases the levels of the transcriptional coactivator PGC1α and the secreted molecule FNDC5, known to regulate BDNF expression, thereby improve spatial learning and memory retention (El Hayek et al., 2019). Lactate administration has also previously shown to increase brain expression of VEGF-A (E et al., 2013; Morland et al., 2017), and the accumulation of lactate in the blood during high-intensity exercise may therefore increase VEGF-A in the brain to stimulate angiogenesis (Ferrara, 2000), which also directly enhances neurogenesis and synaptic function (De Rossi et al., 2016). Studies have shown lactate's ability to mediate changes in liver and brain bioenergetic-associated parameters, including increased VEGF-A expression in the brain, of both young and aged mice receiving supra-lactate threshold treadmill exercise (E et al., 2014; E et al., 2013). Lactate may act through its corresponding receptor, the hydroxy carboxylic acid receptor 1 (HCAR1, aka GPR81), which have been found to be highly enriched in pial fibroblast-like cells and pericyte-like cells, to enhance cerebral VEGF-A and cerebral angiogenesis (Morland et al., 2017). In conjunction with this, Morland and colleagues showed increased brain VEGF-A protein and capillary density in wild-type (WT) mice, but not in HCAR1 knockout (KO) mice, after high-intensity interval exercise and lactate administration giving similar levels to exercise.

Collectively, these studies indicate that lactate may account for some of the exercise-associated neuroprotective changes in the brain, including the induction of VEGF-A expression to drive brain angiogenesis and neurogenesis. Lactate may therefore be a potential endogenous molecule with therapeutic value for the treatment of certain CNS diseases through the HCAR1 receptor.

1.4 Lactate and HCAR1 in the brain

1.4.1 Lactate as a metabolite, energy substrate and signalling molecule

L-lactate (hereinafter referred to as lactate) is a monocarboxylate, originally considered to be an endogenous end-product of anaerobic glycolysis. Lactate production in the brain has long been associated with ischaemia, however, recent evidence shows that it can be found under physiological conditions as well (Magistretti & Allaman, 2018). According to the astrocyte-

neuron lactate shuttle (ANLS) hypothesis (Pellerin & Magistretti, 1994), lactate can be shuttled from astrocytes to neurons and serve as an efficient energy substrate.

Neurons are mainly oxidative, whereas glial cells – particularly astrocytes – show higher glycolytic than oxidative activity. Astrocytes produce lactate from pyruvate through the action of lactate dehydrogenase (LDH) despite the presence of normal oxygen tension, a process known as aerobic glycolysis (Magistretti & Allaman, 2015, 2018; Warburg et al., 1927; Weber & Barros, 2015). Neurons, on the other hand, oxidize lactate to produce pyruvate, which can enter the tricarboxylic acid cycle (TCA) for further energy generation. Thus, neurons may use lactate as a mitochondrial energy substrate. Some studies even suggest that lactate is preferred over glucose when both are available. Recently, it was proposed that intercellular lactate shuttles exist between astrocytes and neurons, by which lactate is transferred from lactate-producing cells to lactate-consuming cells. This constitutes the ANLS hypothesis (figure 1.2) (Brooks, 2009; Magistretti & Allaman, 2015, 2018). The ANLS hypothesis postulates that lactate is shuttled from astrocytes to neighbouring neurons during aerobic glycolysis to fuel these neurons. Furthermore, the neurotransmitter glutamate operates as an initial signal to trigger glucose uptake and aerobic glycolysis in astrocytes. The lactate that is produced by astrocytes is then released through transmembrane MCTs to adjacent neurons to meet their energetic demands (Magistretti & Allaman, 2018; Pellerin & Magistretti, 1994). The MCTs mediate facilitated cotransport of monocarboxylate anions and protons using the concentration gradients as their driving force. By this, lactate is transported across the BBB and different cell membranes to equilibrate the concentration gradients. Higher concentrations reflect sites of lactate production, where the substance migrates towards the sites of action and consumption through the MCTs (Bergersen & Gjedde, 2012; Morland et al., 2015). The cell-specific distribution of the MCTs further facilitates the trafficking of lactate from astrocytes to neurons; with low-affinity MCT1 and MCT4 present in astrocytes and high-affinity MCT2 present in neurons (Pierre & Pellerin, 2005), which may in part explain and support the ANLS hypothesis. However, the proposal of the ANLS hypothesis is not fully acknowledged and has been criticized on various grounds, given its many controversies and remain to be experimentally established (for review, see Dienel, 2012).

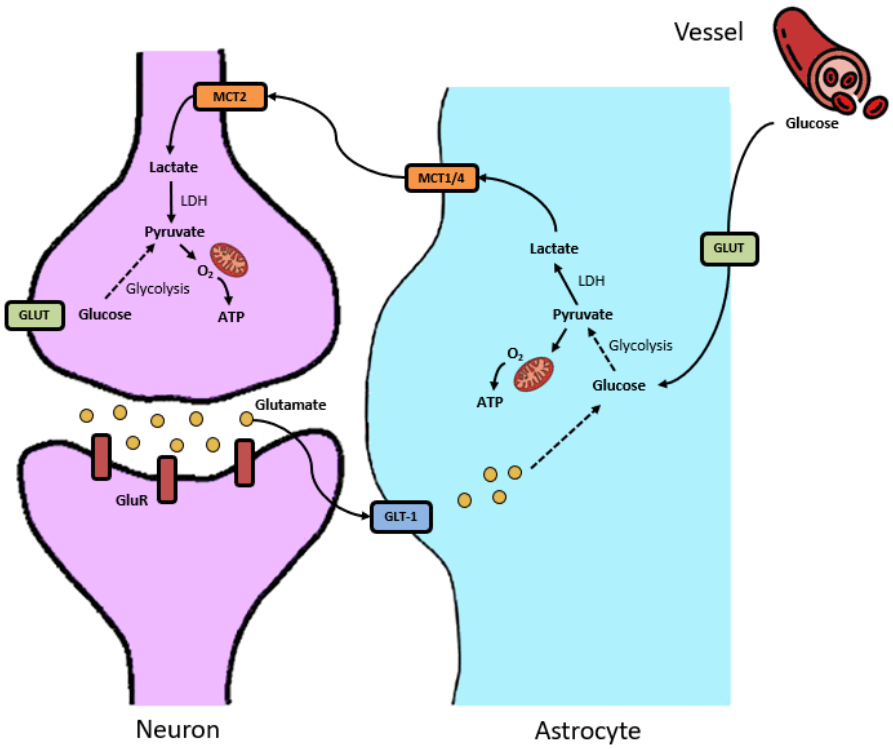

Figure 1.2. The astrocyte-neuron lactate shuttle (ANLS) hypothesis. The release of the neurotransmitter glutamate is actively taken up by astrocytes through GLT-1, and stimulates glucose uptake and aerobic glycolysis to yield lactate which is shuttled to neurons through the MCTs. Within neurons, lactate is converted to pyruvate which enter mitochondria for ATP-generation. Glucose can also enter neurons via transporters (GLUT) to fuel these cells. GLT-1, glutamate transporter 1; GluR, glutamate receptor; GLUT, glucose transporter; LDH, lactate dehydrogenase; MCT, monocarboxylate transporter. Adapted from Newington et al. (2013).

In addition to the metabolic effects, lactate may also be considered a signalling molecule and initiate signalling cascades through the lactate receptor HCAR1. The role of HCAR1 as a metabolic sensor and inflammatory mediator has been extensively reviewed by Hu et al. (2020). In the periphery, HCAR1 is predominantly located in adipocytes than other tissues, and is upregulated during adipocyte differentiation and development. Receptor activation have shown to participate in the regulation of adipocyte function and metabolism through the control of free fatty acids accumulation, which might possibly induce a synergistic effect with insulin (Ge et al., 2008; Jeninga et al., 2009; Offermanns, 2014). The mechanism is suggested to be through the promotion of lipid storage in these cells by downregulating cyclic adenosine monophosphate (cAMP) through G_i action to inhibit lipolysis (reducing fatty acids) in response to insulin-dependent uptake of glucose (Ahmed et al., 2009; Ahmed et al., 2010; Cai et al., 2008; Ge et al., 2008; C. Liu et al., 2009). Recently, HCAR1 has also been discovered to mediate inflammatory immune response. During an inflammatory immune reaction, activated HCAR1 may primarily recruit arrestin beta 2 (ARRB2) to suppress the toll-like receptor (TLR) and the inflammasome NLPR3 that mediates signalling in macrophages and monocytes (Cai et

al., 2008; Hoque et al., 2014; Lerch et al., 2014). Furthermore, lactate pre-treatment with HCAR1 action was related to diminished inflammatory signalling pathways in macrophages of several organs (e.g. liver, spleen and pancreas) (Madaan et al., 2017).

Newly discovered evidences have shown HCAR1 to be active in the mammalian brain as well, where it can be stimulated by physiological concentrations of lactate (about 0.1–30 mM) or by the HCAR1 agonist 3,5- dihydroxybenzoic acid (3,5-DHBA) to reduce cAMP levels (Lauritzen et al., 2014; Morland et al., 2015). HCAR1 immunoreactivity, have shown highest density of HCAR1 at excitatory synapses in hippocampus and cerebellum, but also at the membranes of cerebrovascular endothelial cells (Lauritzen et al., 2014). The present finding of possible HCAR1 receptors in widespread regions of the brain may indicate multiple signalling roles of lactate, including synaptic function, energy metabolism, and cerebral blood flow (Brooks, 2009; Gordon et al., 2008; Hashimoto et al., 2007). In conjunction with this, lactate has been proposed as a "volume transmitter", diffusing longer distances to reach its receptors and exert neuromodulatory effects on a larger population of neurons (Bergersen & Gjedde, 2012; Lauritzen et al., 2014; Morland et al., 2015). The MCTs provide a basis for the volume transmitter concept of lactate, which allows lactate to diffuse between cells and the extracellular space to mediate metabolic signals in the brain (Bergersen & Gjedde, 2012). This concept is further underpinned by lactate-mediated activation of HCAR1 (Lauritzen et al., 2014).

1.4.2 Lactate and HCAR1 involvement in stroke

In conditions where cerebral lactate levels are elevated, such as for instance hypoxic/ischaemic conditions, the lactate receptor will be activated, suggesting a role for HCAR1 in these conditions.

In the brain, HCAR1 activation has been shown to downregulate neuronal activity in cortical neurons, recorded as decreased calcium spiking (Bozzo et al., 2013). The suggested mechanism is inhibition of adenylyl cyclase to downregulate cAMP (Lauritzen et al., 2014). The discovery was further confirmed by de Castro Abrantes and co-workers, who showed that primary cortical neurons from WT but not from HCAR1 KO mice showed decreased calcium spiking activity. The effect was proposed to be mediated through its $G_{i\alpha}$-protein subunit and involve the adenylyl cyclase–cAMP–protein kinase A axis. In addition, HCAR1 was found to interact with other GPCRs, mainly adenosine A1, $GABA_B$, and α_{2A}-adrenergic receptors, through both $G_{i\alpha}$ and $G_{i\beta\gamma}$ subunits which adds a level of complexity to its modulation of neuronal network activity (de

Castro Abrantes et al., 2019). One aspect of the role of HCAR1 may therefore be an overall feedback function against excessive activity, and lowering cAMP through the receptor might serve to regulate multiple cellular processes (for review, see Morland et al., 2015). Briefly summarized, reduced cAMP through HCAR1 activation might counteract the catecholamine-induced increase of cAMP levels which enhance the breakdown of glycogen and lactate production (Leonard, 1975), and thereby save energy, limit acidification and damage in hypoxic conditions. Excess lactate as a result of glucose uptake and its conversion in brain cells might also activate these cells and induce vasodilation and increase CBF (Caesar et al., 2008; Vafaee et al., 2012). Finally, lactate may also limit the activity of cAMP-activated potassium channels, and thereby counteract excessive hyperpolarization. In accordance with this, Carole Berthet's group have shown lactate to be neuroprotective when administrated directly after induced ischaemia through MCAO (Berthet et al., 2012; Berthet et al., 2009).

In addition to modulating neuronal activity, HCAR1 activation also enhances VEGF-A and cerebral angiogenesis, as previously mentioned. VEGF-A increases in response to exercise and lactate, and a direct link between HCAR1 activation and VEGF-A signalling have been suggested. HCAR1 was further found to be localized in the vicinity of the blood vessels; the fibroblast-like cells that surround the pial blood vessels supplying the brain and the pericyte-like cells on the intracerebral microvessels (Morland et al., 2017). Activation of the PI3K/Akt-pathway and mitogen-activated protein kinase (MAPK) 3 and 1 (also known as ERK1 and ERK2)-pathway have been suggested to mediate increased expression and secretion of VEGF-A (L. Wang et al., 2008). Stimulation of HCAR1 with lactate or 3,5-DHBA causes enhanced phosphorylation of these enzymes (Morland et al., 2017). Consequently, these pathways may be involved in HCAR1-induced angiogenesis.

Overall, these findings pinpoint the lactate receptor HCAR1 as an initial mediator of cerebral effects of physical exercise, including as a key regulator of VEGF-A and angiogenesis, perhaps also to enhance neurogenesis. High levels of HCAR1 on fibroblasts in the meninges, especially in pia mater, opens for the possibility that these lactate-sensing fibroblasts may represent a novel therapeutic and preventive target in stroke. As HCAR1 can be stimulated by circulating lactate arriving from the blood as a result of exercise, this may explain the underlying beneficial effects of exercise in stroke. It is therefore of interest to find out if HCAR1-induced vascularization and neurogenesis in response to exercise is neuroprotective in stroke, thereby rescuing cognitive and motor function.

2 Aims of the study

In this study, we hypothesize that lactate-sensing fibroblasts of the meninges represent a novel therapeutic and preventive target in stroke through the HCAR1-mediated signalling, and that this may underlie the beneficial effects of exercise. In light of this, we seek to study the impact of HCAR1-dependent mechanisms in stroke to answer the following questions:

1. In respect to lactate and HCAR1-mediated effects, does exercise have a neuroprotective effect against stroke?
2. In respect to the stroke outcome, which exercise regime (high-intensity or medium intensity) gives the best prevention against stroke?
3. Is HCAR1-induced vascularization and neurogenesis, in response to exercise, neuroprotective in stroke?
4. How does lactate and HCAR1 induce angiogenesis and neurogenesis through exercise to protect against ischaemia?

3 Materials and methods

3.1 Chemicals, reagents and kits

Product	Manufacturer
4′,6-diamidino-2-phenylindole (DAPI)	Sigma-Aldrich, USA
Acetic (glacial) acid	Merck, Germany
Bovine serum albumin (BSA)	Sigma-Aldrich, USA
Chlorhexidine	Fresenius Kabi, Norway
Cresyl violet acetate	Sigma-Aldrich, USA
E-Gel 1 Kb Plus Express DNA Ladder	Invitrogen, USA
E-Gel EX 1% Agarose	Invitrogen, USA
E-Gel Sample Loading Buffer, 1X	Invitrogen, USA
Ethanol	Antibac, Norway
Eukitt Quick-hardening mounting medium	Sigma-Aldrich, USA
GenElute Mammalian Genomic DNA Miniprep Kit (G1N350)	Sigma-Aldrich, USA
Hydrogen chloride	Sigma-Aldrich, USA
Isoflurane	Baxter, USA
Buprenorphine	Indivior, USA
Neo-Clear	Merck, Germany
Newborn calf serum	Invitrogen, USA
OneTaq® Hot Start 2X Master Mix with Standard Buffer	New England BioLabs, USA
Paraformaldehyde	Sigma-Aldrich, USA
Pepsin	Roche, Switzerland
Potassium chloride	Sigma- Aldrich, USA
Potassium dihydrogen phosphate	Merck, Germany
ProLong Gold	Invitrogen, USA
Simplex eye ointment	Actavis, Iceland
Sodium acetate	Sigma-Aldrich, USA
Sodium azide	Sigma-Aldrich, USA
Sodium citrate	Sigma-Aldrich, USA
Sodium chloride	Sigma- Aldrich, USA

Sodium dihydrogen phosphate	Sigma- Aldrich, USA
Sodium L-lactate	Sigma-Aldrich, USA
Sucrose	Sigma-Aldrich, USA
Triton X-100	Sigma-Aldrich, USA
Water, Molecular Biology Grade	5 PRIME GmbH, Germany

3.2 Animals

The animal work described in this study was approved by the Animal Use and Care Committee of the Institute of Basic Medical Sciences, The Faculty of Medicine, University of Oslo, and by the Norwegian Animal Research Authority (FOTS ID 14204 and 12521). All animal experiments were conducted in strict accordance with the national and regional ethical guidelines, and animals were treated by Federation of Laboratory Animal Science Association (FELASA) certified personnel. Whenever possible, precautions and efforts were made to minimize animal discomfort and stress. A total of 144 C57BL/6N male and female mice were included in the study. The generation of HCAR1 KO line has previously been described; the exon encoding murine HCAR1 has been replaced by a cassette encoding β-galactosidase (LacZ) and neomycin resistance by homologous recombination in embryonic stem cells (Ahmed et al., 2010). The mouse line was obtained from Stefan Offermann's laboratory (Max-Planck-Institute for Heart and Lung Research, Department of Pharmacology, Bad Nauheim, Germany), and backcrossed and maintained in a C57Bl/6N background in our laboratory.

All mice, both KO and WT lines, were bred at the animal facilities at the Institute of Basic Medical Sciences, The Faculty of Medicine, University of Oslo. The animals were 5-6 weeks of age at the start of the experiments. The female mice were housed in groups up to 8 per cage, whereas males were separated and housed individually at the start of the experiments to avoid injury due to aggressive behaviour. The mice were maintained in standard GreenLine cages (Sealsafe Plus GM500) in a light regulated room (12:12 hour light:dark schedule) with access to food and water ad libitum. All animals where seen to daily according to the routines in the animal facilities. At any sign of distress, e.g. weight loss, erratic behaviour, lack of grooming etc, the animal in question was taken out of the experiment, according to the animal welfare protocol (FOTS 14204).

3.3 Experimental outline

An overview of the experimental outline is represented in figure 3.1, and summarizes the main procedures described in detail for this chapter. Briefly, a total of 144 animals were genotyped and semi-randomized into four different treatments, before subjected to treadmill running (high- or medium-intensity) or lactate or saline injections for 7 weeks. After 7 weeks of intervention, the animals were subjected to focal ischaemia and allowed to recover for 3 weeks before sacrificed. Additionally, parallelly to the genotyping, the quantitative analysis of capillary density was optimized and a training with the setup of equipment was executed for a week to accustom to the exercise regime prior to the actual intervention. The whole intervention took place over approximately 11 weeks since maximally 12 animals could be operated per day, and the animals were thus subdivided and started up as depicted.

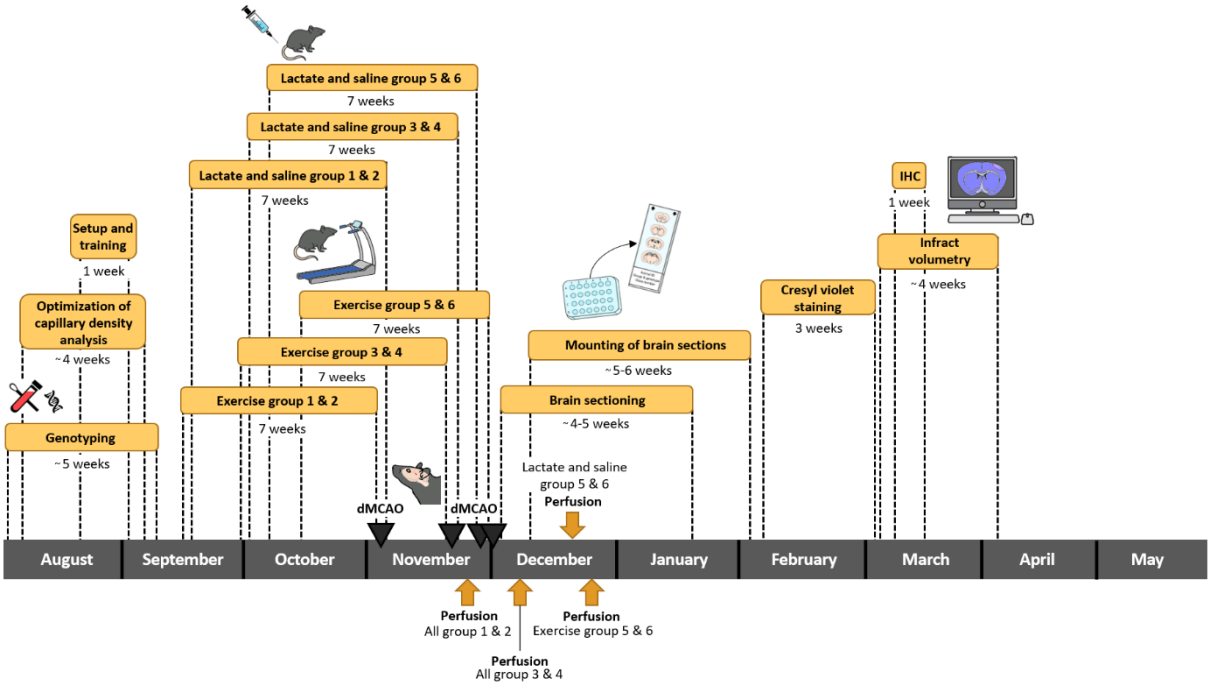

Figure 3.1. Visual overview illustrating the main procedures and the time-lapse throughout the study. A total of 144 mice were either introduced to treadmill running (high- or medium-intensity) or injections (lactate or saline) for 7 weeks. After 7 weeks of intervention, focal ischaemia was induced by dMCAO (triangles) and the animals were perfusion fixed 3 weeks later (arrows) before the brains were processed for further analyses. dMCAO, distal middle cerebral artery occlusion; IHC, immunohistochemistry.

3.4 Genotyping

To check the genotype of the mice, for breeding and for the experiment, genotyping was performed. Genotyping is a method to detect small genetic differences of an individual's DNA

sequence to determine the specific genotype by comparing the DNA sequence to a reference sequence or another sample. Genotypes of HCAR1 KO and WT mouse lines were verified by polymerase chain reaction (PCR) and agarose gel electrophoresis. Ear biopsies were collected routinely at 4-6 weeks of age or in some cases on demand when needed, and genomic DNA was isolated and purified before genotyping.

3.4.1 Extraction and isolation of genomic DNA

Genomic DNA was extracted using the GenElute Mammalian Genomic DNA Miniprep Kit (Sigma-Aldrich, USA), according to the manufacturer's protocol as described below. The kit uses a silica-based membrane, specifically selected for genomic DNA purification.

Ear notches were placed into separate 1.5 ml microcentrifuge tubes, added 180 µl Lysis Solution T and 2 µl Proteinase K (20 mg/ml stock solution), and vortexed to ensure the tissue was fully submerged before incubated on a block heater (Grant Boekel BBD, Boekel Scientific, USA) at 55 °C. Samples were vortexed occasionally during incubation for more rapid digestion of the tissue. The lysis was complete within approximately 2-3 hrs, and the samples were then briefly vortexed to give a homogenic sample. Lysis Solution C (200 µl) was added and thoroughly vortexed for 15 sec, before incubated on a block heater at 70 °C for 10 min. Reaching a homogeneous mixture was essential for efficient lysis. Then, 200 µl 100% ethanol was added and vortexed for 10 sec. Lysis of starting materials with chaotropic salt-containing solutions ensures thorough denaturation of the macromolecules, whereas addition of ethanol causes DNA to bind to the silica membrane of a binding column in the next step.

Binding columns in 2.0 ml collection tubes were prepared with 500 µl Column Preparation Solution, centrifuged for 1 min (13 000 rpm, room temperature) (Heraeus Pico 17 Microcentrifuge, Thermo Fisher Scientific, USA), before the flowthrough liquid was discarded. The Column Preparation Solution maximizes binding of DNA to the membrane, resulting in more consistent yields. The samples were then transferred to the binding columns and centrifuged for 2 min (13 000 rpm, room temperature), and the flowthrough liquid was discarded. A two-step wash was carried out consecutively; 500 µl Wash Solution Concentrate diluted in 100% ethanol was added, centrifuged for 1 min and the flowthrough liquid discarded. This was repeated once. Finally, columns were centrifuged without solutions for 3 min to dry the binding column and make sure it was free of ethanol before eluting the DNA.

The collection tubes containing the flowthrough liquid were discarded, the remaining columns with the samples were transferred to new 2.0 ml collection tubes and 100 µl Elution Solution (10 mM Tris-HCl, 0.5 mM EDTA, pH 9.0) was added directly into the centre of the columns. After 1 min, the samples were centrifuged for 1 min. Columns were discharged, and collection tubes containing pure genomic DNA were collected and stored at -20 °C for further preparation and analysis.

3.4.2 DNA precipitation

DNA concentration was very low after the extraction (in the range of 2-8 ng/µl), and precipitation to concentrate the DNA was therefore carried out using 100% ethanol in the presence of sodium acetate. In the DNA sample, 3M sodium acetate and 100% cold ethanol were added to constitute a final volume of 1/10 and 2.5x portions of the mixture, respectively. That is for 50 µl DNA sample, 17.5 µl 3M sodium acetate and 168.5 µl 100% ethanol were added in a 1.5 ml microcentrifuge tube. Samples were spun for 30 min (13 000 rpm, 4 °C) (Heraeus Fresco 21 Microcentrifuge, Thermo Fisher Scientific, USA), and the supernatant was aspirated using a micropipette. Then, 100 µl 100% cold ethanol was added to each sample, and spun again for 5 min (13 000 rpm, 4 °C). The supernatant was aspirated and the pellet was resuspended in 30 µl DNase/RNase/protease-free distilled water (dH_2O) to give approximately 20-30 ng/µl DNA.

3.4.3 Polymerase chain reaction

The PCR mix for each sample (25 µl) contained 15 µl OneTaq® Hot Start 2X Master Mix with Standard Buffer (New England BioLabs, USA), 1.5 µl 10 µM HCAR1 forward/reverse primer, 1.5 µl 10 µM LacZ forward/reverse primer and 7 µl dH_2O. Finally, 5 µl DNA extract (about 100-150 ng DNA) was added to each 0.2 ml PCR eppendorf tube containing 25 µl PCR mix. Reactions were run in a thermocycler machine (Applied Biosystems 2720 Thermal Cycler, Thermo Fisher Scientific, USA) under the following cycling conditions: 94 °C for 3 min (initial denaturation), followed by 45 cycles at 94 °C for 30 sec (denaturation), 50 °C for 30 sec (annealing), and 72 °C for 1 min (elongation). The cycles were followed by a final step at 72 °C for 10 min and then 4 °C for an undefined time period (cooling), until collected for electrophoresis.

Targeted WT and KO alleles were separately amplified in each sample with specific forward and reverse primer combinations (table 3.1). Primers were customized and ordered from Invitrogen (Thermo Fisher Scientific, USA).

Table 3.1. Sequences of PCR primers used to genotype wild-type and knockout alleles of the HCAR1 and LacZ gene. KO, knockout; WT, wild-type.

Gene	Allele specificity	Sense	Sequence (5′–3′)
HCAR1	WT	Forward	AAG ACC TGG AAG TCA AGC AC
HCAR1	WT	Reverse	CAC CAC AGT GAG GAA GAC AA
LacZ	KO	Forward	TTG GCG TAA GTG AAG CGA C
LacZ	KO	Reverse	AGC GGC TGA TGT TGA ACT G

3.4.4 Agarose gel electrophoresis

Reaction products were run on a 1% agarose gel (Invitrogen, USA) for 10 min using the E-Gel Power Snap electrophoresis system (Invitrogen, USA). The amplified DNA samples (2 µl) were mixed with 10 µl dH_2O and 10 µl loading buffer (E-Gel Sample Loading Buffer 1X, Invitrogen, USA). Similarly, 2 µl of a DNA ladder (E-Gel 1 Kb Plus Express DNA Ladder, Invitrogen, USA) was mixed with 10 µl dH_2O and 10 µl loading buffer. All wells were filled with 20 µl sample or dH_2O, and ran at the E-Gel EX 1-2% program for 10 minutes. The gel was visualized by UV-light.

3.4.5 Interpretation of results

DNA fragments (nucleic acids) are negatively charged, and will move towards the positive electrode in gel electrophoresis when an electric current is applied (figure 3.2). Because all DNA fragments have the same amount of charge per mass, the mixture will be separated according to molecular size where smaller fragments move through the gel faster than larger ones (Corthell, 2014a). Expected sizes of the PCR products for the HCAR1 and LacZ gene are 195 bp and 507 bp, respectively. The ladder contains proteins of known bp-lengths and therefore informs about the sizes of the PCR products and was used to identify WT and KO mice. Heterozygous mice carry both alleles which are displayed as two bands on the gel, and were excluded from the experiment.

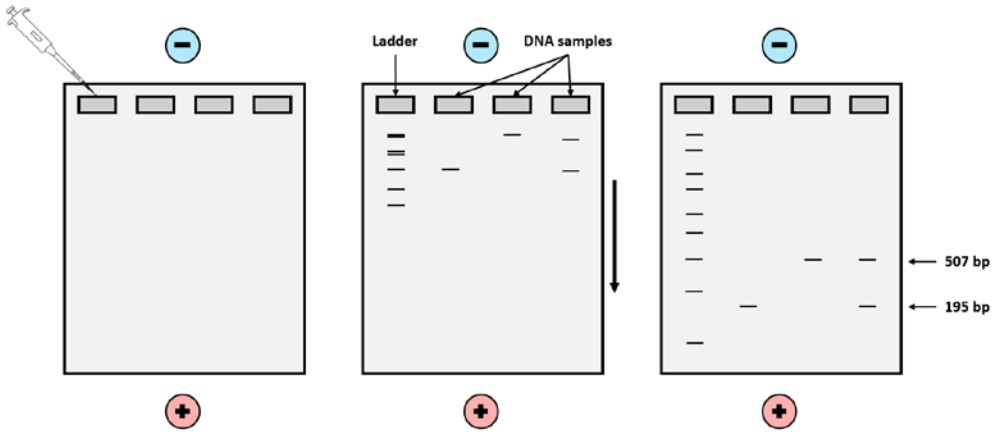

Figure 3.2. Interpretation of genotyping results. The samples, along with a DNA ladder, were loaded into the gel electrophoresis wells. When the power is turned on, the DNA fragments will migrate through the gel towards the positive electrode and be separated by size. The PCR products are expected to generate single bands from HCAR1 or LacZ gene (WT or KO alleles), whereas heterozygote mice display both bands of the PCR products. The right-hand panel shows an example of WT, KO, and heterozygote genotype.

3.5 Animal treatments

144 HCAR1 KO and WT mice were semi-randomized into eight treatment groups: high-intensity exercise, medium-intensity exercise, lactate injections or saline injections for each genotype (figure 3.3). Each group consisted of about 1:1 ratio HCAR1 KO and WT mice, with a balanced male/female distribution.

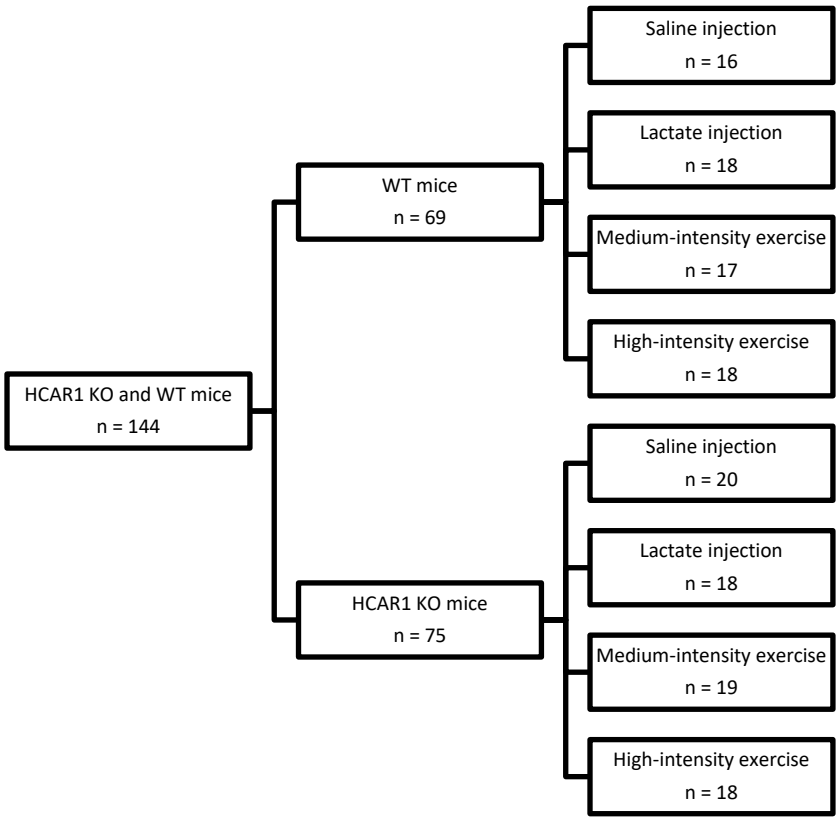

Figure 3.3. Study design and randomization of animals to eight different treatment groups.

3.5.1 Lactate and saline treatment

The lactate treatment group received 2 g/kg sodium L-lactate (≥99.0%, Aldrich, catalogue #71718; dissolved in 0.9% saline; pH-adjusted to 7.4), equal to 18 mmol/kg. The lactate solution concentration was 200 mg/ml, and a volume of 10 µl/g bodyweight was administered. The saline group (control) received the same volume (per kg bodyweight) of 0.9% sterile saline (B. Braun Medical AS, Norway). Intraperitoneal (i.p.) injections were given once a day, 5 consecutive days a week for 7 weeks. Doses were adjusted based on weekly weighing.

3.5.2 Exercise regime

The high- and medium-intensity group exercised once a day, 5 consecutive days a week for 7 weeks, on a six-lane treadmill designed for rodents (Exer 3/6, Columbus Instruments, USA). If necessary, the animals were gently pushed by the experimenter to keep running during the active intervals. The lower part of each treadmill lane contained an electrical grid to give an electrical stimulus (<1.5 mA intensity) if mice were especially unwilling to run, however, most

animals were running voluntary after a short adaptation phase. The treadmill platform was set on 25° incline for both intensity groups.

The training protocol was based on a previously described work (Morland et al., 2017; Rolim et al., 2015), with the following adaptions: Each session consisted of a 10 min warm-up at 8 m/min, followed by 10 intervals at high- or medium-intensity for 4 min, and 2 min of active rest at 5 m/min between each interval. The high-intensity group was running at 80% of maximum running speed (S_{max}), equal to ~80% of maximal oxygen consumption (VO_{2max}), whereas the medium-intensity group was running at 60% of S_{max}. On the first day of exercise for each group, each interval was run at slow speed (15 m/min and 8 m/min, for high- and medium-intensity group, respectively), and to familiarize the animals to treadmill running. On the second day, and then every other week, a maximal exercise-capacity test was executed for each mouse to adjust the running speed of the exercise intervals. The maximal exercise-capacity test was carried out with a 15 min warm-up at 9.6 m/min, followed by gradual increases in speed by 1.8 m/min every 2 min until exhaustion, that is until the mice showed clear signs of exertion (e.g. jumping with both hind paws to keep the pace) and refused to run, despite being pushed back on the treadmill band. Based on the performance, the average 80% and 60% S_{max} was calculated for each high-intensity and medium-intensity group, respectively. The treadmill speed was then progressively increased for the high-intensity group to reach their 80% S_{max}, so they could sustain the 10 consecutive intervals. Increases were carried out every training session, by increasing 0.2 m/min each interval after the fourth interval, maximally 0.6 m/min each session. The medium-intensity group started at a running speed representing 60% of the average S_{max} in the maximal exercise-capacity test, and were kept on the same speed through all intervals of the experiment. Between each training session, the treadmill band was quickly cleaned with 70% ethanol and dried to remove any smell from previous mice, and thoroughly cleaned with soap and ethanol by the end of the day. All animals were carefully handled and observed during the exercises. If individual mice performed below their normal level on the day or had minor injuries, it was allowed short additional breaks. If necessary, it was given a rest day until the next session. Animals that performed below expectations for several consecutive days were withdrawn from the study.

3.6 Permanent coagulation of the distal middle cerebral artery

After 7 weeks of exercise, lactate or saline injections, focal ischaemia was induced by permanent coagulation of the distal MCA (figure 3.4A) according to a previously published protocol (Llovera et al., 2014). All operations were conducted by postdoctoral fellow Samuel Geiseler from the Neurobiology and Toxicology group (Department of Pharmaceutical Biosciences, School of Pharmacy, University of Oslo).

Prior to surgery, mice were anaesthetized in a chamber saturated with 4% isoflurane (~70% N_2O, 30% O_2 + isoflurane) before they were given i.p. injections of buprenorphine 0.3 mg/kg (Temgesic, Indivior, USA) and transferred to a heat pad (37 °C) to maintain body temperature. Reflex examination (toe pinch test) was conducted to ensure the mice were deeply anaesthetized. Anaesthesia was maintained during surgery with approximately 1.5% isoflurane using an anaesthesia mask. Simplex eye ointment (Actavis, Iceland) was applied on both eyes to avoid dryness during and after the surgery.

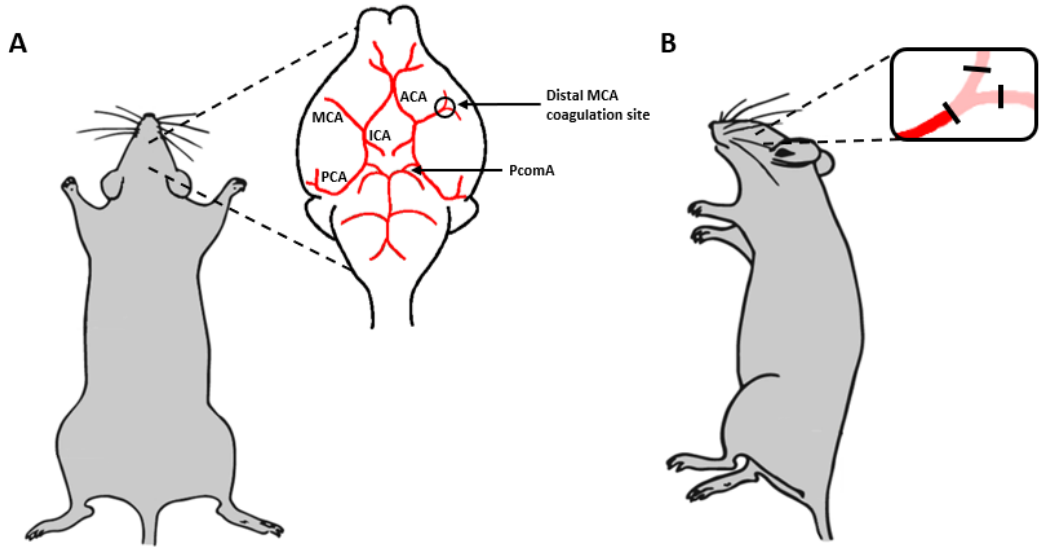

Figure 3.4. Schematic illustration of permanent coagulation of the distal middle cerebral artery. (**A**) Superior view of vessel architecture supplying blood to the brain. Circle represent coagulation site of the MCA. (**B**) Transcranial view of MCA coagulation. Permanent coagulation was conducted proximal and distal to the MCA branching. Black rectangles represent the coagulation sites of the artery. ACA, anterior cerebral artery; ICA, internal carotid artery; MCA, middle cerebral artery; PCA, posterior cerebral artery; PcomA, posterior communicating artery.

The surgical site was first disinfected using 0.1 % chlorhexidine cutaneous solution (Klorhexidin, Fresenius Kabi, Norway). A 1 cm incision was made between the ear and eye using operation scissors, and the skin was separated to localize the temporal muscle. To prevent

drying of the tissue, sterile physiological saline (B. Braun Medical AS, Norway) was applied throughout the operation. The muscle was detached from the skull, in its apical and dorsal part, using the diathermi-forceps of a high-frequency generator (VIO 50 C, Erbe, Germany) adjusted to 12 W in bipolar mode. The distal MCA was identified through the transparent skull, and the bone right above the MCA branch was thinned out using a drill (Dremel, USA). The last layer of bone was carefully withdrawn with ultra-fine forceps. With the diathermi-forceps adjusted to 7 W in bipolar mode, the forceps were placed on each side of the distal MCA as close as possible, but without actually touching, to coagulate the artery with minimal mechanical damage. The coagulation was placed downstream of lenticulostriate arteries, proximal and distal of M1 (figure 3.4B). After 30 sec, the artery was gently touched to ensure permanent coagulation and exclude spontaneous recanalization. In case of observed blood flow as a result of recanalization, electrocoagulation was repeated once. Finally, the temporal muscle was relocated back in its position and the incision was sutured.

After the operation, the mouse was placed in a nursing box at 32 °C for at least 20 min to recover from anaesthesia, and then returned to its cage. I.p. injections of post-operative analgesia (buprenorphine 0.3 mg/kg) were administered 24 hrs after the operation, and then daily for 4 days.

3.7 Gait analysis

On the last day of training and 20 days after the stroke operation, animals of the exercise groups were filmed (GoPro Hero5 Session, GoPro, USA) from above during running. A gait analysis was performed, using a deep-learning algorithm (deeplabcut.com) to asses if the animals had a tendency for imbalanced running after stroke.

Filming of mice after the stroke operation was performed with a 4 min warm-up at 8 m/min. The running speed was adjusted to be 0.2 m/min lower than last session’s running speed for the high-intensity group, whereas the medium-intensity group was running at their last session’s running speed. All recordings were performed during the first to second interval for medium-intensity group, and third to fourth interval for high-intensity group. Otherwise, treadmill running was performed as described earlier.

3.8 Perfusion fixation

The goal of fixation is to rapidly and uniformly preserve the tissue, while keeping its intrinsic structure and natural form. Transcardial perfusion fixation utilises the vascular system of deeply anesthetized animals to deliver the fixative to the tissues of interest. This is particularly important for larger specimens, for instance the intact brain, to prevent the introduction of artefacts and reach all regions of the tissue with the fixative at the same rate (Gage et al., 2012; Kasukurthi et al., 2009). Here, we used the transcardial perfusion method with paraformaldehyde (PFA) as fixative. PFA is the polymerization product of formaldehyde, and exerts its fixative properties the same way as formaldehyde upon depolymerization. To depolymerize, the PFA solution must be heated and treated under alkaline condition, which catalyzes the hydrolysis of the polymers to yield formaldehyde (Kiernan, 2000). Formaldehyde reacts with various side chains of the tissue's proteins to form hydroxymethyl side groups that subsequently cross-link to form methylene bridges. Ultimately, an insoluble product is achieved which leaves the tissue in a chemical state and halts biochemical and proteolytic activities, thereby preventing tissue decomposition (Dey, 2018a). The method described below is a terminal procedure, which combines tissue fixation with euthanasia to harvest the brain. All perfusions were conducted by postdoctoral fellow Samuel Geiseler or associate professor Cecilie Morland from the Neurobiology and Toxicology group.

At 3 weeks after permanent coagulation of the distal MCA, HCAR1 KO and WT mice were deeply anaesthetized with i.p. injections of 0.1 ml/10 g bodyweight ZRF anaesthetic mix, consisting of zolazepam 3.3 mg/ml, tiletamine 3.3 mg/ml, xylazine 0.5 mg/ml and fentanyl 2.6 μg/ml. Reflex examination (toe pinch test) was performed to make sure the depth of anaesthesia had reached a surgical plane, i.e. complete absence of any reflexes and pain-responses. The mouse was then secured in the supine position on the work surface (a polystyrene block) with the paws pinned down using cannulas.

A medial incision was first made with surgical scissors through the abdominal wall, right beneath the rib cage, to open the abdomen cavity. The liver was carefully moved aside to expose the diaphragm and ribs from below. Thereafter, a small incision was made through the diaphragm. This step was critical and the subsequent steps had to be conducted as fast possible, as the first penetration of the diaphragm disturbs the intrapleural pressure and halts the air exchange in the lungs, thereby possibly induce ischaemic damage to the brain. The thorax was

opened by cutting through the entire length of the rib cage up the collarbone. A similar cut was made at the contralateral side to create a rib flap and open the thoracic cavity to expose the heart. A canula connected to a peristaltic pump (Watson-Marlow 323 pump, Watson-Marlow, UK) was inserted into the left ventricle and the mice were perfused transcardially with 4% PFA in 0.1 M sodium phosphate (NaPi) buffer at pH 7.4, at a rate equal the animal's cardiac output (5 ml/min). Simultaneously, a puncture was made on the auricle of the right atrium to allow the blood and perfusate to exit the circulation. Adequate perfusion was ensured by continuing for at least 8 min, or until the liver was completely devoid of blood and the body stiff. Following perfusion, the animal was decapitated and the skin and underlying cranium was carefully removed. Sharp scissors were used to make a cut down the midline and pry off the cranium to expose the brain. The brain was carefully scooped out of the skull using a small spatula and transferred to a tube containing 4% PFA. Post-fixation was carried out in same fixative overnight at refrigerated temperature (4 °C), before the tissue was transferred to and stored in 0.4% PFA for long-term storage until further tissue processing.

3.9 Cryostat sectioning

Cryostat sectioning is the technique of sectioning frozen tissues after rapid freezing the tissue with the help of a cryostat instrument. The process can be carried out in several ways, using various types of microtomes and knife profiles. Here we used a sliding microtome (HM 450, Thermo Scientific, USA) connected to a fast freezing unit (KS 34, Thermo Scientific, USA) to freeze and section the brain with the common wedge-shaped steel knife (profile C). The tissue block is static, while the room tempered microtome knife moves horizontally over the tissue for cryostat sectioning.

Before brain sectioning, the cerebellum was removed using a razor blade and the remaining brain was transferred to separate 15 ml centrifuge tubes containing 30% (w/v) sucrose diluted in NaPi (0.1 M sodium phosphate buffer, pH-adjusted to 7.4) and 0.01% sodium azide to prevent bacterial contamination. The brains were left at refrigerated temperature (4 °C) until saturated and sunk to the bottom, usually within two days, to ensure cryoprotection of the fixed brains.

The microtome plate was rapidly cooled to -40 °C before dripping 30% sucrose solution using a pasteur pipette to create an ice block stage (about 2 x 2 x 1 cm) on the plate. Adjusted to 50

µm, the ice block was trimmed to create a flat surface before the brain was placed on top of the ice block stage with the rostral end pointing up, with the use of blunt forceps. The brain was let to completely freeze, before a few drops of sucrose solution were pipetted around the base of the brain and on top. Embedding of the brain to the frozen medium prevents distortion and separation of the tissue from the stage during sectioning. The brain was then allowed to freeze quickly under the covering with a polystyrene block for some minutes. The temperature was then set to -20 °C, and 20 µm coronal sections were cut from about 3.0 mm rostral from bregma (+3.00 mm) to about 4.6 mm caudal (-4.60 mm) from bregma. Between each cut and harvest, the microtome knife was wiped off. Sections were removed from the knife with a soft paintbrush (Brush Watercolour Round No. 0 and 3/0 pine marten hair, Panduro Hobby, Norway) and placed in four 24-wells plates (4 x 6 wells, Tissue Culture Plates 24 wells sterile, VWR, USA) filled with NaPi with 0.01% sodium azide to ¾ of the volume. To achieve a spatial order, brain sections were placed in wells from left to right starting from A1 to A6 and ending at D1 to D6 (figure 3.5) in all four plates.

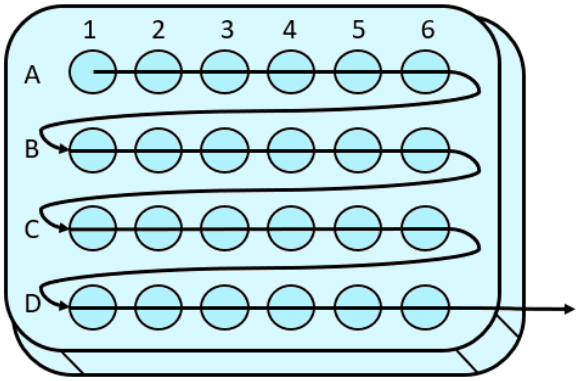

Figure 3.5. Schematic illustration of microtome brain sections transferred and stored into 24-wells plates. A total of four well plates were used for each brain, numbered one to four. Starting with the first plate, brain sections were harvested following the depictured order, and the same pattern continued in the remaining three plates, before repeating all over from the first plate.

At the end of the fourth plate, the same pattern was repeated over again until the whole brain region of interest brain was completely sectioned and all sections harvested. All well plates were covered with parafilm (Parafilm M PM996, Bemis, USA) and stored at refrigerated temperature until mounting and staining.

3.10 Measurement of infarction volume

3.10.1 Buffers and solutions

0.1% Cresyl violet solution

Cresyl violet acetate 1 g/l, in milli-Q water

Phosphate-buffered saline (PBS)

9.8 mM $Na_2HPO_4 \cdot 2H_2O$, 137 mM NaCl, 2.7 mM KCl, 2 mM KH_2PO_4, in milli-Q water (pH 7.4)

Ethanol solution

Anhydrous (100%) ethanol, in PBS to give the respective concentrations

3.10.2 Mounting of brain sections

Every 6th brain section was mounted on 75 x 25 x 1.0 mm microscope slides (Superfrost Plus, Thermo Scientific, USA) under a stereo microscope (Nikon SMZ645, Nikon Instruments, USA) to give a representative cerebral injury to measure the infarct volume. That is, almost every 20 µm brain section from row number one in all four plates were mounted (A1, B1, C1 and D1, see figure 3.6) to cover about 2.5 mm rostral (bregma +2.5) to 3.0 mm caudal from bregma (bregma -3.0). If some brain sections were missing a part or could not be found, neighbouring sections was mounted instead. The brain sections were mounted on the microscope slide by adding a drop of water on the slide and transfer the sections by using a paintbrush (Brush Watercolour Round No. 0 and 3/0 pine marten hair, Panduro Hobby, Norway). The sections were then gently folded out and remaining water was wiped off using soft wipes. Six brain sections were mounted on each glass slide; altogether 6000 sections were mounted. Sections were left at room temperature to dry completely before they were stored at refrigerated temperature.

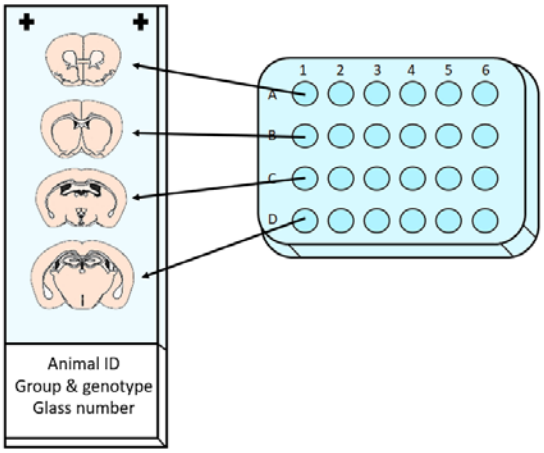

Figure 3.6. Illustration of brain sections selected for infarct volumetry analysis. The arrangement of brain sections in the 24-wells plates allowed for quantification of cerebral infarct volume of every 6th brain section of the entire brain by mounting these sections on the microscope slides, i.e. mainly sections from row number one were selected.

3.10.3 Cresyl violet staining

Cresyl violet (CV) is among the standard histological stains used to detect neurons and apoptotic cells. The reagent heavily stains the condensed chromatin within the cells, leaving a dark violet colour to all nuclei with good contrast visualized under light microscopy (Martin & Chatterjee, 2003). The method is based on the interaction (a chemical reaction) between the alkaline stain and the acidic components (DNA) of the cell nuclei. The dye also stains RNA that is highly concentrated in rough endoplasmic reticulum and ribosomes (Nissl bodies) in the cytoplasm, and hence is also called Nissl staining (Kadar et al., 2009).

The sections were stained according to the protocol in table 3.2. The protocol consists of five main steps; hydration, staining, dehydration, differentiation and clearing. Each procedure was performed using the EasyDip Slide Staining System (Simport Scientific, Canada).

For hydration, the slides were immersed slowly through a series of decreasing concentrations of alcohol (ethanol). CV is hydrophilic in nature and the introduction of water into the tissue sections ensures thorough penetration of the stain during staining. Minimum one-minute immersion times were considered adequate to assure complete removal of the previous solutions. Staining was performed in a water bath at 60 °C for 8 min. Before every use, the CV staining solution (cresyl violet acetate, Aldrich, catalogue #C5042) was reheated to 60 °C and filtered using a paper filter (Qualitative filter paper, grade 403, catalogue #516-0289, VWR, USA). Dehydration is the removal of water from the tissue sections. This was conducted by

passing the sections through increasing concentrations of alcohol to gradually replacing the water content in the tissue sections with ethanol. Differentiation was carried out to remove superfluous CV stain by treating the slides with 1% glacial acetic acid in 95% ethanol for 3 sec, followed by a washing step in 95% ethanol for 5 sec. CV is present as a cationic salt with acetate, and the immersion in acidic conditions will ionize the molecule to a larger extent, thus making it more water-soluble and remove it from the tissue sections. The result is heavily staining of structures with high affinity to the chemical with enhanced contrast. Before proceeding, the slides were examined for possible over- or under-staining. When the sections were over-stained, the differentiation step was repeated for a few additional seconds until desirable staining was achieved. Whereas when brain sections showed signs of under-staining, re-staining was performed for a longer period of time (maximally 15 min). In some cases, the first dehydration step with 70% ethanol (step 9 in table 3.2) was excluded when the sections showed inadequate staining despite repeated re-staining for several additional minutes. Finally, the brain sections were immersed in 100% ethanol for a final dehydration step, before treated with xylene substitute (Neo-Clear, Merck, Germany) for clearing. Clearing with xylene or xylene substitute after dehydration displaces the alcohol from the tissue sections with the clearant, as the xylene substitute is miscible with alcohol. This assures the tissue sections are clear before coverslipped with mounting medium, and also prevents the CV stain to bleed from the tissue sections after coverslipping. To preserve the stained sections for later analysis, coverslipping was performed with Eukitt quick-hardening mounting medium (Sigma-Aldrich, USA) before the slides were left overnight to dry.

Table 3.2 CV staining protocol.

Step	**Medium**	**Time**
1	95% ethanol	15 min
2	70% ethanol	1 min
3	50% ethanol	1 min
4	Phosphate-buffered saline	2 min
5	Phosphate-buffered saline	1 min
6	Cresyl violet at 60 °C	8 min
7	Phosphate-buffered saline	1 min
8	Phosphate-buffered saline	1 min
9	70% ethanol	1 min

10	95% ethanol	1 min
11	1% glacial acetic acid in 95% ethanol	3 sec
12	95% ethanol	5 sec
13	Check staining; repeat from step 10 if over-stained, repeat from step 2 if under-stained	-
14	100% ethanol	1 min
15	Neo-Clear	1 min
16	Cover slides with mounting medium	-

3.10.4 Image acquisition with light microscopy

Surface view images of the whole-coronal brain sections were captured using an automated slide scanner system (Axio Scan Z1, Carl Zeiss Microscopy, Germany). Images were taken at a resolution of 2.6662 pixels per µm (equal to 0.375 µm per pixel) with 20x magnification.

3.10.5 Infarct volumetry after permanent distal middle cerebral artery occlusion

Images of CV-stained coronal sections from 1.645 mm rostral to 2.355 mm caudal from bregma were analysed using the Fiji distribution of ImageJ (Schindelin et al., 2012) (version 2.0.0-rc-69/1.52p; Java 1.8.0_172). The cortex of the ipsilateral (to the stroke) and contralateral hemisphere was outlined according to The Allen Brain Atlas (https://mouse.brain-map.org/experiment/thumbnails/100048576?image_type=atlas) by using the "Polygon selections" tool in the software (figure 3.7). The outlined cortical areas were saved in "ROI Manager" and measured. Resulting values were imported into a pre-defined Excel template and the infarct volume (defined as tissue atrophy plus scarred damaged tissue) was calculated indirectly by the Swanson method (Swanson et al., 1990).

In addition to the actual quantifications, 79 sections were double-blinded and measured to examine the reproducibility of the analysis.

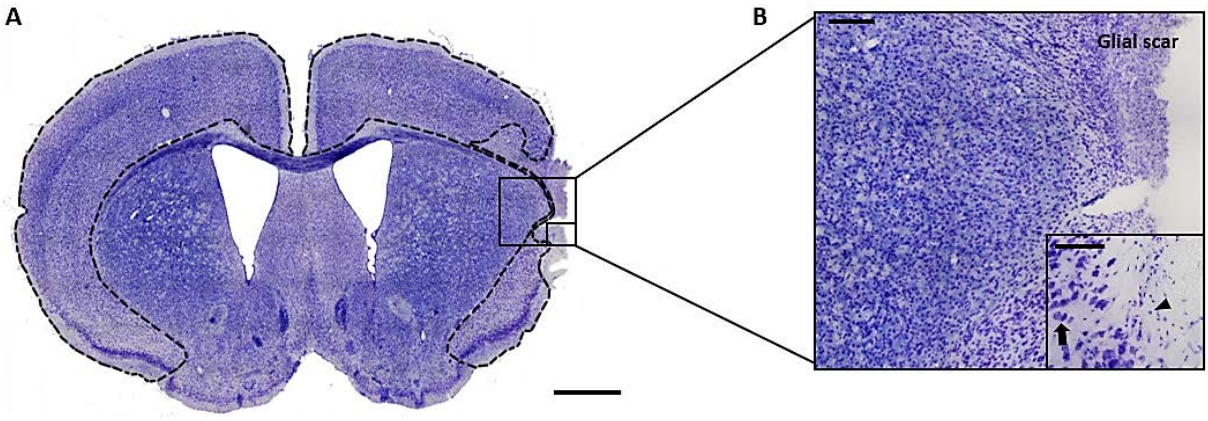

Figure 3.7. Infarct volume quantification of cresyl violet-stained brain sections following permanent dMCAO. (**A**) The ipsilateral and contralateral cortical areas were measured and the infarct volume (tissue atrophy plus scarred damaged tissues) was quantified by subtracting the ipsilateral area from the contralateral area. Dashed lines indicate the cortical areas measured. Scale bar: 1000 µm. (**B**) Higher magnification of the ipsilateral cortex showing the presence of both injured (shrunken neurons with condensed nuclei; indicated by the arrowhead) and non-injured neurons (intact nuclei with regular distribution; indicated by the black arrow). Injured neurons and glial scar were excluded from measurements of cortical areas. Scale bar: 200 µm. Image in square frame (below) was amplified as the previous image (above). Scale bar: 100 µm. Coronal section taken at 0.6 mm rostral of bregma.

To measure the infarct volume (I_{xi}) for a single brain section *x* of animal *i*, the area of ipsilateral cortex (A_I) was subtracted from the area of contralateral cortex (A_C). The differential was then multiplied with the distance (*d*). This gives the following equation:

$$I_{xi} = (A_c - A_I) * d$$

The total infarct volume (TI_i) throughout the analysed region of the brain of each animal was calculated by summing the infarct volumes of all the sections (*n*), as given in the equation below:

$$TI_i = \sum_{x=1}^{n} I_{xi}$$

The theoretical distance of 4 mm between the first and last section (based on the bregma coordinates in the Allen Brain Atlas, as described) was used to calculate the infarct volume from the individual infarct areas measured in each section. Together, the following equation was used to measure the total infarct volume for each animal:

$$TI_i = \sum_{x=1}^{n}((A_C - A_I) * d)_x$$

Where the distance is $d = \frac{4000\ \mu m}{n}$, based on the average distance of *n* sections measured between 1.645 mm rostral and 2.355 mm caudal of bregma (4 mm in total).

The quantifications were performed by an operator who was blinded with regard to treatments and genotypes.

3.11 Immunohistochemistry

The fundamental concept behind immunohistochemistry (IHC) is the specific antigen-antibody binding, which is used to detect targets of interest within the tissue sections (Ramos-Vara, 2005). The antigen-antibody binding is demonstrated by a secondary antibody, capable of binding the primary antibody with high specificity, and is either conjugated to a fluorescent molecule visualized under laser light at specific wave lengths (fluorescent IHC) or a reporter molecule which reacts with a chemical substrate (usually an enzyme) to form a coloured precipitate at the site of antibody binding to protein (colorimetric IHC) (Corthell, 2014b).

Before immunolabelling, an antigen (epitope) retrieval step was included to break methylene bridges formed during fixation. This is particularly for PFA-fixed tissues, in which many amino acid residues of the proteins form methylene bridges within or between the molecules with formaldehyde. These methylene bridges mask may the antigenic sites, which lead to poor immunohistochemical staining. Thus, antigen retrieval allows for the recovery of antigenic sites, which overall improves the staining intensity (Titford, 2009). In addition, prior to primary antibody incubation, a blocking step was essential to prevent non-specific binding of the antibody. Although antibodies show preferential affinity and selectivity for epitopes, non-specific binding may occur at binding sites that closely mimic the targeted epitopes of interest which results in high background staining. Incubation with blocking reagents, typically bovine serum albumin (BSA), casein or normal serum, serve to block the non-specific antibody binding in the tissue and ensures the observed fluorescent staining solely is due to the primary antibody of interest (Corthell, 2014b).

Here, we subjected brain sections to fluorescent IHC in order to visualize and investigate post-stroke angiogenesis and neurogenesis. In the upcoming sections, the immunolabelling of capillaries and neuron markers will be described in detail using different antigen retrieval techniques and specific antibodies. The immersion method with the EasyDip Slide Staining System (Simport Scientific, Canada) was used for antigen retrievals and washing steps, whereas blocking and incubations were performed in moisture chambers while shielded from light. Each procedure had commonalities, including five main steps: antigen retrieval, blocking, primary

antibody incubation, secondary antibody incubation and 4′,6-diamidino-2-phenylindole (DAPI) incubation, separated by washing steps.

3.11.1 Buffers and solutions

Pepsin solution

Pepsin 10 mg/ml, in 0.2 M HCl

Citrate buffer

114 mM sodium citrate, in milli-Q water (pH 8.6)

Phosphate-buffered saline (PBS)

9.8 mM $Na_2HPO_4 \cdot 2H_2O$, 137 mM NaCl, 2.7 mM KCl, 2 mM KH_2PO_4, in milli-Q water (pH 7.4)

Blocking solution

3% newborn calf serum (NCS), 1% bovine serum albumin (BSA), 0.05% triton X-100, in PBS

3.11.2 Mounting of brain sections

From each animal, one 20 µm coronal brain section was mounted on microscope slides (Superfrost Plus, Thermo Scientific, USA) as described earlier. The brain sections were selected to be roughly 0.245 mm rostral from bregma. Additional sections were mounted on separate slides to be included as negative and single-colour controls. Using a pap pen (Super PAP Pen, Electron Microscopy Sciences, USA), a liquid repellent circle was drawn around the mounted sections. This prevented leaking of the labelling reagents by keeping the liquid as a single droplet when immunolabelling was performed, and also allowed differentially staining on sections mounted on the same slides (e.g. controls). The sections were left at room temperature to completely dry off before they were stored at refrigerated temperature overnight or until immunolabelling.

3.11.3 Immunolabelling of capillaries

Enzymatic antigen retrieval was carried out with the protease enzyme pepsin. The pepsin solution was prepared, directly before the immunolabelling procedure to avoid impairment of the enzyme’s activity. The brain sections were immersed in pepsin solution in a water bath at

37 °C for 20 min. After antigen retrieval, the sections were washed (immersed) three times with PBS for 10 min each. Blocking was carried out for 2 hrs with blocking solution at room temperature. Approximately 200 µl blocking solution was sufficient per brain section. Next, the brain sections were incubated with 100 µl primary antibody to collagen type IV (rabbit polyclonal anti-collagen IV; diluted 1:500 in blocking solution; Abcam code ab6586), before shielded from light and left overnight. For negative control, the primary antibody was replaced by blocking solution. Negative control was included to identify spurious binding of the secondary antibody.

The day after, the brain sections were washed by immersion in PBS for 10 min, six times. The antibody staining was revealed using a secondary antibody, Alexa Fluor 488 donkey anti-rabbit IgG (H+L; diluted 1:500 in blocking solution; catalogue #A21206), approximately 100 µl per brain section and incubated for 2 hrs at room temperature while shielded from light. The incubation period was followed by a washing step with PBS three times for 10 min each, before incubation with DAPI (stock solution 1 mg/ml, diluted 1:5000 in PBS) at room temperature for 15 min. DAPI is a fluorescent dye that binds DNA and stains the nuclei blue, and was used as a counterstain. Staining was completed by washing three times with PBS for 10 min before the sections were coverslipped with an anti-fade mountant (ProLong Gold, Invitrogen, USA). Figure 3.8 briefly summarizes the main procedures. Supplementary table 7.1 and 7.2 in Appendix I provide more detailed information about the primary and secondary antibody used.

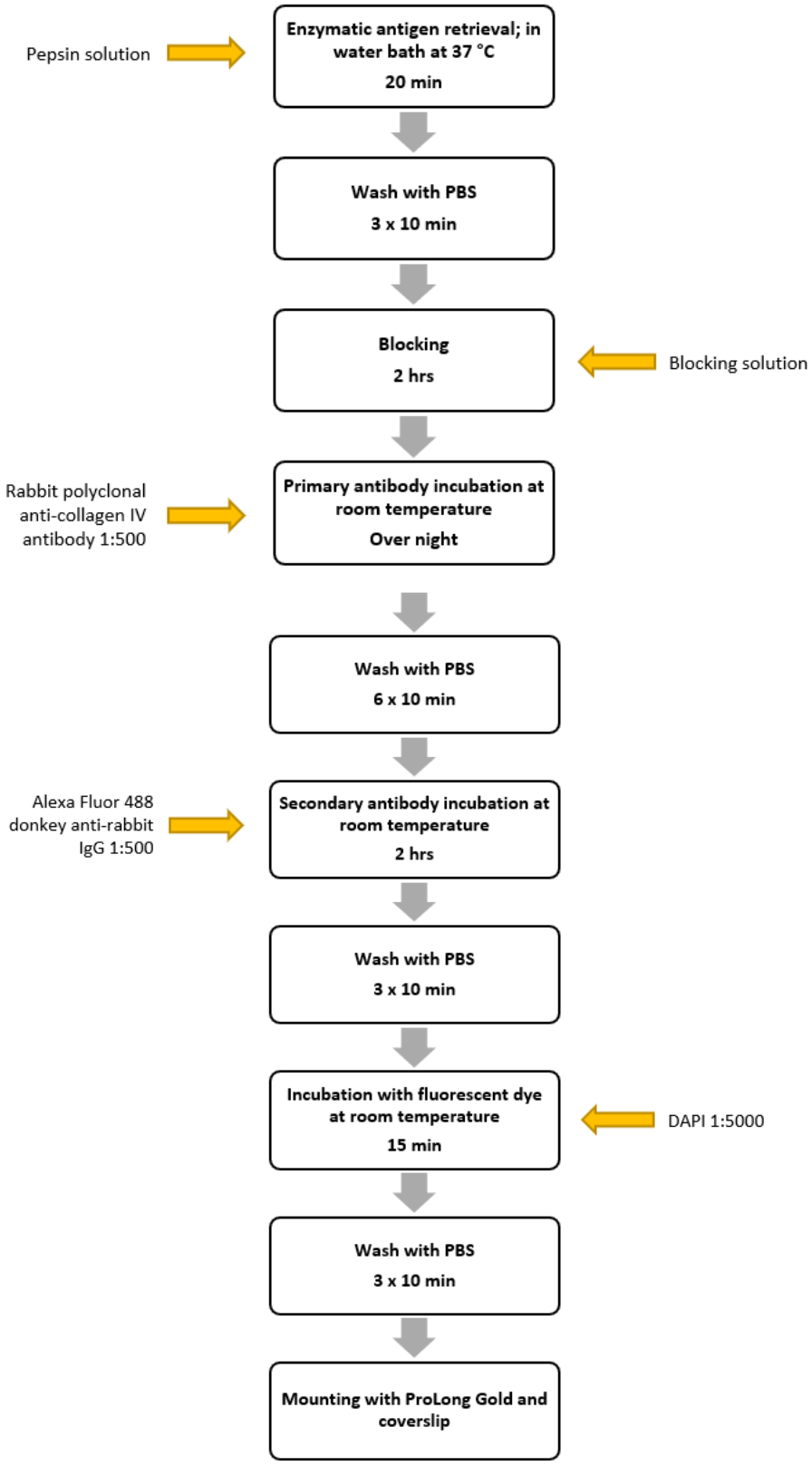

Figure 3.8. Flow chart illustrating the main procedures in fluorescence immunohistochemistry. Immunolabelling of capillaries, arrows indicate reagents used and their respective diluted ratio.

3.11.4 Immunolabelling of neuron markers

Preceding immunolabelling, heat-induced antigen retrieval was executed by immersing the brain sections in citrate buffer (pH 8.6) in a water bath at 80 °C for 30 min. Subsequently, the sections were washed three times with PBS for 10 min each. Blocking was carried out for 2 hrs with blocking solution at room temperature. Approximately 200 µl blocking solution was sufficient per brain section. The blocking reagent was then replaced with primary antibodies to doublecortin (guinea pig polyclonal anti-doublecortin IV; diluted 1:2000 in blocking solution; Abcam code ab18723), nestin (mouse monoclonal anti-nestin; diluted 1:500 in blocking solution; Abcam code ab22035) and MKI67 protein (Ki67) (rabbit polyclonal anti-Ki67; diluted 1:500 in blocking solution; Abcam code ab15580). Roughly 100 µl was applied for each brain section, and the sections were left in a moisture chamber at room temperature overnight while shielded from light. For negative control, one section was incubated with blocking solution. For single-colour controls, three sections were incubated with the following primary antibody combinations: anti-doublecortin and anti-nestin (negative one), anti-nestin and anti-Ki67 (negative two), and anti-Ki67 and anti-doublecortin (negative three). Single-colour controls are valuable in multiplex fluorescent IHC to identify cross-reactivity of the combined antibodies rather than to the target proteins, and also if the fluorophores are “bleeding through” into each other’s channels.

The day after, the brain sections were washed six times with PBS for 10 min. The antibody staining was revealed using the following relevant secondary antibodies: Alexa Fluor 594 goat anti-guinea pig IgG (H+L; diluted 1:500 in blocking solution; catalogue #A11076), Alexa Fluor 488 donkey anti-mouse IgG (H+L; diluted 1:500 in blocking solution; catalogue #A21202) and Alexa Fluor 647 goat anti-rabbit IgG (H+L; diluted 1:500 in blocking solution; catalogue #A27040), approximately 100 µl per section. Incubation with secondary antibodies was carried out for 2 hrs at room temperature while shielded from light, followed by a washing step of PBS three times for 10 min each. Next, the sections were incubated with DAPI (stock solution 1 mg/ml, diluted 1:5000 in PBS) at room temperature for 15 min, before they were washed three times with PBS for 10 min. Finally, the sections were coverslipped with an anti-fade mountant (ProLong Gold, Invitrogen, USA). Figure 3.9 briefly summarizes the main procedures. Supplementary table 7.1 and 7.2 in Appendix I provide more detailed information about the primary and secondary antibodies used.

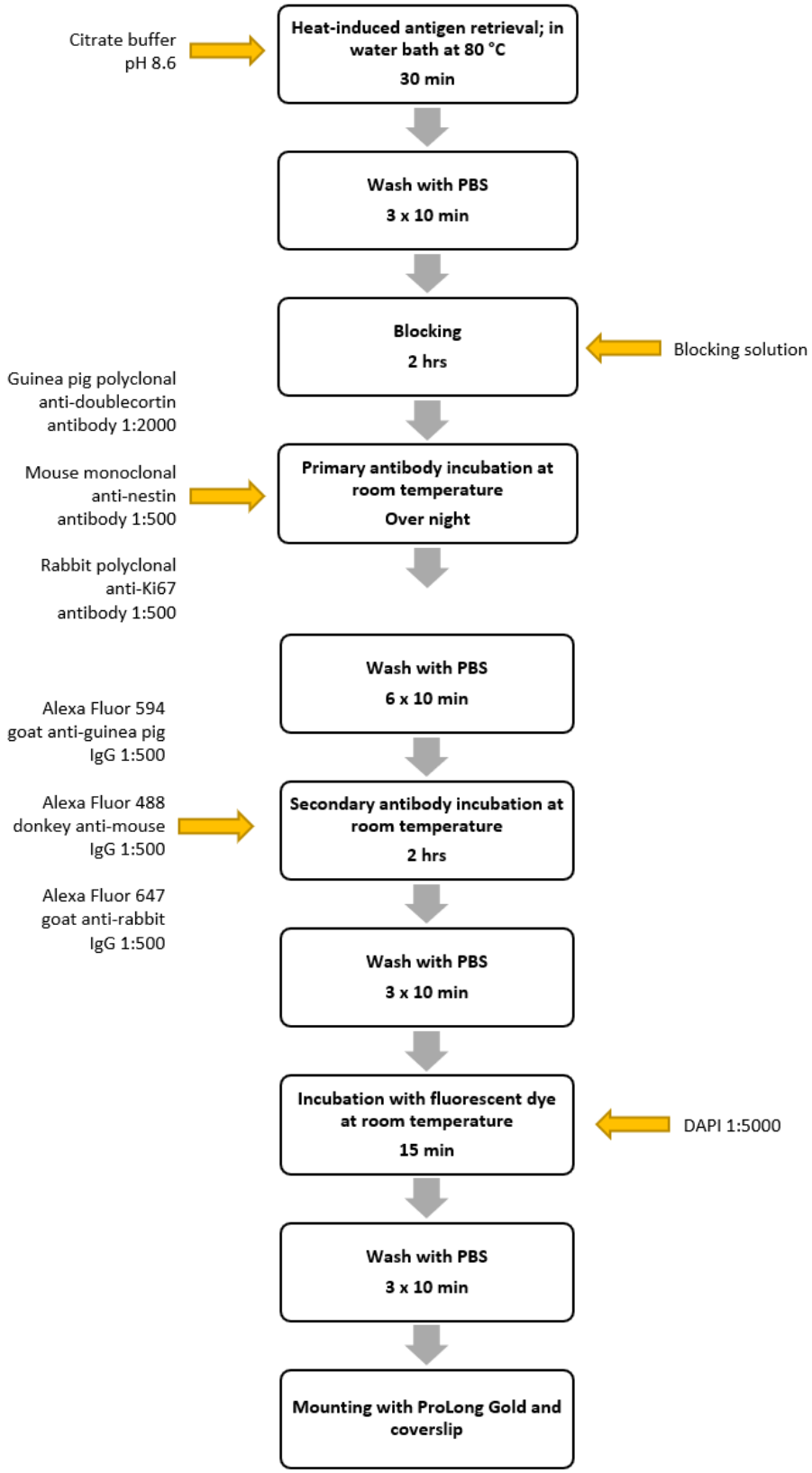

Figure 3.9. Flow chart illustrating the main procedures in fluorescence immunohistochemistry. Immunolabelling of neuron markers, arrows indicate reagents used and their respective diluted ratio.

3.11.5 Image acquisition with confocal microscopy

Images of the immunolabelled sections were not captured due to the COVID-19 outbreak, and will only be described briefly (theoretically) below.

Whole high-resolution fluorescence images of the immunolabelled coronal sections were captured using a confocal laser scanning microscope (LSM 880 with Airyscan, Carl Zeiss Microscopy, Germany) with DPSS 561-10 and Diode 405-30 lasers at Alexa 488 (collagen IV and nestin), Alexa 594 (doublecortin) and Alexa 647 (Ki67). Laser-intensity and gain were adjusted and saved as a pre-setting, and set for all sections prior to image acquisition to ensure consistent settings. The images were captured at 20x magnification with z-stacks.

3.12 Quantitative analysis

Due the COVID-19 outbreak, the quantitative analysis of angiogenesis and neurogenesis were suspended. The following analyses were not executed, but will be described (theoretically) in detail, and are currently in extensive use at the Neurobiology and Toxicology group.

3.12.1 Analysis of angiogenesis and capillary density

Images were analysed using the Fiji software (version 2.0.0-rc-69/1.52p; Java 1.8.0_172). Assessment of angiogenesis was conducted by quantifying the immunolabelled blood vessels at microscopical level using a semi-automated method, adapted with the Trainable Weka Segmentation (TWS) plug-in (Arganda-Carreras et al., 2017). TWS is a machine learning tool which allows the program to automatically annotate structures of interest by training a certain classifier and segment the remaining data automatically. Image segmentation, i.e. partitioning a digital image into multiple segments, was desirable to easily distinguish the fluorescent capillaries from the background. Automatization was performed using macros to automize repetitive procedures. All quantifications were performed by an operator who was blinded with regard to treatments and genotypes.

The Fiji macro consisted of three parts; for the full macro steps, the reader may refer to supplementary figure 7.1 in Appendix III. Before the analysis, the first macro steps were run. These steps adjust the scale in relation to the original pixel resolution of the image, as lower pixel resolutions were used to analyse the images. The macro also opens the “Channels Tool”

function, to actively switch between the channels (wavelengths) of different antibody conjugates, and duplicate the selected image frame for easy comparison and rewinding. To measure the capillaries of the ipsilesional and contralesional hemisphere, a region of interest (ROI) was chosen by overlaying a polygon on the image. ROI was defined as the area surrounding the infarct core by 500 µm distance (figure 3.9A and B). Similarly, the contralesional ROI was defined as the symmetrical position to the stroke lesion, constituting a surrounding area of 500 µm. All measurements were limited to only include the cortex. Next, the second macro steps were run to outline the selected ROI and the contrast was enhanced to better distinguish the fluorescent capillaries from the background. TWS was run, and the classifier was trained to create reliable and reproducible results. Once segmentation was done (figure 3.9C), the final steps of the macro were run to enable analysis of the selected capillaries and find their corresponding occupied surface areas. The resulting segmented image was converted to a "binary" black and white image to allow automatic particle analysis of the objects of interest (figure 3.9D). This process was performed by the "Threshold" function. The "Analyze Particles" function in the macro steps measured the area occupied by the selected capillaries (figure 3.9E).

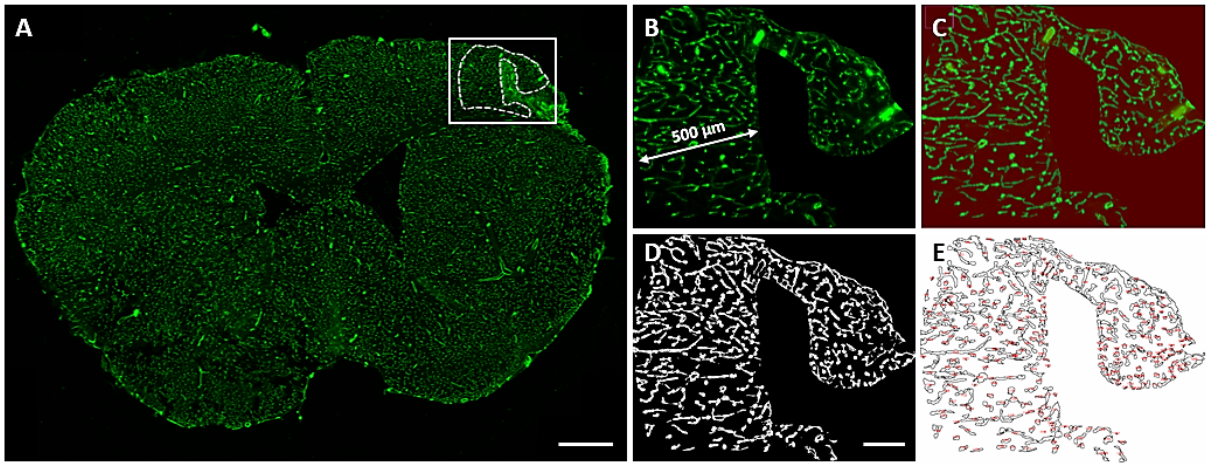

Figure 3.9. Implementation of a semi-automated method to detect and measure capillary density. (**A**) Anti-collagen IV immunolabelled coronal section at 0.345 mm rostral from bregma, and the selection of ROI at ipsilateral hemisphere. The region outlined in white is enlarged in B-E. Scale bar: 1000 µm. (**B**) Outlined and enlarged view of ROI. ROI was defined as 500 µm distance from the stroke area. (**C**) Output after segmentation in TWS. (**D**) Binary black and white image after threshold-adjustments. (**E**) Counting of the highlighted capillaries and their designated surface areas following particle analysis. Scale bar: 300 µm.

Particles to analyse were set from 30 µm-to-infinity to exclude background noises. That is, only objects occupying surface areas $\leq 30\ \mu m^2$ were identified as separate particles. The particles were visually compared to the original image-section to make sure that only capillaries were

included in the final analysis. Capillaries included in the analysis were defined as vessels maximally 10 µm in diameter (Hall et al., 2014; Morland et al., 2017). When the identified particles corresponded to vessels measuring more than 10 µm in diameter, they were interpreted as venules or arterioles and were excluded from the analysis. The area occupied by such larger vessels was subtracted from the total tissue area. By executing this algorithm for both hemispheres independently, the capillary densities of the ipsilesional and contralesional hemispheres were determined. From the obtained data, the surface areas occupied by the capillaries were summarized and the fraction of area (percentage) was calculated in relation to the total tissue area. Figure 3.10 illustrates the principles of the analysis and the macro steps.

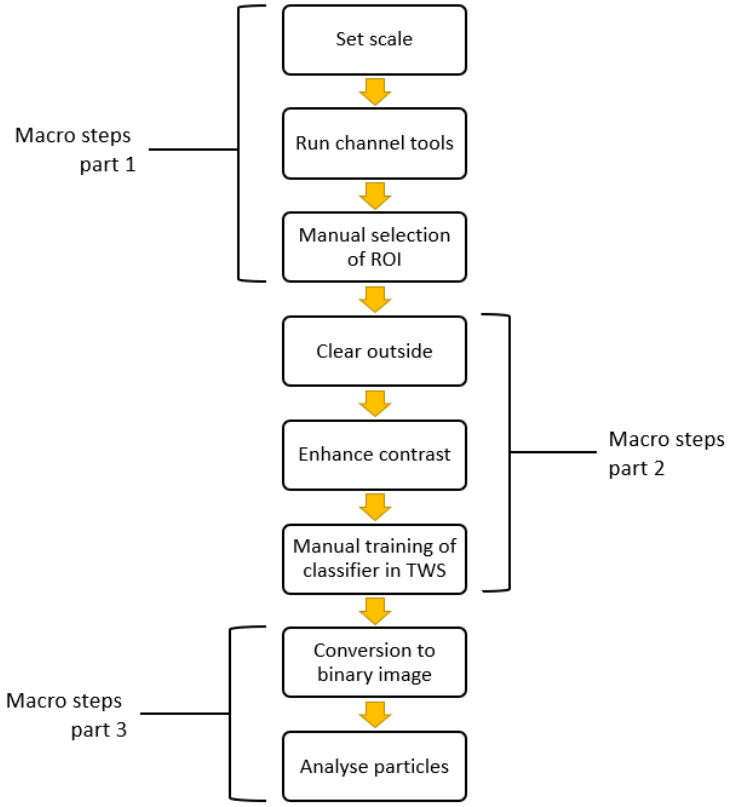

Figure 3.10. Overview of the algorithm for capillary density analysis. The flow chart illustrates the macro steps consisting of three main parts. ROI, region of interest; TWS, trainable weka segmentation.

3.12.2 Analysis of neurogenesis and neuron markers

The images were analysed using the ZEN 3.0 (blue edition) software from ZEISS. Quantification of neurogenesis was executed manually by counting the doublecortin-positive and Ki67-positive cells present in the SGZ and SVZ in the ipsilesional and contralesional hemisphere. Prior to the analysis, the fluorescence intensity from the different channels were

adjusted to minimize background staining and saved as a pre-setting to use on the images. All measurements were performed by an operator who was blinded with regard to the treatments and genotypes.

In a previous set of animals, we have detected Ki67-positive and nestin-positive cells in the neocortex in close proximity to the lesion site. Therefore, this area, as well as the corresponding contralateral site was also analysed. Nestin-positive cells are more densely packed than the Ki-67 and DCX-cells. Combined with a large number of processes which come in close contact with the nuclei of other cells, nestin-positive cells are difficult to count manually. Consequently, the density of nestin-positive cells was estimated by measuring the area occupied by nestin-positive pixels. For these analyses, thresholding and segmentation was performed largely as described for the capillary density measurements. In an experiment using the same combination of antibodies, a PhD student in the Neurobiology and Toxicology group recently demonstrated that manual counting and the pixel area to give highly corresponding results (Lambertus et al., unpublished; Overberg et al., unpublished).

For quantification in the SGZ, the positive-labelled cells of doublecortin, nestin and Ki67 were measured throughout the entire length of DG. The number of neurons labelled with Ki67 or DCX, or the area occupied by nestin-positive pixels was divided by the entire length of the granular cell layer to calculate the neuron density.

Quantification of the SVZ was performed in a similar manner at three distinct regions; ventral zone, dorsal zone and cortical zone, according to the mosaic organization described by Merkle et al. (2007) which relates to the direction of migration for the NSCs. To calculate the density of newborn neurons, the values were divided by the length of the measured zones.

In the perilesional cortex and the similar contralateral cortical area, the total number of DCX and Ki67-positive neurons were analysed, along with the total area covered by nestin-positive pixels. These data were not normalized to a length or area, as they likely represent neurons migrating to lesion site from the SVZ. Therefore, the total number of new neurons in this region was considered a better estimate for possible contribution of neurogenesis in the repair process after stroke. Finally, the neuron densities from the SGZ and SVZ and the neocortex were divided by the thickness of each section to adjust for variation in the thickness, and multiplied by 100 to represent data as cells/100 µm.

3.13 Exclusion criteria

Strict exclusions criteria were applied during the experiment and before the statistical analyses: mice with complications during the surgery (e.g. bleeding, spontaneous recanalization several times and uncertain location of the occlusion site), mice who developed stroke injures beyond the cortical regions of the hemisphere (for instance including part of the underlying striatum) and non-measurable brain sections (due to poor staining or damaged sections which would result in high degree of uncertainty) were excluded from the analyses.

3.14 Statistics

All data are presented as mean ± standard deviation (SD). The value n represents the number of animals. Statistical analyses were performed with IBM SPSS statistics 26 and GraphPad Prism 8. One-way analysis of variance (ANOVA) test was used to compare differences in treatments of the infarct volumes. *P*-values < 0.05 was considered statistically significant, and allowed for further analysis using the Tukey's post hoc test.

4 Results

4.1 Animals

4.1.1 Genotyping

Genotyping was performed to check the genotype and semi-randomize the mice in the different treatment groups. The majority of the PCR samples generated clearly, distinguishable band patterns on the gels for the HCAR1 and the LacZ gene, respectively, giving the expected genotypes (homozygous WT, homozygous KO) (figure 4.1). Heterozygous mice displayed both bands of the HCAR1 and LacZ PCR products. From the genotyping results, 69 WT mice and 75 KO mice were confirmed, giving approximately balanced distribution (1.08 : 0.92 ratio) of the genotypes for the study.

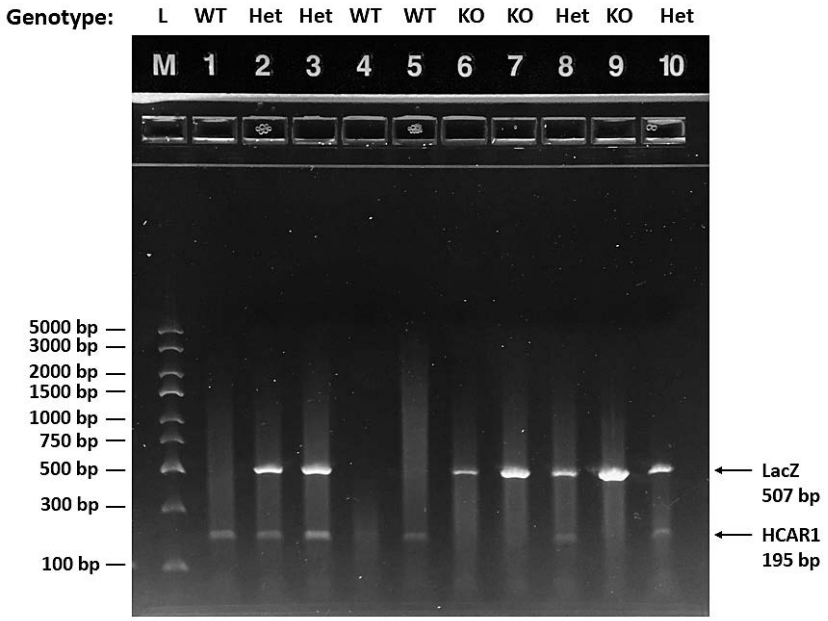

Figure 4.1. Genotyping of WT and HCAR1 KO mice. Arrows indicate the size of the PCR products visualized in the gels. PCR products generating single bands are either from WT or KO alleles, whereas heterozygote mice carry both alleles and display two bands. L, ladder; WT, wild-type; KO, knockout; Het, heterozygote.

4.1.2 Number of animals and distribution

Following the treatments, 5 animals were withdrawn from the study due to the exclusion criteria. The resulting animals (139 mice) were operated with permanent dMCAO, in which 3

female KO mice, 1 male KO mice, 4 WT female mice and 2 WT male mice died during or the day after surgery. This gives an overall mortality rate of ~ 7% from the operations, where KO mice and WT mice had a mortality rate of approximately 5.56% and 8.96%, respectively. In total, a number of 129 mice were perfused before the samples were processed and stained. Figure 4.2 provide a brief overview of the number and distribution of animals throughout the study.

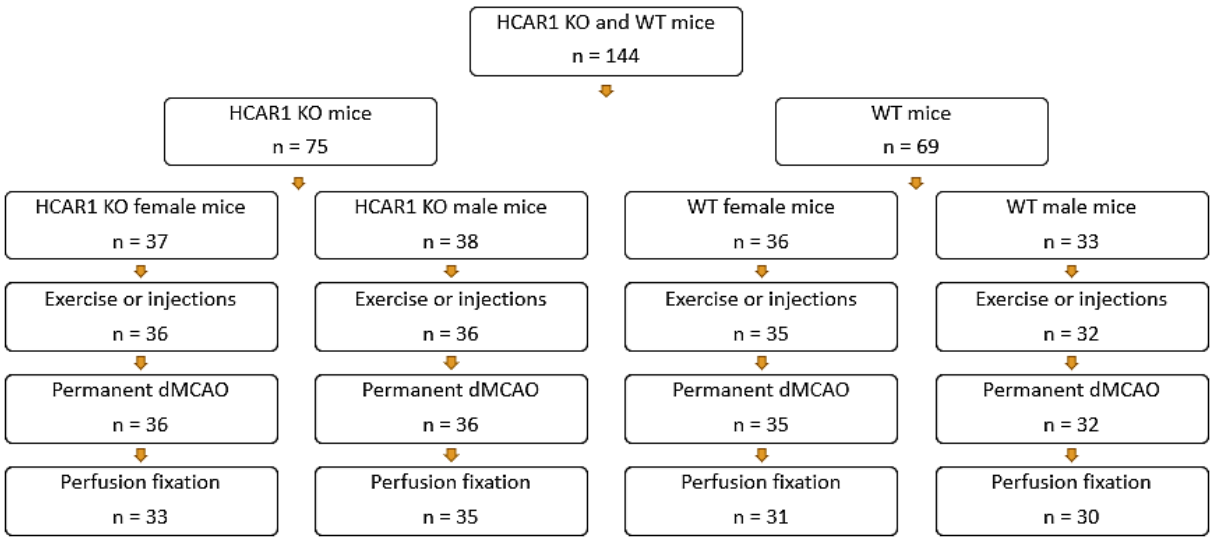

Figure 4.2. Schematic overview of number of animals throughout the study. A total of 144 mice were enrolled for the study, with about equal distribution of genotype and sex. dMCAO, distal middle cerebral artery occlusion; HCAR1, hydroxycarboxylic acid receptor 1; KO, knockout; WT, wild-type.

4.1.3 Bodyweight comparison and development

Throughout the intervention time, mice were either given injections (lactate or saline) or exercised for 7 weeks. Weighing was performed weekly, at the day of operation, and at the day of termination. As bodyweight was used in this study, not only to adjust the dose of lactate or saline, but also for health monitoring, we investigated whether the weight development differed between the sexes, the treatment groups and the genotypes.

As expected, the male mice had slightly higher values in weight than female mice, but both genders showed a steady increase in bodyweight throughout the study. Figure 4.3A shows the gradual increases in weight (gram) for both female and male mice. Figure 4.3B-E shows the mean weight of mice from the different treatment groups and genotypes throughout the experiment. Although there were small week-to-week variations in the bodyweight of individual mice, all the mice increased their weight throughout the intervention period. During

the 3 weeks after the operation, most of the animals continued to increase in bodyweight, but for some animals the bodyweight did not change, or even decreased slightly during this period. Number of animals that decreased in weight during this period was minimal (4 mice in total), and none of the animals lost more than 9.5% of their body weight. Furthermore, we found no differences in weight at the start of the experiment, or in weight development during the experiment, between treatment groups or genotypes. In fact, all mice showed signs of good coat quality, with no differences between the treatment groups and the genotypes. The lactate injected mice, however, showed minor wounds or swellings at the injection site that healed by the next injection time. Alteration of injection site also allowed for faster recovery. Overall, both lactate and saline injected mice, and exercised mice, showed signs of normal behaviour, e.g. nest building, gnawing, digging and grooming, in addition to the gradual increases in bodyweight.

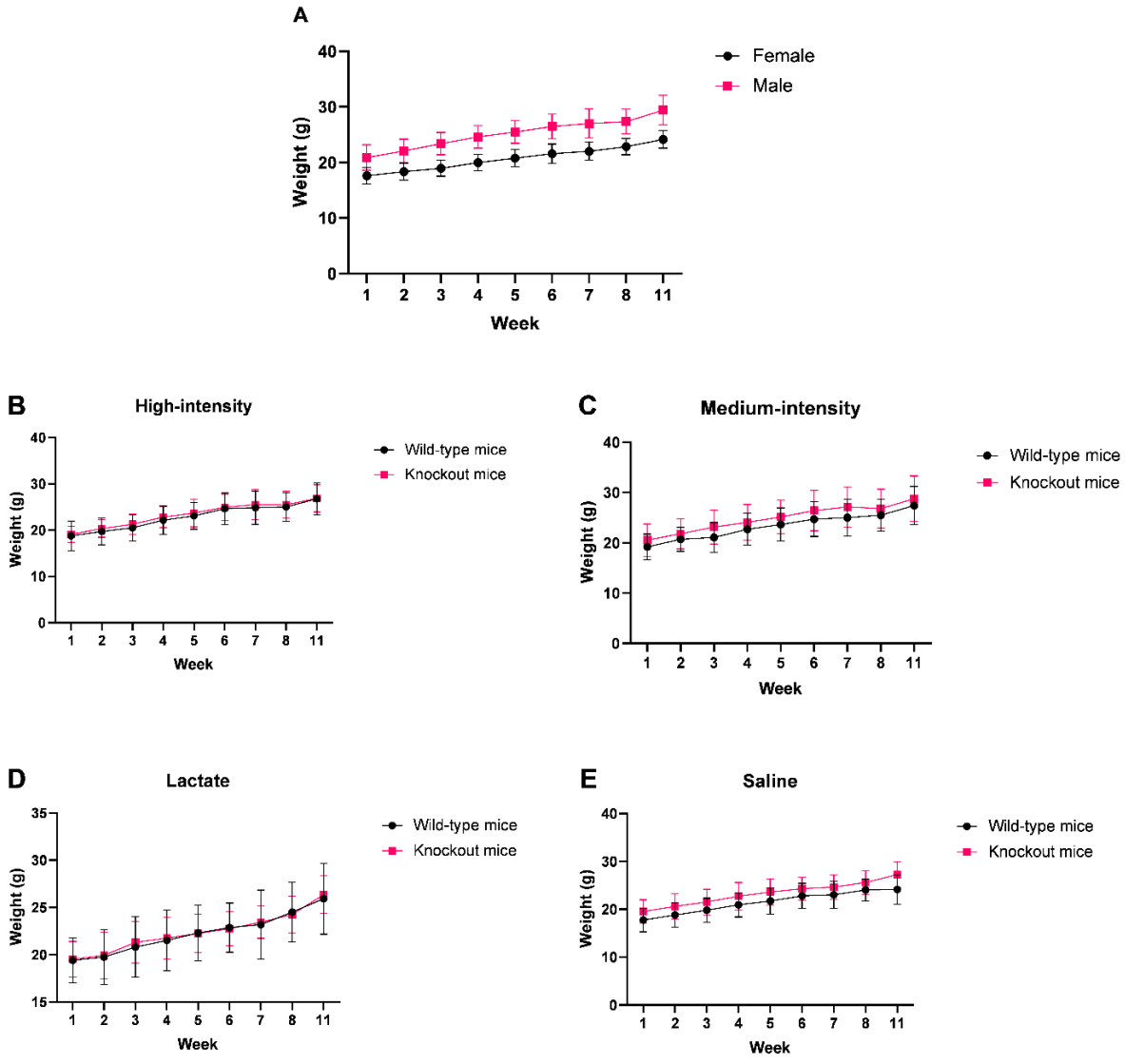

Figure 4.3. Body weight development and comparison. (**A**) Weight development of female and male mice. (**B-E**) Comparison of bodyweight between treatment groups and genotypes. The mice were weighed weekly through 8 consecutive weeks and a final time at the day of perfusion fixation (week 11). The data are represented as mean ± SD. The following number of animals by sex, treatment and genotype were included throughout the study: female mice n = 68, male mice n = 66, WT high-intensity n = 14, KO high-intensity n = 17, WT medium-intensity n = 14, KO medium-intensity n = 15, WT lactate n = 16, KO lactate n = 16, WT saline n = 16 and KO saline n = 20.

4.1.4 Physical performance in maximal exercise-capacity test

To investigate whether exercise could be neuroprotective as a result of HCAR1 activation, WT and HCAR1 KO mice were exposed to high- or medium-intensity interval exercise, 5 consecutive days a week for 7 weeks. A maximal exercise-capacity test was performed every other week. Throughout the intervention period, the genotype did not affect the physical performance since both genotypes overall performed at an equal level in the tests (figure 4.4A and B). The physical performance grouped by intensity (figure 4.4C) shows that the high-intensity group overall performed better through time than the medium-intensity group, as expected. The maximum running speed (m/min) levelled off at the end of the intervention (week 7) for all groups, with ~25% increase in speed throughout the tests. For values of mean and standard deviation from each group for all weeks, the reader may refer to supplementary table 7.4 in appendix IV.

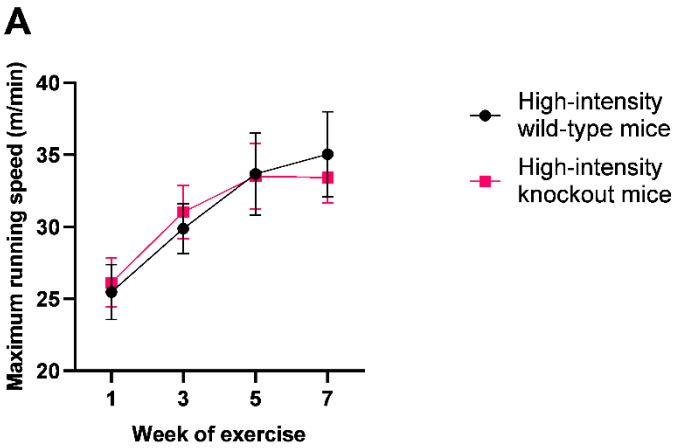

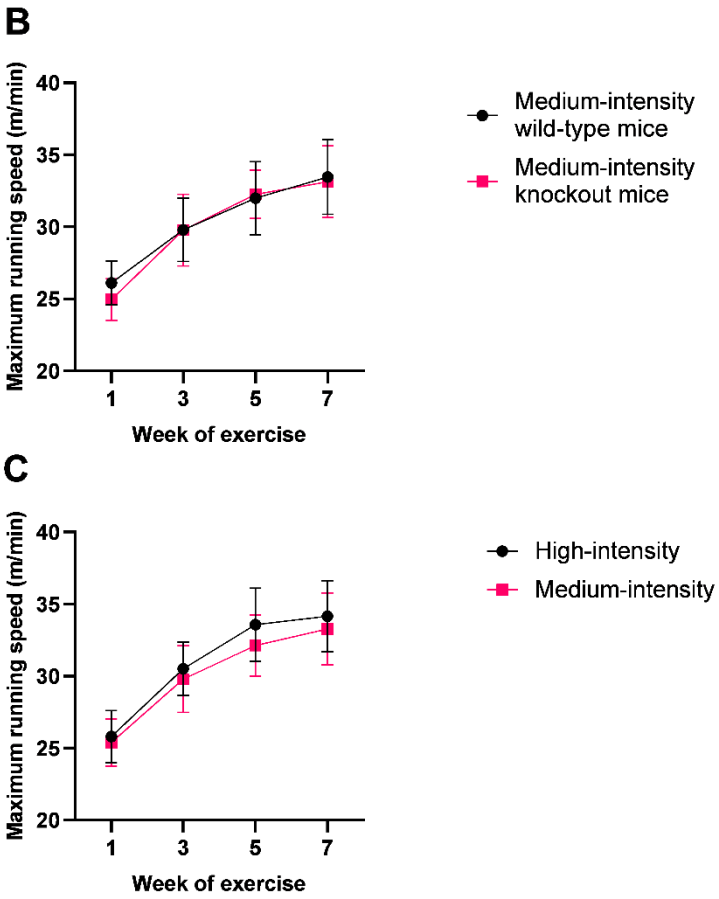

Figure 4.4. Physical performance in maximum exercise-capacity test. (**A**) Comparison of performance of wild-type and knockout mice in the high-intensity group. (**B**) Comparison of physical performance wild-type and knockout mice in the medium-intensity group. (**C**) Comparison of physical performance of high-intensity and medium-intensity groups in the maximum test. The data are represented as mean ± SD. 67 mice were included in the exercise intervention throughout the study, distributed in the following intensity-group by genotype: WT high-intensity n = 16, KO high-intensity n = 18, WT medium-intensity n = 16 and KO medium intensity n = 17.

4.2 Cerebral infarct volume

Due to the circumstances with a large number of images to be analysed within a limited time, the number of animals were reduced to half for the analysis of cerebral infarct volume. In total, 76 animals were included in the measurements, in which 9 animals were excluded due to stroke lesion registered beyond the cortical regions, unsuccessful stroke induction (infarct volume < 3 mm^3) or high degree of inaccuracy due to poor staining or uncertain extrapolation. The resulting 67 animals were distributed as follows for each treatment group and genotype: high-intensity WT mice n = 8, high-intensity KO mice n = 10, medium-intensity WT mice n = 6, medium-intensity KO mice n = 7, lactate WT mice n = 8, lactate KO mice n = 8, saline WT mice n = 12 and saline KO mice n = 8.

4.2.1 Effects of exercise and lactate injections on cerebral infarct volume

To assess whether exercise, through the HCAR1 receptor, had a neuroprotective effect and leading to a smaller infarct volume after stroke, we performed infarct volumetry on cresyl violet-stained serial coronal brain sections of WT and KO mice 3 weeks after permanent dMCAO (figure 4.5). In all the animals that were included in the analysis, we observed a difference in cortical thickness between the left (where stroke was induced) and the right hemisphere. In addition, some sections showed signs of tissue damage. Tissue damage was recognized either as areas where the nuclei were located closer together and were smaller in size, while the remaining cresyl violet labelling was light, or as darker areas with less obvious nuclei, presumably scarred tissue (glial scar). Most brain sections showed clear, distinguishable patterns of stroke, with a high degree of variation in lesion size throughout the brain between the groups and genotypes. The infarct area (defined as atrophy plus visible damaged tissue) mainly encompassed the somatosensory and motor cortex, but in some sections, the infarcts extended all the way down towards the corpus callosum. Minor affection of subcortical structures was found in some animals, and these animals were excluded.

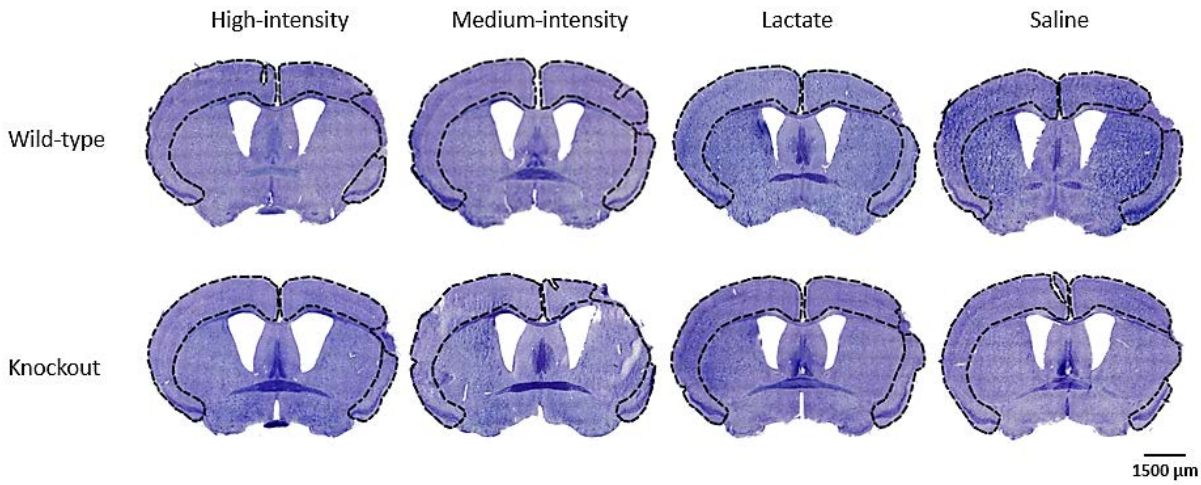

Figure 4.5. Outcome of infarcted tissue size after permanent dMCAO and volumetric infarct analysis. Representative images of cresyl violet-stained sections comparing WT and KO mice in each treatment group, acquired approximately 0.145 mm rostral from bregma. Dashed lines indicate the cortical areas measured of the ipsilateral and contralateral hemisphere. Scale bar: 1500 µm.

We did not find any significant differences between the treatment groups or genotype (P = 0.984 and df = 7, one-way ANOVA) (figure 4.6). For more detailed values of the statistical analysis, the reader may refer to supplementary table 7.5 and 7.6 in appendix IV.

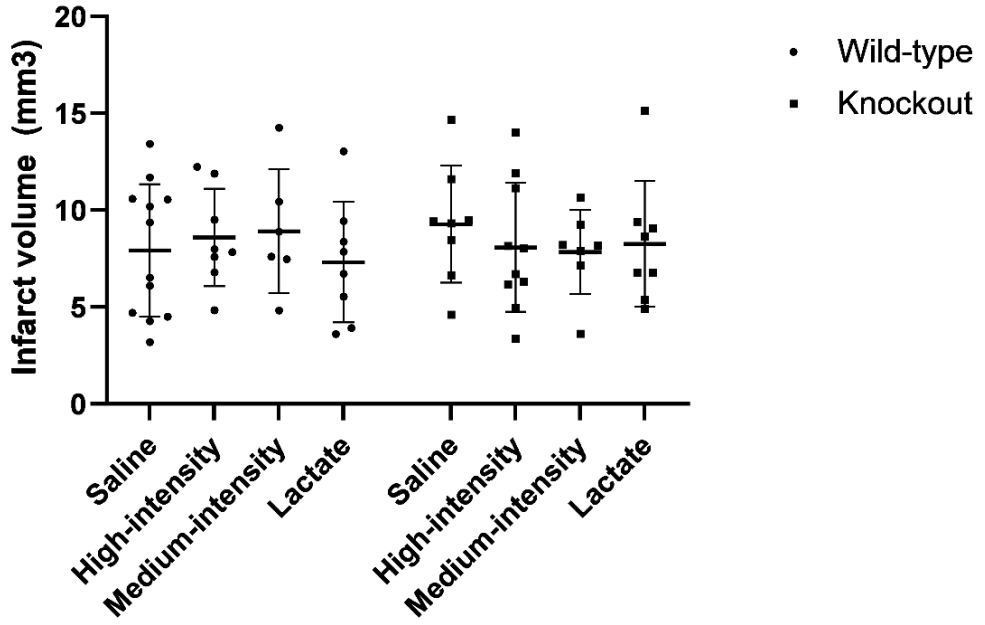

Figure 4.6. Comparison of infarct volumes between the treatment groups and genotypes. WT and HCAR1 KO mice were exposed to saline injections (control), lactate injections or treadmill exercise (high- or medium-intensity), 5 consecutive days a week for 7 weeks in total prior to stroke induction. The mice were perfusion fixed and the brains harvested 3 weeks later for infarct volumetry. Results are presented as mean ± SD for 67 mice in total: WT high-intensity 8.59 ± 2.51 mm^3 (n = 8), KO high-intensity 8.08 ± 3.33 mm^3 (n = 10), WT medium-intensity 8.91 ± 3.20 mm^3 (n = 6), KO medium-intensity 7.85 ± 2.17 mm^3 (n = 7), WT lactate 7.32 ± 3.10 mm^3 (n = 8), KO lactate 8.27 ± 3.24 mm^3 (n = 8), WT saline 7.93 ± 3.42 mm^3 (n = 12) and KO saline 9.28 ± 3.02 mm^3 (n = 8).

4.2.2 Reproducibility of volumetric infarct analysis

As a measure of reproducibility, the infarct volume of some sections (n = 72) were measured twice. The second measurements yielded a resemblance of 99% and 97% (of the first measured areas) of the contralateral and ipsilateral cortical areas, respectively. The standard deviation was 4.5% and 7.1% for the contralateral area and ipsilateral area, respectively. The values are based on second measurements divided by the first measurements. Supplementary table 7.7 (appendix IV) provide the exact ratios and percentage of the measurements.

4.2.3 Distribution of the infarct area relative to bregma coordinates

As another quality control, we investigated how the infarct areas were distributed at different distances in the caudal-rostral direction from bregma, to verify that the lesion was in the supply area of the distal MCA for all groups.

Figure 4.7 provides an overview of the infarct area in the brain, relative to the bregma coordinates measured from mice exposed to high- or medium-intensity interval exercise, lactate injections or saline injections (control mice) of both genotypes.

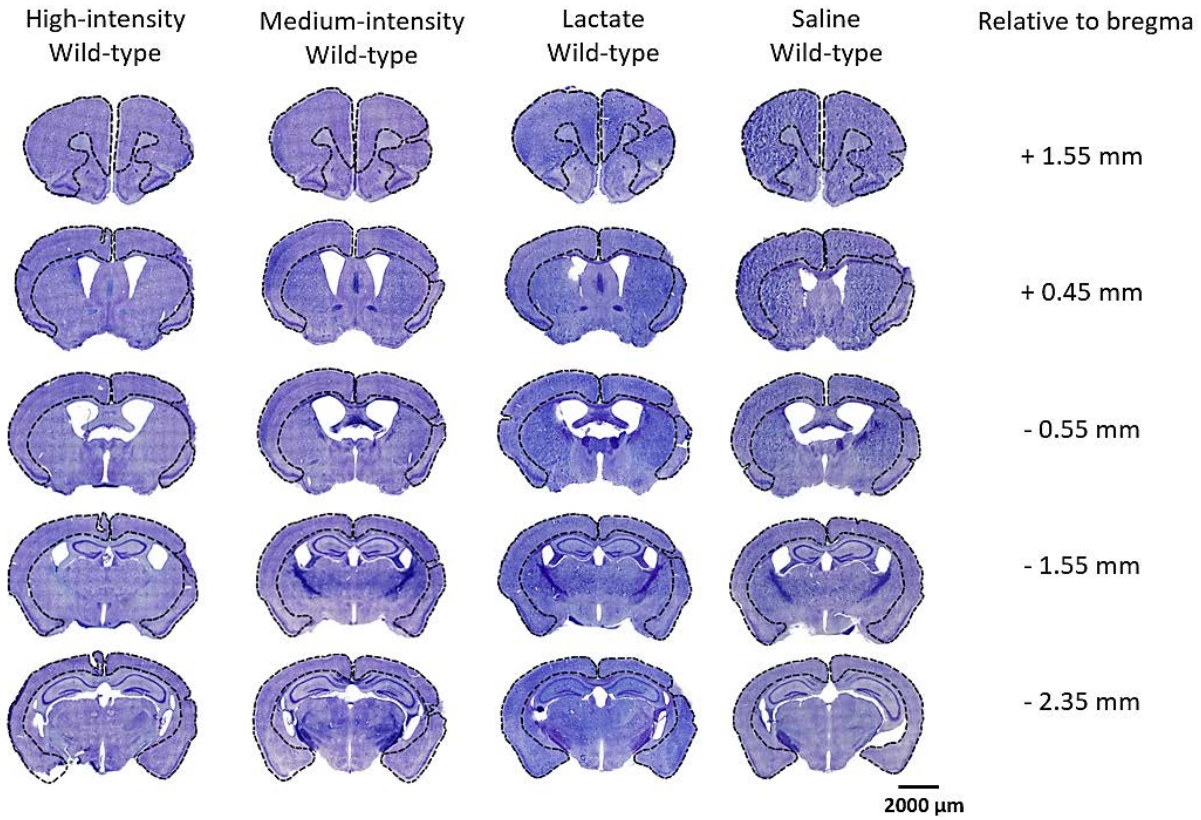

Figure 4.7. Overview of the infarct areas throughout the brain after permanent dMCAO and volumetric infarct analysis. The representative images of cresyl violet-stained coronal brain sections were acquired from individual WT mice, from the different treatment groups, extracted 3 weeks following dMCAO. Each section is represented with their approximate coordinates to bregma. Scale bar: 2000 µm.

Furthermore, we plotted the measured infarct areas form each section against the bregma coordinates from where the sections were obtained. Although there were variations from mouse to mouse, we found that most mice had the largest lesion in the rostral part of the cortex, declining at about bregma -1 (figure 4.8). This did not differ between the treatment groups or the genotypes.

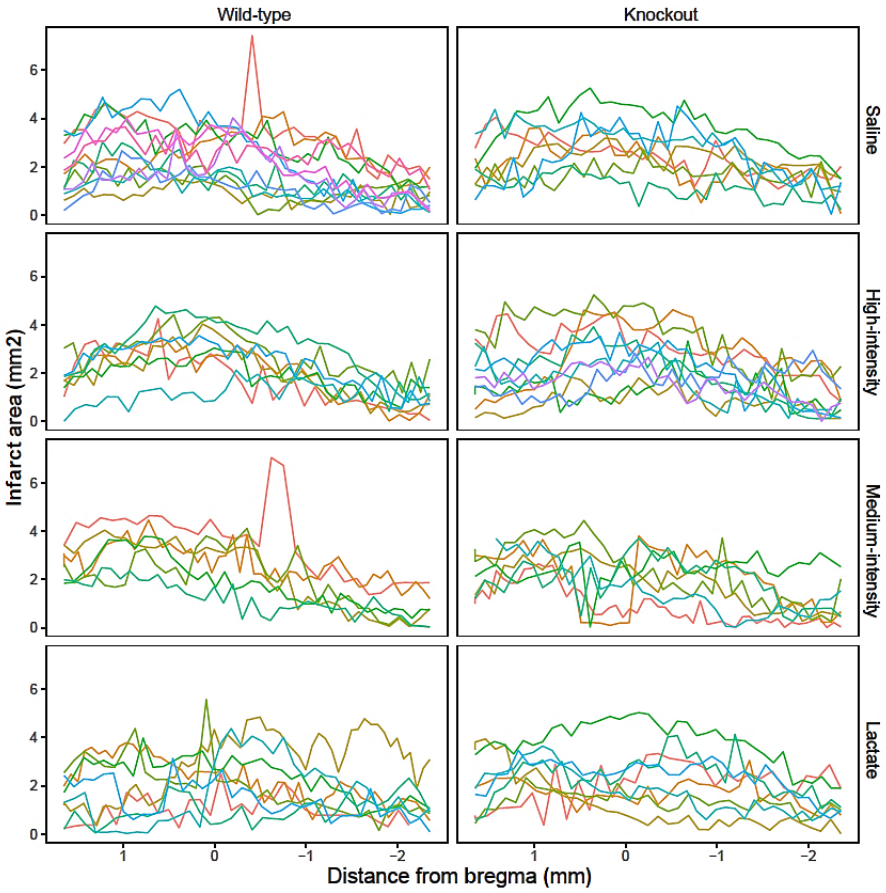

Figure 4.8. Representative overview of infarct areas. The infarct area (mm^2) relative to the bregma coordinates (1.645 mm rostral to 2.355 caudal from bregma) was measured from 67 mice treated with lactate or saline injections, or exercised at high- or medium-intensity for 7 weeks. Each line represents an individual mouse from the respective treatment group and genotype. WT saline n = 12 and KO saline n = 8, WT high-intensity n = 8, KO high-intensity n = 10, WT medium-intensity n = 6, KO medium-intensity n = 7, WT lactate n = 8 and KO lactate n = 8.

4.3 Angiogenesis and neurogenesis

The aim of this study was to investigate the mechanism of exercise-induced angiogenesis and neurogenesis through the HCAR1 receptor. However, data were not generated from the analysis of angiogenesis and neurogenesis as a result of the COVID-19 outbreak. In the following discussion section, we will therefore discuss interpretations of generated data, expected results and arguments for these.

For the quantitative analysis of angiogenesis, test images verified that the collagen IV labelling was successful and clearly outlined the brain vasculature, suggesting that valid results could have been obtained from these sections (figure 4.9).

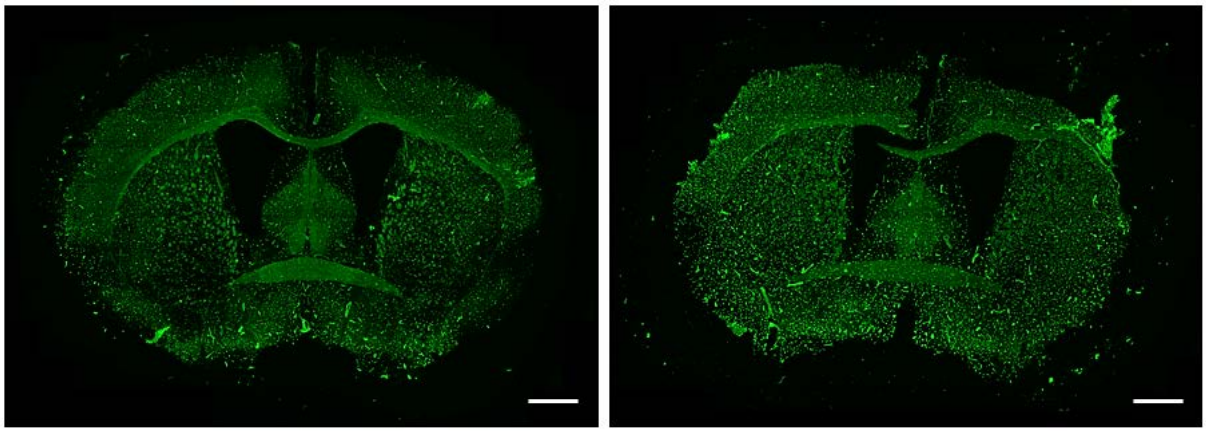

Figure 4.9. Test images of the collagen IV-labelled brain sections for the quantification of capillary density at the stroke area. Acquired approximately 0.245 mm rostral from bregma. Scale bar: 1000 µm.

5 Discussion

5.1 Methodological considerations

5.1.1 Animals

Human stroke can be studied using both *in vitro* or *in vivo* models. *In vitro* models serve as an ethically, non-problematic tool to examine various aspects of stroke, e.g. the effects of hypoxia, hypoglycaemia and excitotoxicity using specific cell types or computer simulation. However, the purpose of the present study was to examine the effects of physical exercise prior to stroke. As presented earlier, human stroke is a highly complex and heterogeneous disorder with diverse manifestations where the magnitude of lesion depends on multiple factors which affect the molecular processes. Both exercise and stroke elicit complex physiological and pathophysiological processes which involve various organs and signal molecules, making it difficult to investigate in detail without the use of animals. Consequently, the most optimal method would involve direct access to brain tissues with the presence of intact blood vessels to investigate the effects of lactate on angiogenesis and the degree of infarct after stroke induction. The use of animal models to investigate the stroke-like events and its sequelae, is therefore inevitable in some cases. Animal models allow researchers to experiment ischaemic stroke under well-controllable and standardized conditions to yield precise analyses and highly reproducible results (Fluri et al., 2015). Although paramount in the research field, the use of animals involves ethical considerations and restrains. Animal research may only be conducted under strict conditions, following "the three Rs" principle (replacement, reduction and refinement) to preserve the highest possible animal welfare standards.

Just like in the majority of stroke experiments, small animals (rodents) are used in this study as they present clear advantages; lower costs of acquisition and keeping, simpler monitoring and tissue processing, and acceptability from an ethical perspective (compared to larger animals). Although the rat's cerebrovascular anatomy and physiology generally resembles humans more than mice (Yamori et al., 1976), larger numbers of mice are more acceptable compared to rats and were necessary to achieve statistically valid results in this study. As mice are appropriate animals for genetic modifications, the mouse model also offer the major advantage of easily creating transgenic and KO models to assess molecular pathophysiology of stroke (Gob et al.,

2015; Kraft et al., 2013; Sommer, 2017). Here we used C57BL/6N HCAR1 KO and WT mice to study the HCAR1-mediated mechanisms in relation to ischaemic stroke. The C57BL/6N inbred strain conserves the LacZ gene in each individual mouse, and thus are considered genetically identical. In addition, this transgene is stable across time and breed frequently. C57BL/6N mice are excellent for exercise and behavioural studies as they are physically active and capable of learning a variety of tasks (Bryant, 2011), which was desirable for this study.

It is, however, important to note that despite the excellent reproducibility of animal models, fully replication of human stroke pathophysiology may not be possible. Extrapolation of results to humans can be unreliable, and the gap between ischaemic stroke in animals and humans extends as we see the many neuroprotective therapies in preclinical stroke studies that have failed to make major progress in clinical transition (Casals et al., 2011). The primary disadvantages of rodents as animal models are the substantial differences in brain size and structure from the human brain, and translation to humans may therefore be challenging without scaling laws to account for these differences (Phipps, 2016). In our study, the animals were treated according to a strict protocol before and after induction of stroke, as is custom for laboratory experiments. The aim was to minimize any variable except the variables being studied. This kept variability at a minimum, and thereby allowed for a limited number of animals to be used to get a robust result (according to reduction of the three R's principle). Nevertheless, these tightly controlled variables may not reflect the complex factors contributing to stroke in the human population as whole. In addition, a homogenous population was enrolled for this study which consisted of young, healthy and genetically similar mice in the same age group. This differs from the typical stroke patient which usually is among the elderly population with risk factors, health complications and comorbidities such as hypertension, dyslipidaemia, obesity and diabetes mellitus (Casals et al., 2011). The combination of risk factors, comorbidities and medications represent individual variation that likely affects the outcome of stoke in humans.

The extent and evolution of the penumbra vary depending on species and stroke model used, time since occlusion, severity of ischaemia and concomitant comorbidities (Touzani et al., 2001). Different mouse strains may exhibit profound differences in infarct volume after MCAO, due to strain differences in arterial collaterals (Yang et al., 1997). And although a handful of evidences show that the potentially salvageable ischaemic penumbra exists in animals and humans after focal ischaemia, the exact time window and location translated

clinically to humans are still unknown. These factors, among many others, must not be overlooked when conducting animal research. Nevertheless, many aspects of stroke have been identified primarily from animal models; the concept of the penumbra and detection of post-stroke neurogenesis are prominent examples of pioneering stroke research (Dirnagl & Endres, 2014), and animal models will continue to expand our understanding of stroke pathophysiology and the study of future therapeutic agents.

5.1.2 Lactate administration

Mice randomized for lactate injections received 2 g/kg sodium L-lactate, equal to 18 mmol/kg. The method was refined based on previous experiments; injections were given intraperitoneally (i.p.) instead of subcutaneously to avoid skin lesions. I.p. administration is a common route, and several benefits follow i.p. injections, including quite long periods of absorption from the repository site and larger volumes can be administered. In regards to rate of absorption, the i.p. route comes second after the intravenous route, with an absorption rate of 25–50% as rapid as the intravenous route (Hirota & Shimizu, 2012). The time-course of the effect of the substance was an important factor in determining the dosage, and is influenced by the rate of absorption. Previous experiments found 2 g/kg i.p. lactate injections to rapidly increase the plasma lactate level, with a peak approximately 15 minutes after injection and remained elevated for at least 1 hour before returning to the baseline levels by 3 hours (E et al., 2013). Similarly, subcutaneous doses of 2.5 g/kg lactate showed peak concentrations after 5 to 15 minutes of the injections, and plasma lactate levels remained elevated at ~5 mM for several hours before returning to baseline levels (Morland et al., 2017). The dose was based on previous experiments to obtain plasma lactate levels similar to during high-intensity exercise (Desai & Bernstein, 2002; Morland et al., 2017; Rolim et al., 2015). EC_{50} values of lactate acting on HCAR1 have been reported from several studies with variable measurements ranging from 1-5 mM (Bozzo et al., 2013; Cai et al., 2008; C. Liu et al., 2009), thus the dose given in the present study was sufficient to increase the baseline levels above EC_{50} values to activate HCAR1 for several hours.

I.p. injections of lactate may undergo hepatic metabolism when passing the liver through the portal vein before reaching systemic circulation. Consequently, lactate can be converted to pyruvate and act a substrate for gluconeogenesis (Brooks, 1986). In light of this, a study showed induced hypophagia in rats receiving i.p. lactate injections, but not s.c. injections (Racotta & Russek, 1977). A newly published study, however, found no significant changes in blood

glucose between i.p. and s.c. lactate injections in mice (Haugen et al., 2020), so the topic remains to be elucidated. The gradual increases in weight observed in both lactate and saline injected mice (figure 4.3D and E) for this study indicate normal behaviour of the mice and excludes the possibility of hypophagia, particularly in mice that received lactate injections. A comparison of mean weight throughout the whole intervention showed gradual increases in weight of all treatment groups and genotypes, and also by gender (figure 4.3). Thus, both lactate injected mice and exercised mice showed signs of overall good health. The variation in weight between each weight-session (week) was due to time of the day the animals were weighed and metabolism. For instance, some animals were weighed at the beginning of a weight-session while others the end of the day, and thus food-intake and secretion varied depending on the time of the day. Nevertheless, the animals in the present study showed no signs of abnormal behaviour and were overall healthy.

Lactate treatments might lead to secondary or factor-dependent effects that should be taken into consideration. Lactate injections have been associated with acute anxiety attacks in some individuals (Pitts & McClure, 1967), so the confounding effect on rodents should be disproved before concluding any effects of lactate acting on HCAR1. This has been previously tested by Morland and co-workers (2017) who observed no differences between the groups. Differences in lactate levels between genotypes and age is another topic of matter, and have been studied (Haugen et al., 2020). No statistically significant differences were found between genotypes and age, but sex differences were reported in which awake male mice showed higher lactate levels than female mice. The sex dependent effect also applied during anaesthetized conditions. These dynamics and possible sex-dependent differences should be kept in mind when conducting animal experiments with lactate.

5.1.3 Exercise regime

Intensity-controlled treadmill running has been demonstrated to be among the exercise regimes that induce the largest and most consistent effects (Wisloff et al., 2001), and exercise intensity appears to be a key factor influencing aerobic priming effects. One precondition with exercise studies that include animals is that they are well-controlled to yield reproducible effects with low variation between the groups. Direct measurements of VO_{2max} to measure aerobic capacity is one method to ensure accurate intensity of endurance exercise and is regarded as the best denotation for aerobic exercises (Åstrand & Rodahl, 1970). Unfortunately, controlling exercise

intensity by measuring VO_{2max} is expensive and time consuming, especially in long-lasting studies including many animals as in this case. A simpler method to indirectly estimate the animal's intensity is therefore S_{max}. This has shown to highly correlate with VO_{2max} (Hoydal et al., 2007). The speed at which VO_{2max} reached a plateau, increased in parallel with the changes in VO_{2max} during the exercise period. S_{max} may therefore be used as a tool to control and adjust the intensity of physical exercise with animals, and was used in the present study.

In this study, the high-intensity group was subjected to an exercise regime that ensured the exercise intensity exceeded the lactate threshold (the onset of blood lactate accumulation) by running at ~80% of S_{max} (equal to ~80% of VO_{2max}) during the intervals. This was considered sufficient to obtain peak lactate levels of ~10 mM (Desai & Bernstein, 2002; Morland et al., 2017), and thus activate the HCAR1 receptor. The high-intensity exercise regime was based on previous experiences and have been validated extensively (Kemi et al., 2002). It is a robust and well-controlled protocol for exercise of both mice sexes, and designed to give optimum enhancement in cardio vascular function. To determine the optimal preventive exercise regime, the high-intensity group was compared with a medium-intensity group running at ~60% of S_{max}. Both intensity-groups showed gradual increases in physical performance throughout the intervention time (figure 4.4C), and as expected there was a tendency that the high-intensity group achieved higher max-test results than medium-intensity. The S_{max} approached a steady-state at the final week of exercise with ~25% increase in speed throughout the tests.

Forced treadmill running was essential to control the total exercise amount and intensity during the sessions were equal for each mouse within each intensity-group. Although forced running is associated to certain negative aspects, it has also shown to effectively induce neuroprotection and reduce the infarct volume in stroke compared to voluntary exercise (Hayes et al., 2008). In addition, it was key that mice in the high-intensity group was running at 80% of maximal running speed to ensure the lactate threshold was exceeded, which is not the case in voluntary running. It is, however, worth to mention and keep in mind the negative aspects of forced running, for instance the intervention interferes with the animal's normal nocturnal-diurnal rhythmicity and can induce stress as it may require negative stimulus such as electric shock or touching the animals to control running (Goh & Ladiges, 2015). These stress responses may result in detrimental effects on the brain, like increases of the stress hormone corticosterone and pro-inflammatory responses (Svensson et al., 2016). Consequently, stress responses may potentially mask the beneficial effects of physical exercise, for instance it is known that

neurogenesis increases as a response of exercise but can be hampered by stress. The exercise regime performed in this study has previously been in use, and shown increased angiogenesis, and hippocampal and subventricular neurogenesis in spite of forced running at high-intensity for 7 weeks (Lambertus et al., unpublished; Morland et al., 2017; Overberg et al., unpublished). This may indicate minimal stress-induction by the given exercise regime. Furthermore, the mice in this study showed signs of voluntary running prior to the warm-up and during the rest phases between the intervals, although some individual mice (mainly within the high-intensity group) refused to run near the end of the intervention-period or after the gradual increases in running speed after the maximal exercise-capacity tests. These were followed-up closely and evaluated as eligible if they still could sustain the 10 consecutive intervals. Nevertheless, the direct interference from the researcher in forced running and the consequences of that should be kept in mind as this might have an impact on the results.

Bias between the genotypes was evaluated by comparing the performance during the maximal exercise-capacity tests (figure 4.4A and B) which showed approximately equal S_{max}. Both KO and WT mice levelled off in S_{max} within 7 weeks of treadmill running, in which WT mice scored slightly higher in seventh week. This confirms previous observations by Morland and co-workers. S_{max} was thus not affected by the genotypes.

5.1.4 Animal models of ischaemic stroke

The selection of stroke model is a crucial aspect of the experimental design and must be well thought through as this can affect the analysis and results. Here we used permanent dMCAO as stroke model based on multiple factors.

As mentioned earlier, the distal MCAO model, unlike the proximal MCAO, produce more restricted damage to the hemisphere which mimics the majority of the human stroke lesions located in the cortical regions supplied by the MCA (Carmichael, 2005; Howells et al., 2010). Avoidance of thalamic, hypothalamic, hippocampal and midbrain damage prevents hyperthermic responses, which may lead to variations in the infarct core (F. Li et al., 1999; Reglodi et al., 2000; Yamashita et al., 1997). Permanent occlusion mimics patients without recanalization/reperfusion which takes consideration to the transport of therapeutics into an ischaemic tissue which is hindered by the occlusion. Thus, these therapeutics rely on good collateral circulation to get to the penumbra, increasing their clinical relevance as opposed to therapeutics tested on transient MCAO which may fail to show positive results in patients

without recanalization/reperfusion. In addition, based on numbers from United States, by choosing permanent MCAO, the majority of the clinical stroke patients (88.7–97.5%) will be represented compared to transient MCAO models which only mimics 2.5–11.3% of the patients (McBride & Zhang, 2017).

Permanent dMCAO by coagulation of the MCA is a relatively quick surgery to perform with an operation time of ~10 minutes (Llovera et al., 2014). The coagulation model in general, is an established, robust and reproducible model and one of the common animal models in experimental stroke research (Howells et al., 2010). A low mortality rate of 5% can be achieved with permanent dMCAO, which is favourable in our study in order to gain low variability and statistically valid results. In fact, for the present study a mortality rate of ~7 % was obtained, which was only slightly higher than estimated by the authors. Traditional MCAO (intraluminal suture model), on the other hand, has a mortality rate of 60% (Longa et al., 1989) which was unfavourable in our experiment which had a long pre-treatment of exercise and injections of the animals prior to stroke induction, but is more suitable for stroke experiments involving post-stroke treatments. It is however important to note that the permanent dMCAO model also has limitations that need to be taken into account. Firstly, craniectomy is needed in order to get access to and coagulate the artery, which can affect intracranial pressure and BBB function. It also presents a risk of post-operational infections in the brain. However, sham operations were executed in a previous experiment to show that the craniectomy, and other factors apart from the actual coagulation, did not induce stroke lesion. No major differences in cortical volume of ipsilateral and contralateral hemisphere were reported based on these findings (Forbord, 2019; Sajedi, 2019). Secondly, injury of the underlying cortex or rupture of a vessel may occur due to drilling or/and electrocoagulation. But by taking precautions (e.g. careful drilling and constant humidification of the tissue), this could however be minimized. From the present study, few cases of subarachnoid haemorrhage during the operations were observed, and were noted to evaluate as possible outliers (e.g. continuous bleeding for more than 5 seconds). Thirdly, identifying the MCA can be challenging due to individual variations of the artery and spontaneous recanalization may occur which might lead to variability in stroke lesion. Thus, even though the model allows visual confirmation of MCAO, successful stroke induction will not be revealed until the final analysis. To ensure complete coagulation of the MCA and successful stroke induction for this study, multiple occlusion sites were used (proximal and distal to the site of bifurcation) and visualised for 30 seconds before the wound was sutured. If recanalization was observed, coagulation was repeated once. Mice who showed several cases

of recanalization were regarded as outliers and excluded. Finally, it is worth to mention that the choice of anaesthesia might have an impact of the infarct volume, as it is known that some anaesthetics might have neuroprotective effects. In this permanent dMCAO protocol, isoflurane was used as anaesthesia gas which have shown to delay or ameliorate ischaemic injury (for review, see Kitano et al., 2007). Given the brief and equal anaesthesia times with this model on the different treatment groups and genotypes, we don't expect this to affect the result of this study.

5.1.5 Fixation

To efficiently preserve the brain while avoiding hypoxic conditions and artefacts, transcardial perfusion fixation was chosen as the fixation method. The common method of immersion fixation was considered unsuited because processing of the brain involves large volumes of neuronal tissue, which makes the technique inappropriate due to poor/slow penetration of the fixative (Srinivasan et al., 2002). Thus, the interruption of blood supply to the brain during tissue harvest would introduce hypoxic damages which was undesirable in our case because ischaemic damage was among the factors investigated. For this study, it was important to obtain whole coronal sections for the later analysis of infarct volume which compared the ipsilateral and contralateral hemisphere. The uniform and rapid fixation of the whole specimens were key to prevent unnecessary variation during fixation to ensure equal processing of all specimens.

There are several reasons why transcardial perfusion fixation is accepted as the gold standard for tissue fixation. The main advantage of perfusion fixation is the uniform distribution of the fixative to preserve the tissue's cytoarchitecture while avoiding hypoxic changes, as mentioned above was a necessary factor. In addition, the method is a low-cost and well-controlled procedure that can be highly adapted by changing buffer and fixative according to the requirements of the experiment (Gage et al., 2012). However, this method has several disadvantages; in addition to be labour- and time-intensive, it requires high volumes of fixative (Eichenbaum et al., 2005).

Several critical parameters need to be taken into consideration during transcardial perfusion to avoid disruptive fixation (e.g. ischaemic damage), and these are dependent on factors such as the species used, the organ to be fixed and further tissue processing. One such critical parameter is the physiological pressure which must mimic the species pressure (Gage et al., 2012). Too high and abrupt increases in flow rate cause swelling of the extravascular space and dilation of

the ventricles, leading to brain swelling and oedema, whereas a low flow rate poses a risk for the fixative to not reach all regions in time to preserve the tissue's ultrastructure (Eichenbaum et al., 2005). In the present study, the infusion rate of the fixative was set to match the estimate cardiac output in mice to avoid these issues. Opening the right auricle allowed for the blood and fixative to escape from circulation to prevent over-pressurizing the cardio-vascular system.

Transcardial perfusion is commonly performed with either glutaraldehyde or paraformaldehyde (PFA) as perfusion fixatives, but other alternatives are possible based on the chemical properties of the molecules of interest and the morphology required. These aldehydes act by cross-linking proteins, and hence are called cross-linking fixatives. The fixative used in this protocol was PFA, which is a polymer of formaldehyde. Some of the advantages of formaldehyde include high penetration rate, well-preserved cell morphology and effective fixation for routine laboratory staining due to better preserved antigenicity. The chemical is also cheap, stable and easy to prepare. Although excellent for the present study, no ideal fixative exists for preservation of tissue components, and limitations follow the chosen fixative; artefacts in highly vascular tissues and suboptimal occupational safety are some of them (Dey, 2018a).

The alternative cross-linking fixative glutaraldehyde has two aldehyde groups separated by three methylene bridges which results in extensive and rapid irreversible cross-linking of proteins, and therefore provides better fixation of the ultrastructure and morphology. This makes glutaraldehyde excellent as fixative for electron microscopy. Glutaraldehyde, however, penetrates tissues more slowly than formaldehyde due to larger molecule weight and causes unspecific binding to proteinaceous reagents, notably antibodies, which results in poor antigenicity. These are major drawbacks to its use since removal or blocking prior to immunohistochemistry are required (Dey, 2018a; Kiernan, 2000). The fixative is also less stable and more costly than formaldehyde, and causes autofluorescence which disturbs later analyses.

In the present study, we needed to combine morphological investigations of the stroke area with fluorescence microscopy. Based on the arguments presented above, formaldehyde was chosen as the most practical and suitable fixative to be used in the study.

5.1.6 Cryostat sectioning

To measure the stroke size, we needed to produce brain sections for further processing. One important basic factor in the sectioning process, is the plasticity of the tissue block which affects

the quality and consistency of the sections. When the tissue is frozen, the water content turns the tissue block into a brittle component which might cause variations in sectioning (Tokuyasu, 1973). This variability in plasticity can be controlled with optimum temperature during cryoprotection and sectioning.

Before the brains were sectioned, cryoprotection was conducted by saturating the brains in 30% sucrose solution. By infiltrating the tissue with a cryoprotectant solution before freezing, the water content in the tissue decreased, which left the brain less brittle and ensured consistent sectioning (Tokuyasu, 1973). The addition of sucrose also minimized freezing damage by preventing the formation of large crystals (known as freezing artefacts) during freezing (Rosene et al., 1986). Proper combination of sucrose concentration and freezing temperature was essential for smooth sectioning. Too low temperature causes brittle sections, whereas too high temperature causes folding of brain sections. 30% sucrose concentration combined with -20 °C freezing temperature was found to be satisfactory for this purpose, based on previous experiences for fine sectioning.

Brains were sectioned using a sliding microtome connected to cryostat. The sliding microtome allowed brain sections to be cut manually and stored in separate wells for later mounting of selected sections. Its simple design and easy maintenance allowed any operator to use the instrument. The sliding microtome is, however, restricted to cut mainly large and thick section. For this study's purpose, 20 µm sections were considered appropriate for further histological staining and immunolabelling, and the sliding microtome was therefore appropriate for use.

Critical aspects of the sliding microtome sectioning included distorted placement of the brain on the ice block stage due to skewed manual cutting of the cerebellum, which resulted in oblique sections. In addition, the manual storage in consecutive wells had to be in a spatial order which required accuracy of the operator. These technical and procedural deviations following brain sectioning were noted and corrected when the infarct volume measurements were performed.

5.1.7 Histological staining

In order to examine the cortical area and distinguish apoptotic/necrotic cells from living cells, histological staining was performed to provide contrast to the visually uniform brain sections. The CV staining technique introduced and described in the method section was based on previous experiences and found to be satisfactory for our purpose.

CV is among the stains routinely used to quantify cerebral infarct volume and area, as stained cells can be clearly defined and easily measured when appropriate staining is achieved. The CV stain offers the advantage of cost-efficiency, ease and is suitable with a variety of fixatives and processing conditions, including frozen sections of formaldehyde-fixed tissues (Gittins & Harrison, 2004; M. M. Powers & Clark, 1955). The staining technique used in this study was relatively short in time and multiple sections could be stained simultaneously.

However, the robustness of the method was not optimal, as the sections showed various degrees of stain intensity and folding during the staining procedure. To cope with these challenges, comprehensive troubleshooting was necessary, and lead to an additional dehydration step with 70% ethanol after staining and washing and replacement of distilled water with PBS in all steps. These adjustments, however, lead to uneven staining, and adaptations in combination with a compromise of staining intensity and folding were eventually necessary during the staining to yield quantifiable stained sections. For instance, re-staining was conducted up to maximally 15 min, differentiation shortened to less than 3 seconds and, in some cases, the dehydration step with 70% ethanol was excluded. In general, such individual adjustments to each section or batch would not have been acceptable when direct comparisons of staining intensity were used to define the stroke area and measure the infarct volume. The method used in this study measured the infarct volume indirectly where the analyses were based on anatomical hallmarks (cortical areas of each hemisphere). Optimal staining for each section was therefore a prerequisite to enhance the quality and accuracy to these measurements.

Alternative staining of neurons includes hematoxylin-eosin (HE), triphenyltetrazolium chloride (TTC) and neuron-specific nuclear protein (NeuN). In HE staining, hematoxylin stains all nuclei and leaves a bluish shade, while eosin is used as counterstain of the cytoplasm and leaves a pinkish shade. Together these shades provide good contrast to the sections (Dey, 2018b). TTC is a reagent for oxidative enzymes. The salt accepts a proton from succinate dehydrogenase, thereby reducing it to an insoluble form which leaves a red precipitate (Altman, 1974; Bederson et al., 1986; Bednar et al., 1994; Belayev et al., 1999; Cole et al., 1990). Areas with inactive enzymes, for instance the infarct core, will not be stained red and hence appears pale. These stains, however, were not suitable in the present study. Previous experiments conducted showed inconsistent HE staining of the brain sections (Forbord, 2019; Sajedi, 2019). TTC, on the other hand, easily reveal detectable lesion areas, but is only for suitable for vital and unfixed brain tissues with active enzymes. Since we were relying on immunohistochemical analyses as well

(which require fixed tissue), a staining procedure that could be combined with formaldehyde fixation was chosen. Comparative studies have shown significant correlations for quantification of cerebral stroke with HE and TTC staining (Dettmers et al., 1994; Hatfield et al., 1991; Isayama et al., 1991; Liszczak et al., 1984; McGee-Russell et al., 1970), and TTC and CV staining (Tureyen et al., 2004). This indicate that these staining techniques are considered equitable and suitable for measurements of stroke areas, regardless of their differences.

NeuN is a more specific marker for neurons. It is an antibody which recognizes a neuron-specific antigen (Mullen et al., 1992). NeuN staining offers the advantage of selectivity and clear staining of neuronal perikarya (soma) and nuclei (Blaya et al., 2014; Lu et al., 2002). This allows more accurate staining and quantification of neurons. In contrast to NeuN staining, CV staining is not specific for neurons and may lead to misclassification of small neurons as glia, or *vice versa* (Gittins & Harrison, 2004). In this study, accurate quantification of neurons was not critically important to measure the infarct volume. In addition, NeuN staining would be more expensive and time-consuming due to incubation with primary antibodies. CV was therefore the most suitable option for histological staining to achieve stained sections that could be analysed.

5.1.8 Measurement of cerebral infarct volume

A particularly important factor in the study of stroke is the quantification of infarction size, in which it is key to have a reliable methodology to generate data and results. In order to quantify the infarct area and volume in this study, a low-cost manual image analysis was combined with the Swanson method (Swanson et al., 1990). The quantification of the infarct volume was conducted by analysing multiple, closely spaced sections per brain, which has shown to be a feasible approach to estimate the total infarct volume of the brain (Osborne et al., 1987). This approach can, however, be tedious since infarct regions are manually outlined on a digitized image for each section, but offers the advantage of excellent reliability and reproducibility. In fact, our analysis showed a reproducibility of 99% and 97% of the contralesional and ipsilesional hemisphere, respectively, confirming the reliability of the analysis. Lowest percentage and extreme values were mainly a result of bad stained and damaged sections (e.g. folding or extrapolation).

The inference of oedema on the infarct size have shown to introduce errors in the volume quantification, as swelling of the brain can induce enlargement of the infarcted tissue (Brint et

al., 1988). To correct for the oedema, the infarct area was measured by the Swanson method. This was especially important in our study which evaluated the neuroprotective role of lactate on the infarction size, where overestimation by possible brain swelling needed to be adjusted. This algorithm utilised the difference between the areas of the non-infarcted ipsilesional hemisphere and the contralesional hemisphere to correct for brain oedema, and is based on the assumption that swelling only occurs in the infarcted tissue. Thus, the non-ischaemic tissue stays true to size, and the infarct area can be calculated indirectly. This assumption, however, makes the method vulnerable to artefacts when changes in the ipsilesional hemisphere occurs due to swelling outside the infarcted tissue (McBride et al., 2015).

Three different approaches may originally be applied to calculate and compare the infarct volume between the groups and genotypes. The infarct volume can be either calculated based on the actual distance between each section, or based on the average distance of the total number of sections measured between 1.645 mm rostral and 2.355 mm caudal of bregma (4 mm in total). The third approach compares the measurements as the percentage size of stroke.

According to the Swanson method, the total infarct volume of the brain (TI_i) to an animal (i) is calculated with the distance (d) between each section (x) out of n sections measured. That is, d = 120 µm for every 6th section of 20 µm measured, in the following equation:

$$TI_i = \sum_{x=1}^{n}((A_C - A_I) * d)_x$$

Theoretically, given that the distance was 120 µm and the measured region of the brain constituted 4 mm, one would expect approximately 33 sections per brain. This was not the case, although all sections were sectioned at 20 µm, anatomical differences in brain size and small variations within the bregma coordinates resulted in brain sections ranging from 31 to 39. Moreover, this approach did not correct for any sections lost during mounting or staining, or when neighbouring sections were mounted which caused deviations in the distance between the sections. A more accurate approach was therefore to calculate the average distance based on number of sections (n) analysed and the length of the measured region (4 mm). This gives an estimated distance calculated by $d = \frac{4000\ \mu m}{n}$, and adjusts for the irregularities due to deviations in the distance. However, since the mean calculated distance only takes the number of analysed sections in account, there is a higher chance of deviations if there is an increase of sections excluded. Fewer number of sections per brain results in higher values of mean distance. Thus,

brains with many excluded sections would give an overestimation of the total infarct area. The ideal approach would therefore be to provide the exact distance between the sections whenever a section was missing or skipped in the analysis, but was not feasible in this study.

The infarct size can also be evaluated by measuring the size of stroke as percentage. That is, the percentage area of ipsilateral cortex (A_I) is calculated from the area of contralateral cortex (A_C) for each section (x), before the average percentage is given per animal (i) based on total number of sections (n). The equation below summarises these calculations:

$$\mathrm{TI}_i = \frac{\sum_{x=1}^{n} \left(\frac{A_I}{A_C} * 100\%\right)_x}{n}$$

This approach, when examined separately for each section of the brain, gives an indication of the localisation with the greatest stroke lesion. When divided by *n* sections, an indication of the average stroke size is provided. However, an absolute value in stroke size is not provided as opposed to the other methods, making it less accurate for comparison. Additionally, the use of average percentage only includes the analysed sections, thus it does not provide a full estimate of the total infarct size between 1.645 mm rostral and 2.355 mm caudal of bregma. Based on these aspects, the second approach was found appropriate to calculate the total infarct volume since it adjusted for the irregularities in number of brain sections in relation to the distance, and overall is a more accurate approach by taking consideration to these factors. Although overestimation can pose a challenge with this method, Swanson and colleagues showed spaced intervals ranging from 200-740 µm had little effect on the obtained values for the infarct volumes. Our interval consisted of sections ranging from 31 to 39, as mentioned previously, which correspond to a spaced distance of maximally 160 µm. Furthermore, a distance over 740 µm was not exceeded when sections were excluded from the analysis. Thus, the distance was considered narrow enough to not affect the values for the infarct volumes.

5.1.9 Immunohistochemistry

Colorimetric and fluorescent immunohistochemistry

Colorimetric IHC is typically used for qualitative experiments, as the colorimetric staining works by an enzymatic reaction which continues until the reagents are exhausted or loss of physical space to deposit the product. Fluorescent IHC, on the other hand, is preferable for

quantitative experiments and multiple immunohistochemical staining (Corthell, 2014b). With multiple fluorescent immunostaining, several fluorescent channels can be viewed separately and merged into a pseudo-coloured image. This offers an advantage over colorimetric IHC, as signal co-localization between a certain fluorescent counterstain and of the detection system can easily be identified and adds credibility to the specificity of the primary antibody. In addition, separate views allow observation of weak stains without interference from other signals (Renshaw, 2013). Together, these aspects of fluorescent IHC staining were favourable in our study since several protein markers were to be immunolabelled and analysed. These markers were used to identify anatomical structures, for instance the vascular basement membrane of capillaries and proteins expressed by newborn neurons, which did not require identical fluorescence intensity for each section. Hence, the quantification was sufficient as long as the intensity was acceptable in order to recognize and identify these structures. However, fluorescence comes with major pitfalls: the fluorescence dies out within time and must be kept in refrigerated temperature and shielded from light, and autofluorescence of tissue components or fixatives can make interpretation of fluorescence results difficult. The analyses needed therefore to be performed briefly after the immunolabelling.

Antigen retrieval

Antigen retrieval can either be heat-mediated (known as heat-induced antigen retrieval) or enzymatic-mediated (known as enzymatic antigen retrieval). Heat-induced antigen retrieval uses heat in combination with alkaline buffer to cleave the methylene bridges to expose and penetrate to the antigenic sites, whereas enzymatic antigen retrieval uses protease enzymes to digest the tissue and allow better penetration of the antibodies. The optimal antigen retrieval technique is dependent on multiple variables, including the antigen, the tissue, the fixation method and/or the primary antibodies used (Renshaw, 2013). It is important to keep in mind that no universal antigen retrieval solution is available, and hence, the best solution for each individual labelling procedure must often be found experimentally. Heat-induced antigen retrieval is often the preferred technique to achieve satisfactory results in IHC (for review, see Shi et al., 2001). Although many publications have reported satisfactory results with heat-induced antigen retrieval, not all antigen structures modified by formalin are compatible and/or can be restored using this conventional technique. For some proteins, the high temperature may induce destruction of antigens, leading to false-negative results of IHC staining (Renshaw,

2013). In such cases, a combination of lower temperatures and enzymatic digestion may provide better results.

For the assessment of post-stroke neurogenesis, the heat-induced antigen retrieval was considered suitable to achieve satisfactory immunostaining. However, previous experiments showed poor staining of capillaries with primary antibody to collagen IV with this technique, and enzymatic antigen retrieval with pepsin was experimented and found to be more suited. As enzymatic antigen retrieval can damage the morphology of the tissue, the concentration and treatment time needed to be optimized. In addition, we needed to test whether pepsin would disturb the immunolabelling with the neurogenesis markers. Confirmed incompatibility of these antigen retrievals ultimately lead to separate immunolabelling of capillaries and neurons to achieve satisfactory IHC staining.

Mainly two methods are available for antigen retrieval; directly apply the solutions on the tissue slides using a pipette (the pipette method) or immerse a rack of tissue slides into a container of the solution (the immersion method). Each method was tested out before the actual experiment, and the latter provided several advantages over the former. The most worth-mentioning advantage is the prevention of over-retrieval of antigens (varying treatment time), as only slight differences (2-3 minutes) can have significant effects on the intensity of the subsequent immunohistochemical staining, cause disassociation of the tissue sections and/or destruction of the antigens (Corthell, 2014b). The method also allowed treatment of large batches of slides, and was therefore also more efficient and less time-consuming which was desirable in our situation. The immersion method, however, uses more reagent compared to the pipette method.

Antibodies

Antibodies (known as immunoglobulins, Ig) are the cornerstones for IHC and are proteins produced and secreted by plasma cells in response to antigenic stimulation. The “Y”-shaped basic structure consists of four polypeptides; two heavy chains and two light chains. The two tips of the “Y” (Fab region) constitute the antigen binding sites and account for the antigen specificity. The base of the two “Y”-arms (Fc region) allows antibody binding to cells or complements. Antigenic stimulation occurs when antibodies bind the epitope (the antigenic determinant site) of biological components that are capable of evoking an immunogenic response (antigens) (Dey, 2018c; Yuan & Arikkath, 2014). In this study, various antibodies were used as markers to investigate angiogenesis and neurogenesis in exercise and stroke.

Vascular basement laminae immunolabelling with primary antibodies specifically against collagen type IV was used as a marker to measure the capillary density in the brain. Collagen IV is a major structural constituent of the basement membrane which forms a complex network that underlies the endothelial cells (Boudko et al., 2018). Endothelial cells have the capability to express, synthetize and deposit collagen IV, and this have shown to be a central event in blood vessel formation, vascular survival and maturation *in vivo* (Bonanno et al., 2000; Mundel & Kalluri, 2007; Nicosia et al., 1991). The use of antibody against collagen IV for immunolabelling of capillaries was first used by Madsen and Holmskov (1995) who showed reliable results in skeletal muscles, and was further confirmed by Qu et al. (1997). More recent studies have successfully used anti-collagen IV immunolabelling of capillary basement membranes of the human and rodent brain (Challa et al., 2002; Morland et al., 2017; R. L. Zhang et al., 2014), which yielded clear and continuous vascular patterns, and reliable results. For the present study, the anti-collagen IV staining was therefore considered to be an adequate approach for capillary density measurements that are within the range of previously published data.

Adult neurogenesis can be studied with different approaches, one of them being the use of several stage-specific molecular markers expressed. Doublecortin (DCX), nestin and Ki67 were used as markers for the different stages of neurogenesis. DCX is a microtubule-associated protein expressed in intermediate NPs, neuroblasts and immature neurons, and have shown to be retained in neurogenic areas such as in the SGZ of the hippocampal DG (Couillard-Despres et al., 2005; Francis et al., 1999; Rao & Shetty, 2004). The protein also regulates and directs neuronal migration of the SVZ cells by regulating the organization and stability of the microtubules (Gleeson et al., 1999; Ocbina et al., 2006). Moreover, DCX expression is thought to be specific for newly born neurons as the protein is not re-expressed during gliogenesis or regenerative axonal growth (Couillard-Despres et al., 2005; Rao & Shetty, 2004). Thus, DCX was represented as a good marker for neurogenesis at the SGZ and SVZ of the brain for this study. Nestin is an intermediate filament specifically expressed transiently in RGLs and early intermediate NPs, and vanishes when the cells convert into differentiation (Lendahl et al., 1990). Nestin positive NSCs have been frequently used as a marker involved in adult neurogenesis (Gilyarov, 2008). Howbeit, nestin should be used with caution, as re-expression in gial cells have been observed as a result of cerebral ischaemia (Duggal et al., 1997), traumatic brain injury (Sahin Kaya et al., 1999) and neurotoxicity (Yoo et al., 2005), which limits its specificity. Ki67 is a nuclear protein expressed in all dividing cells in all phases of the cell cycle

(G1, S, G2, M), except the resting phase (G0) and early phases of G1 (D. C. Brown & Gatter, 2002; Scholzen & Gerdes, 2000). Studies have reported Ki67 expression at different levels during mitosis in all mammalian species, including rodents and humans (Endl & Gerdes, 2000; Scholzen & Gerdes, 2000). Furthermore, the protein has shown to be an effective and reliable marker in the initial phase of adult neurogenesis (Kee et al., 2002). Based on the (co-) expression of these three markers, a distinction can be made between the subtypes of progenitor cells and the different stages of neurogenesis (e.g. mitotic and post-mitotic neurons). The above-mentioned markers are frequently used for multiple staining in IHC and subsequent confocal microscopy for the identification and quantification of newborn cells, and therefore are considered evaluated and suited for use in this study. Nevertheless, some of the antigens are susceptible to formalin fixation-induced epitope masking, for instance nestin and Ki67 (Ansorg et al., 2015), but by combining immunolabelling with antigen retrieval this was prevented for the present study.

Specificity of polyclonal and monoclonal antibodies

Antibodies can either be polyclonal or monoclonal. Polyclonal antibodies are generated from different clones of B cells and directed against a variety of epitopes of the single antigen (i.e. multiple epitopes against the same protein), whereas monoclonal antibodies are generated from a single B cell and are specific to a single epitope. Hence, the monoclonal antibodies take the advantage of high specificity towards their targets and reduced cross-reactivity (Dey, 2018c; Yuan & Arikkath, 2014). The antibody's specificity is the ability to detect specific epitopes of the antigen. The high specificity of monoclonal antibodies for single epitopes makes them less robust to detect the antigen of interest since physical and chemical instabilities can induce small changes which result in complete absence of the specific epitope. In contrast, polyclonal antibodies can detect multiple epitopes which make them more resistant to physical and chemical instabilities. Polyclonal antibodies, are on the other hand, more vulnerable to batch-to-batch variations, cross-reactivity and non-specific binding to epitopes present in more than one antigen. In the present study, mainly polyclonal antibodies were used to detect the targets of interest. These antibodies have been extensively tested in our laboratory as well as in studies from other research groups. Furthermore, blocking step and single-colour controls were performed to rule out the possible challenges with polyclonal antibodies.

Antibody validation

The use of antibodies requires validation of their specificity and reproducibility, as this have a wide impact on the interpretation of the experiment. By including proper controls, an indication of the specificity of the antibody is provided. The gold standard is to test on tissues or cell lines known to not express the protein of interest, e.g. KO models or RNA interferences (Yuan & Arikkath, 2014). These methods provide the best negative controls to identify spurious binding of the antibodies, but are expensive, especially when multiple antibodies are to be included in the experiment as in our case. An alternative approach is the utilisation of blocking peptides to eliminate the signals, so-called absorption tests. Blocking peptides are sequenced similar to the antibody, and incubated along with it in excess amount. If the antibody is specific, loss of signal (staining) is expected with the blocking peptide. Although this method is useful to pinpoint an antibody's specificity, testing of selectivity is not accounted for since off-target binding of the antibody will be completely inhibited (Bordeaux et al., 2010). In addition, the absolute amount of antigen that constitutes an "excess" amount can be difficult to find, since antibodies can bind tightly to the tissue antigen or loosely to the soluble antigen (Saper & Sawchenko, 2003). Western blotting can also be performed to confirm that the antibody recognizes only one antigen in the tissue. In western blotting, proteins are extracted from cells or tissues and separated by size using gel electrophoresis, before the target protein is transferred to a membrane and identified via conjugation with specific primary and secondary (enzymatic or fluorescent labelled) antibodies (J. Liu et al., 2014). An indication of the antibody's specificity to the target is provided when a single band is observed at the known molecular weight of the target. Presence of multiple bands or bands at other molecular weights indicate unspecific binding of the same target in different states of post-translational modifications, breakdown products or splice variants of the protein. This method is a less stringent, but reasonable test, to carry out and considered appropriate as a first validation step if KO models are not available for testing (Bordeaux et al., 2010; Saper & Sawchenko, 2003). The test, however, is unsuited for formalin-fixed tissues as fully denatured proteins are needed for antibodies to recognize antigens and bind. Here, antibody validation was not performed since the applied antibodies have extensively been evaluated in the literature and shown to be reliable, as mentioned earlier. For that reason, the specificity of the antibodies was considered established and reliable. Since the purpose of IHC was to identify cells or structures of the tissue, rather than the proteins itself, the labelled morphology could be verified and compared to the published literature.

5.2 Interpretation and discussion of findings

5.2.1 Infarct volume

Effect of exercise preconditioning on stroke outcome

The aim of the present study was to explore the neuroprotective effects of exercise against stroke in relation to lactate and HCAR1-mediated signalling. We did not observe any significant effect of exercise or lactate injections on the infarct volume 3 weeks after stroke induction (figure 4.6).

It is well-known that exercise provide beneficial effects by reducing risk factors of stroke in humans (Lee et al., 2003; J. Li & Siegrist, 2012; Willey et al., 2011). Previous studies conducted on animal models have also demonstrated exercise to be neuroprotective in stroke, including the attenuation of brain damage (He et al., 2014; J. Li et al., 2004; Liebelt et al., 2010; Naderi et al., 2018; R. Y. Wang et al., 2001). One of the mechanism is thought to be through the increase of neurotrophic factors, for instance VEGF-A, which increases as a result of exercise to induce angiogenesis and neurogenesis (Morland et al., 2017; Overberg et al., unpublished). Minimum amount of exercise preconditioning to induce brain ischaemic tolerance have shown to range from 2-3 weeks (for review, see F. Zhang et al.,2011). The duration of preconditioning in this study was 7 weeks, which should be sufficient to induce neuroprotection in ischaemic stroke. However, our findings indicate no link between exercise and stroke outcome, and that exercise do not provide neuroprotection prior to stroke. Though only half of the animals were included in the statistical analysis, the result was nevertheless robust given the high P-value ($P = 0.984$) and the number of animals were sufficient to yield statistically valid results (n = 7-12 in each group). A number of factors may affect the results and explain these contradictory findings.

One important aspect is that part of the neuroprotective effects of exercise are also mediated through the amelioration of risk factors related to stroke (Lee et al., 2003; J. Li & Siegrist, 2012; Willey et al., 2011), which would not come forth with the use of young and healthy animals (6 weeks of age at the start of our experiment). For instance, the protective effects of exercise may partly be mediated through reduced blood pressure (Whelton et al., 2002) and insulin resistance (Dylewicz et al., 1999), improved endothelial function (Endres et al., 2003) and lipid

metabolism (Schenk & Horowitz, 2007), and reduced excess body weight (Goodpaster et al., 2010), which altogether improves the stroke outcome. This kind of variation and risk factors among stroke patients were not reflected in our animals, but we did observe variations in weight development and physical performance (figure 4.3 and 4.4). Our mouse population (albeit genetically similar and only among healthy individuals) therefore to some degree represented the natural diversity in physical condition and health which also would be the case in humans.

Another aspect of the experimental design that is worth to mention is the use of forced treadmill running for the entire intervention period, which could have an impact on the stroke outcome. As mentioned previously, forced running can introduce a chronic stress response which may result in detrimental effects in the event of brain injury. Svensson et al. (2016) showed that mice subjected to forced treadmill running had increased inflammatory mediators and neuronal damage in the hippocampus following global cerebral ischaemia compared to non-exercised mice. The potential masking of the positive effects of exercise by chronic induction of stress could be one explanation to the lack of effects when investigating the pre-ischaemic effects of exercise. However, the lack of neuroprotective effect was observed in lactate-injected mice as well, which excludes the confounding factor on the stroke outcome of the exercised mice. In addition, no signs of external stress were observed among the mice. In fact, all mice in the exercise groups showed gradual increases in weight, good coat quality and of signs of normal behaviour, e.g. nest building, gnawing, digging and grooming, throughout the intervention period. Furthermore, we observed that the mice showed signs of voluntary running prior to the warm-up and during the rest phases between the intervals, which indicate that the exercise regime did not induce any major stress or discomfort.

In this study, we measured the infarct volume (here, defined as tissue atrophy plus scarred damaged tissue) of mice perfused 3 weeks after permanent dMCAO. Few studies have been published that investigate stroke outcome of cortical regions 3 weeks after focal ischaemia. Comparison of infarct volumes from previous experiments showed that the mean values were in the same area as in the present study, ranging from 6-12 mm^3 of mice perfused 3 weeks after permanent dMCAO (Forbord, 2019; Sajedi, 2019). As for mice perfused 1 week after permanent dMCAO, higher mean values have been reported ranging from 9-15 mm^3 (Forbord, 2019; Llovera et al., 2014; Sajedi, 2019). The experiment performed by Forbord and Sajedi showed significant lower infarct volumes of WT mice receiving lactate injections compared to WT mice with saline of brains perfused 3 weeks after dMCAO. This indicate that lactate may

have a more a “long-term” protective mechanism (within 3 weeks recovery phase) when given shortly after stroke (24 and 48 hours after), whereas exercise and lactate given over an extended period of 7 weeks prior to stroke does not show the same neuroprotective effect in permanent dMCAO. It is worth to note that in a reperfused brain, injuries due to intermediate processes, e.g. oxidative stress, infiltration of immune cells, BBB dysfunction, and platelet and complementary activation, may occur when using transient MCAO (Cadenas, 2018; Heo et al., 2005; Peters et al., 1998; M. S. Sun et al., 2018; Yu et al., 2017). We therefore cannot exclude the same outcome of high- or medium-intensity exercise or lactate treatment in a transient stroke model, and that this may have protected against ischaemia-reperfusion brain injury.

Effect of exercise-intensity in stroke

A part of the present study was to compare the high- and medium-intensity exercise regimes to determine which one provides best prevention against stroke. The results presented in this study showed no neuroprotective effects in stroke of high- or medium-intensity exercise compared to the controls, and no significant difference in stroke outcome was found between these intensities.

Studies have reported varying running speed of exercise preconditioning to be preventive in stroke. J. Li and co-workers (2004) demonstrated reduced infarct volume in rats exercised at low-to-medium-intensity (15 m/min) prior to transient MCAO, but not permanent MCAO. However, more animal experiments have used high-intensity exercise regimes (20-30 m/min) as exercise preconditioning for the prevention of stroke (Chen et al., 2007; He et al., 2014; Liebelt et al., 2010; R. Y. Wang et al., 2001). A more recent study by Pin-Barre and co-workers (2017) investigated the effects of high- and medium-intensity in stroke recovery (e.g. promotion of cerebral plasticity), in which high-intensity exercise above the lactate threshold proved to be more effective after cerebral ischaemia than medium-intensity exercise under the lactate threshold. Thus, variable findings and conclusions have been published.

For this study, given the better physical performance in the maximum exercise-capacity test of mice exercised at high-intensity (figure 4.4) we would expect these mice to have better neuroprotection than medium-intensity. However, seeing that no beneficial effects were observed in stroke outcome of both high- and medium-intensity exercised mice, the lack of effect in our study due to suboptimal exercise is less likely. One explanation could be that we investigated the long-term neuroprotective effects of exercise and lactate (3 weeks recovery

phase) which show no effects in stroke size, as opposed to the published studies which investigated the neuroprotective effects shortly after focal ischaemia (e.g. one-week recovery phase). Nevertheless, we believe that investigating the long-term effects is the most relevant, as at one week tissue rescue is still possible (Forbord, 2019; Sajedi, 2019).

Does HCAR1 mediate exercise-induced neuroprotection after stroke?

In the present study, we hypothesised that lactate-sensing fibroblasts of the meninges could mediate exercise-induced brain vascularization via HCAR1 activation, and this would augment CBF during stroke through the increased network of collaterals in the penumbra and thereby improve the stroke outcome. Here, we observed no link between exercise, lactate and HCAR1 in the infarct size between the genotypes.

Published literature has demonstrated the beneficial effects of exercise prior to stroke to be mediated through various mechanisms (Endres et al., 2003; He et al., 2014; Jia et al., 2009; Liebelt et al., 2010), but no consensus has been reached regarding the initial signal. So far, no study has been conducted regarding exercise preconditioning with the involvement of lactate and HCAR1 relative to stroke. The role of lactate and/or HCAR1 post-stroke, on the other hand, have previously been investigated in some studies. Berthet and colleagues reported that lactate administered after transient focal ischaemia improved neurologic outcome and reduced infarct volume, and that the effects persisted 2 weeks after stroke induction (Berthet et al., 2012; Berthet et al., 2009). More recent experiments investigated the role of lactate and HCAR1 after permanent dMCAO. WT and HCAR1 KO mice treated with 2 g/kg lactate injections (24 and 48 hours after focal ischaemia) were perfused 3 weeks after stroke induction and showed improved stroke outcome compared to WT control mice treated with saline injections (Forbord, 2019; Sajedi, 2019). These reported findings highlight the pivotal role of lactate through both HCAR1-dependent and -independent mechanisms in stroke.

Thus, it may appear that lactate have beneficial effects when given post-stroke, whereas exercise preconditioning and lactate administrations given over an extended period prior to stroke do not show neuroprotection. Since exercise and lactate did not show an overall impact on the stroke outcome, it would be interesting to look closer at the pre-ischaemic effects of exercise and lactate, through HCAR1-activation, on angiogenesis and neurogenesis at the stroke area. Morland et al. (2017) have already demonstrated HCAR1 to mediate exercise-induced brain vascularization in the hippocampal DG, and the neocortex, but did not investigate this in

relation to stroke. Furthermore, novel data from our research group show that exercise or lactate treatment in mice (following the same high-intensity exercise regime and lactate treatment in the current study) induce neurogenesis in the SVZ, in a HCAR1-dependent manner (Overberg et al., unpublished). Neurons derived from the subventricular neurogenic niche may migrate towards the cortical area in response to stroke.

Based on these insights, an interesting addition to the evaluation of the role of HCAR1 in cerebral ischaemia would therefore be whether increased brain vascularization and neurogenesis, through HCAR1-mediated increase of VEGF-A, would occur in stroke, and if so, whether it would be sufficient to rescue the penumbra and ameliorate the stroke outcome. Nevertheless, our findings show that exercise preconditioning and lactate administrations given 7 weeks prior to stroke do not effectively protect against ischaemia-induced cell death, whereas lactate treatments given in the later phases after the stroke incident (> 24 hours) improves the outcome based on previous published literatures.

5.2.2 Angiogenesis and neurogenesis

General interpretation and expectation of results

Based on the given treatments, significant differences between the capillary density and neurogenesis of ipsilateral and contralateral cortex could be expected. The interpretation of such findings would be based on significant differences ($P < 0.05$) in WT mice that received lactate injections or exercised, whereas HCAR1 KO mice with corresponding treatments show no significant differences ($P > 0.05$). This indicates that the angiogenic and neurogenic effects are a result of lactate-induced HCAR1 activation, and other effects of lactate through other mechanisms, e.g. metabolic pathways, will be excluded. If significant differences are observed in both genotypes from the exercise group but not mice given lactate injections, it can be interpreted that the findings are independent of lactate and HCAR1 activation. From our experiment, approximately equal angiogenic and neurogenic effects can be expected for high-intensity exercise and lactate injected WT mice, since the lactate dose administered in this study is expected to increase the plasma concentration on the same level as during high-intensity exercise. It is, nevertheless, important to keep in mind that stressors and other factors may incur differently between exercise and injections, and hence variations may occur between the effects of these WT mice. Lastly, increases of angiogenic and neurogenic effects in WT mice receiving

medium-intensity regime are also expected. Since the medium-intensity group performed slightly below the high-intensity group, we may expect lower increase in capillary density and neurogenesis compared to the high-intensity exercised mice. WT and KO mice who received saline injections are not expected to show significant differences in the induction of angiogenesis and neurogenesis. However, WT mice with saline injections may have slightly greater differences of the ipsilateral and contralateral cortex compared to KO mice, since baseline levels of lactate may be in the EC_{50} range (Hoydal et al., 2007; Iversen et al., 2012; Schwarzkopf et al., 2013) which can be a contributing factor. For the analysis of neurogenesis, different markers were used to indicate how far the process has accelerated. Since the brains were extracted 3 weeks after the induction of focal ischaemia, we expect that tissue remodelling and reconstruction following injury has already occurred. Higher values of DCX-positive cells per 100 µm will therefore be expected compared to the other markers which demonstrate an earlier phase of the process.

Angiogenesis in cortical regions after focal ischaemia

The present study investigated whether HCAR1-mediated exercise could induce angiogenesis in the brain. The angiogenic factor VEGF-A regulates angiogenesis (Ferrara, 2000), and previous studies have shown increased angiogenesis in the brain via VEGF-A after exercise in rodents (Ding et al., 2006; Isaacs et al., 1992; Morland et al., 2017; Swain et al., 2003). Furthermore, lactate has been postulated to exert the exercise-induced increase of cerebral VEGF-A and angiogenesis. E et al. (2013) showed increased VEGF expression in mice after high-intensity exercise and lactate injections. A more recent study published by Morland and co-workers (2017), confirmed the enhancement of cerebral angiogenesis in the sensorimotor cortex and the hilus of the DG of hippocampus after exercise and lactate administration. The effect of VEGF-A and angiogenesis was particularly evident in the hippocampus in WT mice but not HCAR1 KO mice, and the authors suggested the effects to be mediated through HCAR1. In both cases, the lactate dose administered was equal to the present study, whereas the treatment period and high-intensity exercise regime to Morland et al. (2017) corresponded to our intervention. Based on these previous findings, we therefore should expect an increase in angiogenesis following the given lactate treatment and exercise regime.

VEGF-A and angiogenesis relative to ischaemia have shown neuroprotective effects in several studies when administered late (minimum 24 hours after ischaemia) (Y. Sun et al., 2003; Z. G.

Zhang et al., 2000), while other studies have demonstrated the neuroprotective effect of VEGF-A indirectly by impeding its activity (Bao et al., 1999; Hayashi et al., 1998). In regards to localisation, increased angiogenesis was notably observed in the striatal ischaemic penumbra and not at the DG by Y. Sun et al. (2003), in contrast to the observed effects by Morland et al. (2017). This was also observed by Sajedi (2019), who further investigated the angiogenic effect of lactate and HCAR1 in an acute setting after stroke and found no significant effects between WT mice and HCAR1 KO mice in the DG. An explanation to this finding may be that lactate has a preventive effect when administered post-stroke rather than pre-stroke, and the impact of stroke may drive angiogenesis towards the injured area to a greater extent, since post-stroke increases of VEGF-A and angiogenesis have been observed (Hayashi et al., 1997; Lennmyr et al., 1998; Z. G. Zhang et al., 2000). Consequently, the implication of lactate to enhance angiogenesis has been found in ICH, in which exogenous lactate infusion potentiated angiogenesis, while inhibition of endogenous lactate with lactate dehydrogenase blocked angiogenesis (Zhou et al., 2018). The mechanism was suggested to be through a lactate-facilitated activation of the NF-κB signalling pathway to induce VEGF transcription.

Altogether, these findings pinpoint the principal role of lactate in the regulation of angiogenesis, which can be evident both after exercise and stroke. We therefore, theoretically, should expect an effect of exercise and lactate on cerebral angiogenesis. In addition, based on previous findings we argue that HCAR1 may mediate these effects. However, since no impact was observed in stroke outcome in this study, it is questionable whether the increased capillary density is observed 3 weeks after stroke. If so, such findings would indicate that the effect of collaterals would not be sufficient to rescue the penumbra and reduce the stroke size in our experimental model, and that exercise- and lactate-mediated HCAR1-activation induces angiogenesis but do not show neuroprotection in the later phases after stroke.

Neurogenesis at the subgranular zone

Another aspect of the study aimed to elucidate the effects of exercise on neurogenesis, via HCAR1, in stroke. Adult neurogenesis at the SGZ of the hippocampus as a response to exercise has previously been observed by others (E et al., 2014; Itoh et al., 2011; Lambertus et al., unpublished; Overberg et al., unpublished; van Praag et al., 2005), and should therefore be expected. Moreover, several studies have pinpointed lactate as an explanatory mechanism for exercise-induced neurogenesis. Morland et al. (2017) have previously shown that exercise and

lactate administration increased VEGF-A levels in hippocampus in WT mice but not in HCAR1 KO mice. This site is known to undergo adult neurogenesis as a response to exercise (Goncalves et al., 2016). It is therefore conceivable that the angiogenic effect of exercise and lactate also promotes neurogenesis. Surprisingly, further investigations conducted by the same research group on the same animals reported exercise-induced neurogenesis at the SGZ to be independent of lactate and HCAR1 activation (Overberg et al., unpublished). In contrast, Lev-Vachnish et al. (2019) showed increased neurogenesis in the hippocampus after lactate administration, although likely through a metabolic effect. These controversial results of HCAR1-mediated neurogenesis open up for further investigations to confirm its role in the hippocampal neurogenesis.

The promotion and augmentation of angiogenesis will also activate neurogenesis after focal cerebral ischaemia (Fabel et al., 2003; Jin et al., 2002; Y. Sun et al., 2003). Together, these combined processes, mediated by exercise-induced growth factors (e.g. VEGF-A), regulates the migration of NSCs into the ischaemic area, and consequently their proliferation into functional neurons may to rescue the brain function. Based on these assumptions, the effects of lactate and HCAR1 in stroke have been investigated. The administration of lactate post-stroke (24 and 48 hours) showed no significant differences in neurogenesis at the SGZ between the treatments and genotypes (Sajedi, 2019), but the author stated that huge variations in the regions analysed were a possible contributing factor to the insignificance. In addition, the intervention was given as an acute treatment 24 and 48 hours after induced dMCAO, as opposed to the published work presented by Overberg and colleagues (unpublished), and Morland and colleagues (2017). In line with these treatments, the present experimental intervention consisted of a treatment given over 7 weeks (exercise and lactate injections) before the induction of focal ischaemia, and was therefore regarded as a preventive strategy.

Based on these findings, an increase of neurogenesis should, theoretically, be expected as result of exercise, regardless of lactate being part of the underlying mechanism. We did, however, not observe any difference in the infarct size of exercised mice and lactate injected mice versus the controls. Thus, it is uncertain if same effects will be observed in the present study.

Neurogenesis at the subventricular zone

Exercise-induced adult neurogenesis at the SVZ is a less established phenomenon with fewer published studies and controversial findings (J. Brown et al., 2003; Mastrorilli et al., 2017).

However, neurogenesis at the SVZ have shown to be more prominent as a response of stroke, and this may be an important factor to trigger and stimulate the process (Jin et al., 2001; R. L. Zhang et al., 2001). The combined effects of exercise and stroke on the neurogenic response have been demonstrated by J. Jin and co-workers (2010), who showed that long-term exercise, after ICH injury, fertilized the proliferation, survival and migration of NPs in the SVZ towards injured areas.

Based on these findings, it is conceivable that lactate, through HCAR1-activation, mediates the initial signal to induce subventricular neurogenesis as a result of exercise, and that this may contribute to the neuronal injury recovery. However, previous experiments have shown ambiguous results. In an acute setting of cerebral stroke, Sajedi (2019) investigated the effects of HCAR1-induced neurogenesis at the SVZ after lactate administrations 24 and 48 hours after dMCAO, but did not find any significant differences between WT and HCAR1 KO mice. Variations in sections measured relative to bregma should be noted as a possible cause to the reported findings. On the other hand, Overberg and colleagues showed that the effects of lactate treatment alone increased neurogenesis at the SVZ in WT mice, but not HCAR1 KO mice. Moreover, WT mice exercised at high-intensity also tended to induce neurogenesis, although this was not significant between the genotypes. Based on these findings, the authors concluded that it was uncertain whether HCAR1 mediated the increased neurogenesis alone, or that the lactate injections in WT mice was an additional effect on top of a smaller exercise-induced neurogenesis (through HCAR1-independent mechanisms). Altogether, some correlations between exercise and neurogenesis, and lactate and exercise in relation to stroke can be drawn from these studies, which highlights the principal role of HCAR1 in the regulation of neurogenesis at the SVZ.

Unlike the intervention described by Sajedi, our study focused on exercise as a preventative strategy rather than post-stroke rehabilitation. The lactate treatment and exercise regime described in this study were identical to the treatments presented by Overberg and colleagues, and we should therefore expect induced neurogenesis at the SVZ from either lactate treatment or exercise, and that this would, theoretically, rescue the penumbra. However, since we did not observe neuroprotective effects of exercise in stroke outcome it is uncertain that same effects would be observed in our experimental model. One possibility is that exercise preconditioning to induce subventricular neurogenesis would not be sufficient to ameliorate stroke damage, and therefore show no effect on the stroke outcome 3 weeks after stroke.

6 Conclusion

HCAR1 expressed on lactate-sensing fibroblasts of the meninges have been identified as a key regulator of cerebral VEGF-A and angiogenesis. Lactate levels increase as a response of exercise and activates HCAR1 in a similar manner as lactate administration, and this may underlie the beneficial effects of exercise to improve stroke recovery. Here, we found no effects of exercise or lactate treatment on the stroke outcome compared to the controls. Furthermore, WT mice did not show improved stroke outcome compared to HCAR1 KO mice. In conclusion, based on the results presented here, prolonged exercise preconditioning (7 weeks) does not protect against ischaemia-induced cell death 3 weeks after stroke. In view of the previous potential effects demonstrated by HCAR1 and lactate, the next step would be to further examine whether exercise and lactate result in a pronounced effect on angiogenesis and neurogenesis to get a broader view of the processes of brain remodelling prior to stroke. Furthermore, it would be interesting to investigate the different mechanisms involved in pre- or post-stroke of lactate and HCAR1-activation.

References

Aberg, M. A., Aberg, N. D., Hedbacker, H., Oscarsson, J., & Eriksson, P. S. (2000). Peripheral infusion of igf-i selectively induces neurogenesis in the adult rat hippocampus. *J Neurosci, 20*(8), 2896-2903.

Ahmed, K., Tunaru, S., & Offermanns, S. (2009). Gpr109a, gpr109b and gpr81, a family of hydroxy-carboxylic acid receptors. *Trends Pharmacol Sci, 30*(11), 557-562. 10.1016/j.tips.2009.09.001

Ahmed, K., Tunaru, S., Tang, C., Muller, M., Gille, A., Sassmann, A., . . .Offermanns, S. (2010). An autocrine lactate loop mediates insulin-dependent inhibition of lipolysis through gpr81. *Cell Metab, 11*(4), 311-319. 10.1016/j.cmet.2010.02.012

Altman, F. P. (1974). Studies on the reduction of tetrazolium salts. 3. The products of chemical and enzymic reduction. *Histochemie, 38*(2), 155-171. 10.1007/bf00499663

Alvarez-Buylla, A., & Lim, D. A. (2004). For the long run: Maintaining germinal niches in the adult brain. *Neuron, 41*(5), 683-686. 10.1016/s0896-6273(04)00111-4

Ansorg, A., Bornkessel, K., Witte, O. W., & Urbach, A. (2015). Immunohistochemistry and multiple labeling with antibodies from the same host species to study adult hippocampal neurogenesis. *J Vis Exp,* (98). 10.3791/52551

Arganda-Carreras, I., Kaynig, V., Rueden, C., Eliceiri, K. W., Schindelin, J., Cardona, A., & Sebastian Seung, H. (2017). Trainable weka segmentation: A machine learning tool for microscopy pixel classification. *Bioinformatics, 33*(15), 2424-2426. 10.1093/bioinformatics/btx180

Arsenijevic, Y., & Weiss, S. (1998). Insulin-like growth factor-i is a differentiation factor for postmitotic cns stem cell-derived neuronal precursors: Distinct actions from those of brain-derived neurotrophic factor. *J Neurosci, 18*(6), 2118-2128.

Arvidsson, A., Collin, T., Kirik, D., Kokaia, Z., & Lindvall, O. (2002). Neuronal replacement from endogenous precursors in the adult brain after stroke. *Nat Med, 8*(9), 963-970. 10.1038/nm747

Bao, W. L., Lu, S. D., Wang, H., & Sun, F. Y. (1999). Intraventricular vascular endothelial growth factor antibody increases infarct volume following transient cerebral ischemia. *Zhongguo Yao Li Xue Bao, 20*(4), 313-318.

Bates, D. O., Hillman, N. J., Williams, B., Neal, C. R., & Pocock, T. M. (2002). Regulation of microvascular permeability by vascular endothelial growth factors. *J Anat, 200*(6), 581-597. 10.1046/j.1469-7580.2002.00066.x

Bederson, J. B., Pitts, L. H., Germano, S. M., Nishimura, M. C., Davis, R. L., & Bartkowski, H. M. (1986). Evaluation of 2,3,5-triphenyltetrazolium chloride as a stain for detection and quantification of experimental cerebral infarction in rats. *Stroke, 17*(6), 1304-1308. 10.1161/01.str.17.6.1304

Bednar, M. M., Fanburg, J. C., Anderson, M. L., Raymond, S. J., Dooley, R. H., & Gross, C. E. (1994). Comparison of triphenyltetrazolium dye with light microscopic evaluation in a rabbit model of acute cerebral ischaemia. *Neurol Res, 16*(2), 129-132. 10.1080/01616412.1994.11740210

Belayev, L., Busto, R., Zhao, W., Fernandez, G., & Ginsberg, M. D. (1999). Middle cerebral artery occlusion in the mouse by intraluminal suture coated with poly-l-lysine: Neurological and histological validation. *Brain Res, 833*(2), 181-190. 10.1016/s0006-8993(99)01528-0

Benjamin, E. J., Muntner, P., Alonso, A., Bittencourt, M. S., Callaway, C. W., Carson, A. P., . . .Virani, S. S. (2019). Heart disease and stroke statistics-2019 update: A report from the american heart association. *Circulation, 139*(10), e56-e528. 10.1161/cir.0000000000000659

Bergersen, L. H., & Gjedde, A. (2012). Is lactate a volume transmitter of metabolic states of the brain? *Front Neuroenergetics, 4*, 5. 10.3389/fnene.2012.00005

Berthet, C., Castillo, X., Magistretti, P. J., & Hirt, L. (2012). New evidence of neuroprotection by lactate after transient focal cerebral ischaemia: Extended benefit after intracerebroventricular injection and efficacy of intravenous administration. *Cerebrovasc Dis, 34*(5-6), 329-335. 10.1159/000343657

Berthet, C., Lei, H., Thevenet, J., Gruetter, R., Magistretti, P. J., & Hirt, L. (2009). Neuroprotective role of lactate after cerebral ischemia. *J Cereb Blood Flow Metab, 29*(11), 1780-1789. 10.1038/jcbfm.2009.97

Blaya, M. O., Bramlett, H. M., Naidoo, J., Pieper, A. A., & Dietrich, W. D. (2014). Neuroprotective efficacy of a proneurogenic compound after traumatic brain injury. *J Neurotrauma, 31*(5), 476-486. 10.1089/neu.2013.3135

Bloor, C. M. (2005). Angiogenesis during exercise and training. *Angiogenesis, 8*(3), 263-271. 10.1007/s10456-005-9013-x

Bogousslavsky, J., Van Melle, G., & Regli, F. (1988). The lausanne stroke registry: Analysis of 1,000 consecutive patients with first stroke. *Stroke, 19*(9), 1083-1092. 10.1161/01.str.19.9.1083

Bonanno, E., Iurlaro, M., Madri, J. A., & Nicosia, R. F. (2000). Type iv collagen modulates angiogenesis and neovessel survival in the rat aorta model. *In Vitro Cell Dev Biol Anim, 36*(5), 336-340. 10.1290/1071-2690(2000)036<0336:Ticmaa>2.0.Co;2

Bordeaux, J., Welsh, A., Agarwal, S., Killiam, E., Baquero, M., Hanna, J., . . .Rimm, D. (2010). Antibody validation. *Biotechniques, 48*(3), 197-209. 10.2144/000113382

Boudko, S. P., Danylevych, N., Hudson, B. G., & Pedchenko, V. K. (2018). Basement membrane collagen iv: Isolation of functional domains. In R. P. Mecham (Ed.), *Methods in cell biology* (Vol. 143, pp. 171-185): Academic Press.

Bozzo, L., Puyal, J., & Chatton, J. Y. (2013). Lactate modulates the activity of primary cortical neurons through a receptor-mediated pathway. *PLoS One, 8*(8), e71721. 10.1371/journal.pone.0071721

Brint, S., Jacewicz, M., Kiessling, M., Tanabe, J., & Pulsinelli, W. (1988). Focal brain ischemia in the rat: Methods for reproducible neocortical infarction using tandem occlusion of the distal middle cerebral and ipsilateral common carotid arteries. *J Cereb Blood Flow Metab, 8*(4), 474-485. 10.1038/jcbfm.1988.88

Brooks, G. A. (1986). The lactate shuttle during exercise and recovery. *Med Sci Sports Exerc, 18*(3), 360-368. 10.1249/00005768-198606000-00019

Brooks, G. A. (2009). Cell-cell and intracellular lactate shuttles. *J Physiol, 587*(Pt 23), 5591-5600. 10.1113/jphysiol.2009.178350

Brown, D. C., & Gatter, K. C. (2002). Ki67 protein: The immaculate deception? *Histopathology, 40*(1), 2-11. 10.1046/j.1365-2559.2002.01343.x

Brown, J., Cooper-Kuhn, C. M., Kempermann, G., Van Praag, H., Winkler, J., Gage, F. H., & Kuhn, H. G. (2003). Enriched environment and physical activity stimulate hippocampal but not olfactory bulb neurogenesis. *Eur J Neurosci, 17*(10), 2042-2046. 10.1046/j.1460-9568.2003.02647.x

Bruno, V., Battaglia, G., Copani, A., D'Onofrio, M., Di Iorio, P., De Blasi, A., . . .Nicoletti, F. (2001). Metabotropic glutamate receptor subtypes as targets for neuroprotective drugs. *J Cereb Blood Flow Metab, 21*(9), 1013-1033. 10.1097/00004647-200109000-00001

Bryant, C. D. (2011). The blessings and curses of c57bl/6 substrains in mouse genetic studies. *Ann N Y Acad Sci, 1245*, 31-33. 10.1111/j.1749-6632.2011.06325.x
Cadenas, S. (2018). Ros and redox signaling in myocardial ischemia-reperfusion injury and cardioprotection. *Free Radic Biol Med, 117*, 76-89. 10.1016/j.freeradbiomed.2018.01.024
Caesar, K., Hashemi, P., Douhou, A., Bonvento, G., Boutelle, M. G., Walls, A. B., & Lauritzen, M. (2008). Glutamate receptor-dependent increments in lactate, glucose and oxygen metabolism evoked in rat cerebellum in vivo. *J Physiol, 586*(5), 1337-1349. 10.1113/jphysiol.2007.144154
Cai, T. Q., Ren, N., Jin, L., Cheng, K., Kash, S., Chen, R., . . .Waters, M. G. (2008). Role of gpr81 in lactate-mediated reduction of adipose lipolysis. *Biochem Biophys Res Commun, 377*(3), 987-991. 10.1016/j.bbrc.2008.10.088
Caplan, L. R. (2009). *Caplan's stroke: A clinical approach: Fourth edition*: Butterworth-Heinemann.
Carleton, A., Petreanu, L. T., Lansford, R., Alvarez-Buylla, A., & Lledo, P. M. (2003). Becoming a new neuron in the adult olfactory bulb. *Nat Neurosci, 6*(5), 507-518. 10.1038/nn1048
Carmeliet, P., & Tessier-Lavigne, M. (2005). Common mechanisms of nerve and blood vessel wiring. *Nature, 436*(7048), 193-200. 10.1038/nature03875
Carmichael, S. T. (2005). Rodent models of focal stroke: Size, mechanism, and purpose. *NeuroRx, 2*(3), 396-409. 10.1602/neurorx.2.3.396
Casals, J. B., Pieri, N. C., Feitosa, M. L., Ercolin, A. C., Roballo, K. C., Barreto, R. S., . . .Ambrosio, C. E. (2011). The use of animal models for stroke research: A review. *Comp Med, 61*(4), 305-313.
Caspersen, C. J., Powell, K. E., & Christenson, G. M. (1985). Physical activity, exercise, and physical fitness: Definitions and distinctions for health-related research. *Public Health Rep, 100*(2), 126-131.
Challa, V. R., Thore, C. R., Moody, D. M., Brown, W. R., & Anstrom, J. A. (2002). A three-dimensional study of brain string vessels using celloidin sections stained with anti-collagen antibodies. *J Neurol Sci, 203-204*, 165-167. 10.1016/s0022-510x(02)00284-8
Chan, P. H. (1996). Role of oxidants in ischemic brain damage. *Stroke, 27*(6), 1124-1129. 10.1161/01.str.27.6.1124
Chen, Y. W., Chen, S. H., Chou, W., Lo, Y. M., Hung, C. H., & Lin, M. T. (2007). Exercise pretraining protects against cerebral ischaemia induced by heat stroke in rats. *Br J Sports Med, 41*(9), 597-602. 10.1136/bjsm.2006.033829
Clayton, J. A., Chalothorn, D., & Faber, J. E. (2008). Vascular endothelial growth factor-a specifies formation of native collaterals and regulates collateral growth in ischemia. *Circ Res, 103*(9), 1027-1036. 10.1161/circresaha.108.181115
Cole, D. J., Drummond, J. C., Ghazal, E. A., & Shapiro, H. M. (1990). A reversible component of cerebral injury as identified by the histochemical stain 2,3,5-triphenyltetrazolium chloride (ttc). *Acta Neuropathol, 80*(2), 152-155. 10.1007/bf00308918
Correale, J., & Villa, A. (2009). Cellular elements of the blood-brain barrier. *Neurochem Res, 34*(12), 2067-2077. 10.1007/s11064-009-0081-y
Corthell, J. T. (2014a). Agarose gel electrophoresis. In J. T. Corthell (Ed.), *Basic molecular protocols in neuroscience: Tips, tricks, and pitfalls* (pp. 21-25). San Diego: Academic Press.
Corthell, J. T. (2014b). Immunohistochemistry. In J. T. Corthell (Ed.), *Basic molecular protocols in neuroscience: Tips, tricks, and pitfalls* (pp. 91-103). San Diego: Academic Press.

Cotman, C. W., & Berchtold, N. C. (2002). Exercise: A behavioral intervention to enhance brain health and plasticity. *Trends Neurosci, 25*(6), 295-301.
Couillard-Despres, S., Winner, B., Schaubeck, S., Aigner, R., Vroemen, M., Weidner, N., . . .Aigner, L. (2005). Doublecortin expression levels in adult brain reflect neurogenesis. *Eur J Neurosci, 21*(1), 1-14. 10.1111/j.1460-9568.2004.03813.x
Crack, P. J., & Taylor, J. M. (2005). Reactive oxygen species and the modulation of stroke. *Free Radic Biol Med, 38*(11), 1433-1444. 10.1016/j.freeradbiomed.2005.01.019
de Castro Abrantes, H., Briquet, M., Schmuziger, C., Restivo, L., Puyal, J., Rosenberg, N., . . .Chatton, J. Y. (2019). The lactate receptor hcar1 modulates neuronal network activity through the activation of galpha and gbetagamma subunits. *J Neurosci, 39*(23), 4422-4433. 10.1523/jneurosci.2092-18.2019
De Rossi, P., Harde, E., Dupuis, J. P., Martin, L., Chounlamountri, N., Bardin, M., . . .Meissirel, C. (2016). A critical role for vegf and vegfr2 in nmda receptor synaptic function and fear-related behavior. *Mol Psychiatry, 21*(12), 1768-1780. 10.1038/mp.2015.195
Desai, K. H., & Bernstein, D. (2002). Exercise and oxygen consumption in the mouse. In B. D. Hoit & R. A. Walsh (Eds.), *Cardiovascular physiology in the genetically engineered mouse* (pp. 277-302). Boston, MA: Springer US.
Dettmers, C., Hartmann, A., Rommel, T., Kramer, S., Pappata, S., Young, A., . . .Baron, J. C. (1994). Immersion and perfusion staining with 2,3,5-triphenyltetrazolium chloride (ttc) compared to mitochondrial enzymes 6 hours after mca-occlusion in primates. *Neurol Res, 16*(3), 205-208. 10.1080/01616412.1994.11740228
Dey, P. (2018a). Fixation of histology samples: Principles, methods and types of fixatives. In P. Dey (Ed.), *Basic and advanced laboratory techniques in histopathology and cytology* (pp. 3-17). Singapore: Springer Singapore.
Dey, P. (2018b). Haematoxylin and eosin stain of the tissue section. In *Basic and advanced laboratory techniques in histopathology and cytology* (pp. 69-79). Singapore: Springer Singapore.
Dey, P. (2018c). Immunocytochemistry in histology and cytology. In *Basic and advanced laboratory techniques in histopathology and cytology* (pp. 149-169). Singapore: Springer Singapore.
Dienel, G. A. (2012). Brain lactate metabolism: The discoveries and the controversies. *J Cereb Blood Flow Metab, 32*(7), 1107-1138. 10.1038/jcbfm.2011.175
Ding, Y. H., Li, J., Zhou, Y., Rafols, J. A., Clark, J. C., & Ding, Y. (2006). Cerebral angiogenesis and expression of angiogenic factors in aging rats after exercise. *Curr Neurovasc Res, 3*(1), 15-23.
Dirnagl, U., & Endres, M. (2014). Found in translation: Preclinical stroke research predicts human pathophysiology, clinical phenotypes, and therapeutic outcomes. *Stroke, 45*(5), 1510-1518. 10.1161/strokeaha.113.004075
Dirnagl, U., Iadecola, C., & Moskowitz, M. A. (1999). Pathobiology of ischaemic stroke: An integrated view. *Trends Neurosci, 22*(9), 391-397.
Doetsch, F., & Alvarez-Buylla, A. (1996). Network of tangential pathways for neuronal migration in adult mammalian brain. *Proc Natl Acad Sci U S A, 93*(25), 14895-14900. 10.1073/pnas.93.25.14895
Doyle, K. P., Simon, R. P., & Stenzel-Poore, M. P. (2008). Mechanisms of ischemic brain damage. *Neuropharmacology, 55*(3), 310-318. 10.1016/j.neuropharm.2008.01.005
Duggal, N., Schmidt-Kastner, R., & Hakim, A. M. (1997). Nestin expression in reactive astrocytes following focal cerebral ischemia in rats. *Brain Res, 768*(1-2), 1-9. 10.1016/s0006-8993(97)00588-x

Durukan, A., & Tatlisumak, T. (2007). Acute ischemic stroke: Overview of major experimental rodent models, pathophysiology, and therapy of focal cerebral ischemia. *Pharmacol Biochem Behav, 87*(1), 179-197. 10.1016/j.pbb.2007.04.015

Dylewicz, P., Przywarska, I., Szczesniak, L., Rychlewski, T., Bienkowska, S., Dlugiewicz, I., & Wilk, M. (1999). The influence of short-term endurance training on the insulin blood level, binding, and degradation of 125i-insulin by erythrocyte receptors in patients after myocardial infarction. *J Cardiopulm Rehabil, 19*(2), 98-105.

E, L., Burns, J. M., & Swerdlow, R. H. (2014). Effect of high-intensity exercise on aged mouse brain mitochondria, neurogenesis, and inflammation. *Neurobiol Aging, 35*(11), 2574-2583. 10.1016/j.neurobiolaging.2014.05.033

E, L., Lu, J., Selfridge, J. E., Burns, J. M., & Swerdlow, R. H. (2013). Lactate administration reproduces specific brain and liver exercise-related changes. *J Neurochem, 127*(1), 91-100. 10.1111/jnc.12394

Edelberg, J. M., & Reed, M. J. (2003). Aging and angiogenesis. *Front Biosci, 8*, s1199-1209.

Edvinsson, L., & Krause, D. (2001). *Cerebral blood flow and metabolism*.

Egginton, S., Zhou, A. L., Brown, M. D., & Hudlicka, O. (2001). Unorthodox angiogenesis in skeletal muscle. *Cardiovasc Res, 49*(3), 634-646. 10.1016/s0008-6363(00)00282-0

Eichenbaum, K. D., Eichenbaum, J. W., Fadiel, A., Miller, D. C., Demir, N., Naftolin, F., . . .Pevsner, P. H. (2005). Minimally invasive method for murine brain fixation. *Biotechniques, 39*(4), 487-488, 490. 10.2144/000112003

El Hayek, L., Khalifeh, M., Zibara, V., Abi Assaad, R., Emmanuel, N., Karnib, N., . . .Sleiman, S. F. (2019). Lactate mediates the effects of exercise on learning and memory through sirt1-dependent activation of hippocampal brain-derived neurotrophic factor (bdnf). *J Neurosci, 39*(13), 2369-2382. 10.1523/jneurosci.1661-18.2019

Encinas, J. M., Michurina, T. V., Peunova, N., Park, J. H., Tordo, J., Peterson, D. A., . . .Enikolopov, G. (2011). Division-coupled astrocytic differentiation and age-related depletion of neural stem cells in the adult hippocampus. *Cell Stem Cell, 8*(5), 566-579. 10.1016/j.stem.2011.03.010

Endl, E., & Gerdes, J. (2000). The ki-67 protein: Fascinating forms and an unknown function. *Exp Cell Res, 257*(2), 231-237. 10.1006/excr.2000.4888

Endres, M., Gertz, K., Lindauer, U., Katchanov, J., Schultze, J., Schrock, H., . . .Laufs, U. (2003). Mechanisms of stroke protection by physical activity. *Ann Neurol, 54*(5), 582-590. 10.1002/ana.10722

Engel, O., Kolodziej, S., Dirnagl, U., & Prinz, V. (2011). Modeling stroke in mice - middle cerebral artery occlusion with the filament model. *J Vis Exp*, (47). 10.3791/2423

Esposito, M. S., Piatti, V. C., Laplagne, D. A., Morgenstern, N. A., Ferrari, C. C., Pitossi, F. J., & Schinder, A. F. (2005). Neuronal differentiation in the adult hippocampus recapitulates embryonic development. *J Neurosci, 25*(44), 10074-10086. 10.1523/jneurosci.3114-05.2005

Fabel, K., Fabel, K., Tam, B., Kaufer, D., Baiker, A., Simmons, N., . . .Palmer, T. D. (2003). Vegf is necessary for exercise-induced adult hippocampal neurogenesis. *Eur J Neurosci, 18*(10), 2803-2812. 10.1111/j.1460-9568.2003.03041.x

Farmer, J., Zhao, X., van Praag, H., Wodtke, K., Gage, F. H., & Christie, B. R. (2004). Effects of voluntary exercise on synaptic plasticity and gene expression in the dentate gyrus of adult male sprague-dawley rats in vivo. *Neuroscience, 124*(1), 71-79. 10.1016/j.neuroscience.2003.09.029

Ferrara, N. (2000). Vascular endothelial growth factor and the regulation of angiogenesis. *Recent Prog Horm Res, 55*, 15-35; discussion 35-16.

Fisher, M. (2010). The challenge of mixed cerebrovascular disease. *Ann N Y Acad Sci, 1207*, 18-22. 10.1111/j.1749-6632.2010.05758.x
Fluri, F., Schuhmann, M. K., & Kleinschnitz, C. (2015). Animal models of ischemic stroke and their application in clinical research. *Drug Des Devel Ther, 9*, 3445-3454. 10.2147/dddt.S56071
Folkman, J., & Shing, Y. (1992). Angiogenesis. *J Biol Chem, 267*(16), 10931-10934.
Forbord, K. F. (2019). *Hcar1-dependent effect of therapeutic lactate in post-stroke pathophysiology in mice* (Master). University of Oslo, Oslo.
Francis, F., Koulakoff, A., Boucher, D., Chafey, P., Schaar, B., Vinet, M. C., . . .Chelly, J. (1999). Doublecortin is a developmentally regulated, microtubule-associated protein expressed in migrating and differentiating neurons. *Neuron, 23*(2), 247-256. 10.1016/s0896-6273(00)80777-1
Gage, G. J., Kipke, D. R., & Shain, W. (2012). Whole animal perfusion fixation for rodents. *J Vis Exp*, (65). 10.3791/3564
Ge, H., Weiszmann, J., Reagan, J. D., Gupte, J., Baribault, H., Gyuris, T., . . .Li, Y. (2008). Elucidation of signaling and functional activities of an orphan gpcr, gpr81. *J Lipid Res, 49*(4), 797-803. 10.1194/jlr.M700513-JLR200
Geiseler, S. J., & Morland, C. (2018). The janus face of vegf in stroke. *Int J Mol Sci, 19*(5). 10.3390/ijms19051362
Gerriets, T., Li, F., Silva, M. D., Meng, X., Brevard, M., Sotak, C. H., & Fisher, M. (2003). The macrosphere model: Evaluation of a new stroke model for permanent middle cerebral artery occlusion in rats. *J Neurosci Methods, 122*(2), 201-211.
Gilberto González, R., A. Hirsch, J., Koroshetz, W., Lev, M., & W. Schaefer, P. (2006). *Acute ischemic stroke: Imaging and intervention*.
Gilyarov, A. V. (2008). Nestin in central nervous system cells. *Neurosci Behav Physiol, 38*(2), 165-169. 10.1007/s11055-008-0025-z
Gittins, R., & Harrison, P. J. (2004). Neuronal density, size and shape in the human anterior cingulate cortex: A comparison of nissl and neun staining. *Brain Res Bull, 63*(2), 155-160. 10.1016/j.brainresbull.2004.02.005
Gleeson, J. G., Lin, P. T., Flanagan, L. A., & Walsh, C. A. (1999). Doublecortin is a microtubule-associated protein and is expressed widely by migrating neurons. *Neuron, 23*(2), 257-271. 10.1016/s0896-6273(00)80778-3
Gob, E., Reymann, S., Langhauser, F., Schuhmann, M. K., Kraft, P., Thielmann, I., . . .Kleinschnitz, C. (2015). Blocking of plasma kallikrein ameliorates stroke by reducing thromboinflammation. *Ann Neurol, 77*(5), 784-803. 10.1002/ana.24380
Goh, J., & Ladiges, W. (2015). Voluntary wheel running in mice. *Curr Protoc Mouse Biol, 5*(4), 283-290. 10.1002/9780470942390.mo140295
Goncalves, J. T., Schafer, S. T., & Gage, F. H. (2016). Adult neurogenesis in the hippocampus: From stem cells to behavior. *Cell, 167*(4), 897-914. 10.1016/j.cell.2016.10.021
Goodpaster, B. H., Delany, J. P., Otto, A. D., Kuller, L., Vockley, J., South-Paul, J. E., . . .Jakicic, J. M. (2010). Effects of diet and physical activity interventions on weight loss and cardiometabolic risk factors in severely obese adults: A randomized trial. *Jama, 304*(16), 1795-1802. 10.1001/jama.2010.1505
Gordon, G. R., Choi, H. B., Rungta, R. L., Ellis-Davies, G. C., & MacVicar, B. A. (2008). Brain metabolism dictates the polarity of astrocyte control over arterioles. *Nature, 456*(7223), 745-749. 10.1038/nature07525
Haas, T. L., Milkiewicz, M., Davis, S. J., Zhou, A. L., Egginton, S., Brown, M. D., . . .Hudlicka, O. (2000). Matrix metalloproteinase activity is required for activity-

induced angiogenesis in rat skeletal muscle. *Am J Physiol Heart Circ Physiol, 279*(4), H1540-1547. 10.1152/ajpheart.2000.279.4.H1540

Hall, C. N., Reynell, C., Gesslein, B., Hamilton, N. B., Mishra, A., Sutherland, B. A., . . .Attwell, D. (2014). Capillary pericytes regulate cerebral blood flow in health and disease. *Nature, 508*(7494), 55-60. 10.1038/nature13165

Hansen-Smith, F. M., Hudlicka, O., & Egginton, S. (1996). In vivo angiogenesis in adult rat skeletal muscle: Early changes in capillary network architecture and ultrastructure. *Cell Tissue Res, 286*(1), 123-136. 10.1007/s004410050681

Hashimoto, T., Hussien, R., Oommen, S., Gohil, K., & Brooks, G. A. (2007). Lactate sensitive transcription factor network in l6 cells: Activation of mct1 and mitochondrial biogenesis. *Faseb j, 21*(10), 2602-2612. 10.1096/fj.07-8174com

Hatfield, R. H., Mendelow, A. D., Perry, R. H., Alvarez, L. M., & Modha, P. (1991). Triphenyltetrazolium chloride (ttc) as a marker for ischaemic changes in rat brain following permanent middle cerebral artery occlusion. *Neuropathol Appl Neurobiol, 17*(1), 61-67. 10.1111/j.1365-2990.1991.tb00694.x

Haugen, O. P., Vallenari, E. M., Belhaj, I., Smastuen, M. C., Storm-Mathisen, J., Bergersen, L. H., & Amellem, I. (2020). Blood lactate dynamics in awake and anaesthetized mice after intraperitoneal and subcutaneous injections of lactate-sex matters. *PeerJ, 8*, e8328. 10.7717/peerj.8328

Hayashi, T., Abe, K., & Itoyama, Y. (1998). Reduction of ischemic damage by application of vascular endothelial growth factor in rat brain after transient ischemia. *J Cereb Blood Flow Metab, 18*(8), 887-895. 10.1097/00004647-199808000-00009

Hayashi, T., Abe, K., Suzuki, H., & Itoyama, Y. (1997). Rapid induction of vascular endothelial growth factor gene expression after transient middle cerebral artery occlusion in rats. *Stroke, 28*(10), 2039-2044. 10.1161/01.str.28.10.2039

Hayes, K., Sprague, S., Guo, M., Davis, W., Friedman, A., Kumar, A., . . .Ding, Y. (2008). Forced, not voluntary, exercise effectively induces neuroprotection in stroke. *Acta Neuropathol, 115*(3), 289-296. 10.1007/s00401-008-0340-z

He, Z., Wang, X., Wu, Y., Jia, J., Hu, Y., Yang, X., . . .Leung, M. C. (2014). Treadmill pre-training ameliorates brain edema in ischemic stroke via down-regulation of aquaporin-4: An mri study in rats. *PLoS One, 9*(1), e84602. 10.1371/journal.pone.0084602

Henderson, G., Flower, R. J., Ritter, J. M., Dale, M. M., & Rang, H. P. (2016). *Rang and dale's pharmacology* (8th ed. ed.Pharmacology). Edinburgh: Elsevier Churchill Livingstone.

Heo, J. H., Han, S. W., & Lee, S. K. (2005). Free radicals as triggers of brain edema formation after stroke. *Free Radic Biol Med, 39*(1), 51-70. 10.1016/j.freeradbiomed.2005.03.035

Hillman, C. H., Erickson, K. I., & Kramer, A. F. (2008). Be smart, exercise your heart: Exercise effects on brain and cognition. *Nat Rev Neurosci, 9*(1), 58-65. 10.1038/nrn2298

Hirota, J., & Shimizu, S. (2012). Routes of administration. In H. J. Hedrich (Ed.), *The laboratory mouse (second edition)* (pp. 709-725). Boston: Academic Press.

Hoque, R., Farooq, A., Ghani, A., Gorelick, F., & Mehal, W. Z. (2014). Lactate reduces liver and pancreatic injury in toll-like receptor- and inflammasome-mediated inflammation via gpr81-mediated suppression of innate immunity. *Gastroenterology, 146*(7), 1763-1774. 10.1053/j.gastro.2014.03.014

Howells, D. W., Porritt, M. J., Rewell, S. S., O'Collins, V., Sena, E. S., van der Worp, H. B., . . .Macleod, M. R. (2010). Different strokes for different folks: The rich diversity of animal models of focal cerebral ischemia. *J Cereb Blood Flow Metab, 30*(8), 1412-1431. 10.1038/jcbfm.2010.66

Hoydal, M. A., Wisloff, U., Kemi, O. J., & Ellingsen, O. (2007). Running speed and maximal oxygen uptake in rats and mice: Practical implications for exercise training. *Eur J Cardiovasc Prev Rehabil, 14*(6), 753-760. 10.1097/HJR.0b013e3281eacef1

Hu, J., Cai, M., Liu, Y., Liu, B., Xue, X., Ji, R., . . .Lou, S. (2020). The roles of grp81 as a metabolic sensor and inflammatory mediator. *J Cell Physiol*. 10.1002/jcp.29739

Huang, Y., & McNamara, J. O. (2004). Ischemic stroke: "Acidotoxicity" is a perpetrator. *Cell, 118*(6), 665-666. 10.1016/j.cell.2004.09.004

Hui, C., Tadi, P., & Patti, L. (2019, 2019 May 16). Ischemic stroke. Retrieved 07.08.19 from https://www.ncbi.nlm.nih.gov/books/NBK499997/

Iadecola, C., & Alexander, M. (2001). Cerebral ischemia and inflammation. *Curr Opin Neurol, 14*(1), 89-94.

Iadecola, C., Salkowski, C. A., Zhang, F., Aber, T., Nagayama, M., Vogel, S. N., & Ross, M. E. (1999). The transcription factor interferon regulatory factor 1 is expressed after cerebral ischemia and contributes to ischemic brain injury. *J Exp Med, 189*(4), 719-727. 10.1084/jem.189.4.719

Isaacs, K. R., Anderson, B. J., Alcantara, A. A., Black, J. E., & Greenough, W. T. (1992). Exercise and the brain: Angiogenesis in the adult rat cerebellum after vigorous physical activity and motor skill learning. *J Cereb Blood Flow Metab, 12*(1), 110-119. 10.1038/jcbfm.1992.14

Isayama, K., Pitts, L. H., & Nishimura, M. C. (1991). Evaluation of 2,3,5-triphenyltetrazolium chloride staining to delineate rat brain infarcts. *Stroke, 22*(11), 1394-1398. 10.1161/01.str.22.11.1394

Itoh, T., Imano, M., Nishida, S., Tsubaki, M., Hashimoto, S., Ito, A., & Satou, T. (2011). Exercise increases neural stem cell proliferation surrounding the area of damage following rat traumatic brain injury. *J Neural Transm (Vienna), 118*(2), 193-202. 10.1007/s00702-010-0495-3

Iversen, N. K., Malte, H., Baatrup, E., & Wang, T. (2012). The normal acid-base status of mice. *Respir Physiol Neurobiol, 180*(2-3), 252-257. 10.1016/j.resp.2011.11.015

Jeninga, E. H., Bugge, A., Nielsen, R., Kersten, S., Hamers, N., Dani, C., . . .Kalkhoven, E. (2009). Peroxisome proliferator-activated receptor gamma regulates expression of the anti-lipolytic g-protein-coupled receptor 81 (gpr81/gpr81). *J Biol Chem, 284*(39), 26385-26393. 10.1074/jbc.M109.040741

Jia, J., Hu, Y. S., Wu, Y., Liu, G., Yu, H. X., Zheng, Q. P., . . .Cao, Z. J. (2009). Pre-ischemic treadmill training affects glutamate and gamma aminobutyric acid levels in the striatal dialysate of a rat model of cerebral ischemia. *Life Sci, 84*(15-16), 505-511. 10.1016/j.lfs.2009.01.015

Jin, J., Kang, H. M., & Park, C. (2010). Voluntary exercise enhances survival and migration of neural progenitor cells after intracerebral haemorrhage in mice. *Brain Inj, 24*(3), 533-540. 10.3109/02699051003610458

Jin, K., Minami, M., Lan, J. Q., Mao, X. O., Batteur, S., Simon, R. P., & Greenberg, D. A. (2001). Neurogenesis in dentate subgranular zone and rostral subventricular zone after focal cerebral ischemia in the rat. *Proc Natl Acad Sci U S A, 98*(8), 4710-4715. 10.1073/pnas.081011098

Jin, K., Sun, Y., Xie, L., Peel, A., Mao, X. O., Batteur, S., & Greenberg, D. A. (2003). Directed migration of neuronal precursors into the ischemic cerebral cortex and striatum. *Mol Cell Neurosci, 24*(1), 171-189.

Jin, K., Zhu, Y., Sun, Y., Mao, X. O., Xie, L., & Greenberg, D. A. (2002). Vascular endothelial growth factor (vegf) stimulates neurogenesis in vitro and in vivo. *Proc Natl Acad Sci U S A, 99*(18), 11946-11950. 10.1073/pnas.182296499

Jin, R., Yang, G., & Li, G. (2010). Inflammatory mechanisms in ischemic stroke: Role of inflammatory cells. *J Leukoc Biol, 87*(5), 779-789. 10.1189/jlb.1109766

Kadar, A., Wittmann, G., Liposits, Z., & Fekete, C. (2009). Improved method for combination of immunocytochemistry and nissl staining. *J Neurosci Methods, 184*(1), 115-118. 10.1016/j.jneumeth.2009.07.010

Kasukurthi, R., Brenner, M. J., Moore, A. M., Moradzadeh, A., Ray, W. Z., Santosa, K. B., . . .Hunter, D. A. (2009). Transcardial perfusion versus immersion fixation for assessment of peripheral nerve regeneration. *J Neurosci Methods, 184*(2), 303-309. 10.1016/j.jneumeth.2009.08.019

Kee, N., Sivalingam, S., Boonstra, R., & Wojtowicz, J. M. (2002). The utility of ki-67 and brdu as proliferative markers of adult neurogenesis. *J Neurosci Methods, 115*(1), 97-105. 10.1016/s0165-0270(02)00007-9

Kemi, O. J., Loennechen, J. P., Wisloff, U., & Ellingsen, O. (2002). Intensity-controlled treadmill running in mice: Cardiac and skeletal muscle hypertrophy. *J Appl Physiol (1985), 93*(4), 1301-1309. 10.1152/japplphysiol.00231.2002

Kernan, W. N., Ovbiagele, B., Black, H. R., Bravata, D. M., Chimowitz, M. I., Ezekowitz, M. D., . . .Wilson, J. A. (2014). Guidelines for the prevention of stroke in patients with stroke and transient ischemic attack. *Stroke, 45*(7), 2160-2236. doi:10.1161/STR.0000000000000024

Kiernan, J. A. (2000). Formaldehyde, formalin, paraformaldehyde and glutaraldehyde: What they are and what they do. *Microscopy Today, 8*(1), 8-13. 10.1017/S1551929500057060

Kitano, H., Kirsch, J. R., Hurn, P. D., & Murphy, S. J. (2007). Inhalational anesthetics as neuroprotectants or chemical preconditioning agents in ischemic brain. *J Cereb Blood Flow Metab, 27*(6), 1108-1128. 10.1038/sj.jcbfm.9600410

Koch, S., & Claesson-Welsh, L. (2012). Signal transduction by vascular endothelial growth factor receptors. *Cold Spring Harb Perspect Med, 2*(7), a006502. 10.1101/cshperspect.a006502

Koh, S. H., & Park, H. H. (2017). Neurogenesis in stroke recovery. *Transl Stroke Res, 8*(1), 3-13. 10.1007/s12975-016-0460-z

Kornack, D. R., & Rakic, P. (2001). The generation, migration, and differentiation of olfactory neurons in the adult primate brain. *Proc Natl Acad Sci U S A, 98*(8), 4752-4757. 10.1073/pnas.081074998

Kovacs, Z., Ikezaki, K., Samoto, K., Inamura, T., & Fukui, M. (1996). Vegf and flt. Expression time kinetics in rat brain infarct. *Stroke, 27*(10), 1865-1872; discussion 1872-1863. 10.1161/01.str.27.10.1865

Kraft, P., Gob, E., Schuhmann, M. K., Gobel, K., Deppermann, C., Thielmann, I., . . .Kleinschnitz, C. (2013). Fty720 ameliorates acute ischemic stroke in mice by reducing thrombo-inflammation but not by direct neuroprotection. *Stroke, 44*(11), 3202-3210. 10.1161/strokeaha.113.002880

Krupinski, J., Kaluza, J., Kumar, P., Kumar, S., & Wang, J. M. (1994). Role of angiogenesis in patients with cerebral ischemic stroke. *Stroke, 25*(9), 1794-1798. 10.1161/01.str.25.9.1794

Kureishi, Y., Luo, Z., Shiojima, I., Bialik, A., Fulton, D., Lefer, D. J., . . .Walsh, K. (2000). The hmg-coa reductase inhibitor simvastatin activates the protein kinase akt and promotes angiogenesis in normocholesterolemic animals. *Nat Med, 6*(9), 1004-1010. 10.1038/79510

Lambertus, M., Overberg, L. T., Andersson, K. A., Hadzic, A., Haugen, O. P., Storm-Mathisen, J., . . .Morland, C. (unpublished). *High intensity is required in exercise-derived neurogenesis*.

Lauritzen, K. H., Morland, C., Puchades, M., Holm-Hansen, S., Hagelin, E. M., Lauritzen, F., . . .Bergersen, L. H. (2014). Lactate receptor sites link neurotransmission, neurovascular coupling, and brain energy metabolism. *Cereb Cortex, 24*(10), 2784-2795. 10.1093/cercor/bht136

Lee, C. D., Folsom, A. R., & Blair, S. N. (2003). Physical activity and stroke risk: A meta-analysis. *Stroke, 34*(10), 2475-2481. 10.1161/01.str.0000091843.02517.9d

Lendahl, U., Zimmerman, L. B., & McKay, R. D. (1990). Cns stem cells express a new class of intermediate filament protein. *Cell, 60*(4), 585-595. 10.1016/0092-8674(90)90662-x

Lennmyr, F., Ata, K. A., Funa, K., Olsson, Y., & Terent, A. (1998). Expression of vascular endothelial growth factor (vegf) and its receptors (flt-1 and flk-1) following permanent and transient occlusion of the middle cerebral artery in the rat. *J Neuropathol Exp Neurol, 57*(9), 874-882. 10.1097/00005072-199809000-00009

Leonard, B. E. (1975). A study of the neurohumoral control of glycolysis in the mouse brain in vivo: Role of noradrenaline and dopamine. *Z Naturforsch C Biosci, 30*(3), 385-391. 10.1515/znc-1975-5-614

Lerch, M. M., Conwell, D. L., & Mayerle, J. (2014). The anti-inflammasome effect of lactate and the lactate gpr81-receptor in pancreatic and liver inflammation. *Gastroenterology, 146*(7), 1602-1605. 10.1053/j.gastro.2014.04.025

Lev-Vachnish, Y., Cadury, S., Rotter-Maskowitz, A., Feldman, N., Roichman, A., Illouz, T., . . .Okun, E. (2019). L-lactate promotes adult hippocampal neurogenesis. *Front Neurosci, 13*, 403. 10.3389/fnins.2019.00403

Leventhal, C., Rafii, S., Rafii, D., Shahar, A., & Goldman, S. A. (1999). Endothelial trophic support of neuronal production and recruitment from the adult mammalian subependyma. *Mol Cell Neurosci, 13*(6), 450-464. 10.1006/mcne.1999.0762

Li, F., Omae, T., & Fisher, M. (1999). Spontaneous hyperthermia and its mechanism in the intraluminal suture middle cerebral artery occlusion model of rats. *Stroke, 30*(11), 2464-2470; discussion 2470-2461. 10.1161/01.str.30.11.2464

Li, J., Luan, X., Clark, J. C., Rafols, J. A., & Ding, Y. (2004). Neuroprotection against transient cerebral ischemia by exercise pre-conditioning in rats. *Neurol Res, 26*(4), 404-408. 10.1179/016164104225016038

Li, J., & Siegrist, J. (2012). Physical activity and risk of cardiovascular disease--a meta-analysis of prospective cohort studies. *Int J Environ Res Public Health, 9*(2), 391-407. 10.3390/ijerph9020391

Liebelt, B., Papapetrou, P., Ali, A., Guo, M., Ji, X., Peng, C., . . .Ding, Y. (2010). Exercise preconditioning reduces neuronal apoptosis in stroke by up-regulating heat shock protein-70 (heat shock protein-72) and extracellular-signal-regulated-kinase 1/2. *Neuroscience, 166*(4), 1091-1100. 10.1016/j.neuroscience.2009.12.067

Liszczak, T. M., Hedley-Whyte, E. T., Adams, J. F., Han, D. H., Kolluri, V. S., Vacanti, F. X., . . .Zervas, N. T. (1984). Limitations of tetrazolium salts in delineating infarcted brain. *Acta Neuropathol, 65*(2), 150-157. 10.1007/bf00690469

Liu, C., Wu, J., Zhu, J., Kuei, C., Yu, J., Shelton, J., . . .Lovenberg, T. W. (2009). Lactate inhibits lipolysis in fat cells through activation of an orphan g-protein-coupled receptor, gpr81. *J Biol Chem, 284*(5), 2811-2822. 10.1074/jbc.M806409200

Liu, J., Haorah, J., & Xiong, H. (2014). Western blotting technique in biomedical research. In H. Xiong & H. E. Gendelman (Eds.), *Current laboratory methods in neuroscience research* (pp. 187-200). New York, NY: Springer New York.

Llovera, G., Roth, S., Plesnila, N., Veltkamp, R., & Liesz, A. (2014). Modeling stroke in mice: Permanent coagulation of the distal middle cerebral artery. *J Vis Exp*, (89), e51729. 10.3791/51729

Lo, E. H., Dalkara, T., & Moskowitz, M. A. (2003). Mechanisms, challenges and opportunities in stroke. *Nat Rev Neurosci, 4*(5), 399-415. 10.1038/nrn1106
Lois, C., Garcia-Verdugo, J. M., & Alvarez-Buylla, A. (1996). Chain migration of neuronal precursors. *Science, 271*(5251), 978-981. 10.1126/science.271.5251.978
Longa, E. Z., Weinstein, P. R., Carlson, S., & Cummins, R. (1989). Reversible middle cerebral artery occlusion without craniectomy in rats. *Stroke, 20*(1), 84-91. 10.1161/01.str.20.1.84
Lopez-Lopez, C., LeRoith, D., & Torres-Aleman, I. (2004). Insulin-like growth factor i is required for vessel remodeling in the adult brain. *Proc Natl Acad Sci U S A, 101*(26), 9833-9838. 10.1073/pnas.0400337101
Lopez, M. F., Sarracino, D. A., Prakash, A., Athanas, M., Krastins, B., Rezai, T., . . .Ning, M. (2012). Discrimination of ischemic and hemorrhagic strokes using a multiplexed, mass spectrometry-based assay for serum apolipoproteins coupled to multi-marker roc algorithm. *Proteomics Clin Appl, 6*(3-4), 190-200. 10.1002/prca.201100041
Love, S. (2003). Apoptosis and brain ischaemia. *Prog Neuropsychopharmacol Biol Psychiatry, 27*(2), 267-282. 10.1016/s0278-5846(03)00022-8
Lu, D., Sanberg, P. R., Mahmood, A., Li, Y., Wang, L., Sanchez-Ramos, J., & Chopp, M. (2002). Intravenous administration of human umbilical cord blood reduces neurological deficit in the rat after traumatic brain injury. *Cell Transplant, 11*(3), 275-281.
Madaan, A., Nadeau-Vallee, M., Rivera, J. C., Obari, D., Hou, X., Sierra, E. M., . . .Chemtob, S. (2017). Lactate produced during labor modulates uterine inflammation via gpr81 (hca1). *Am J Obstet Gynecol, 216*(1), 60.e61-60.e17. 10.1016/j.ajog.2016.09.072
Madsen, K., & Holmskov, U. (1995). Capillary density measurements in skeletal muscle using immunohistochemical staining with anti-collagen type iv antibodies. *Eur J Appl Physiol Occup Physiol, 71*(5), 472-474. 10.1007/bf00635884
Magistretti, P. J., & Allaman, I. (2015). A cellular perspective on brain energy metabolism and functional imaging. *Neuron, 86*(4), 883-901. 10.1016/j.neuron.2015.03.035
Magistretti, P. J., & Allaman, I. (2018). Lactate in the brain: From metabolic end-product to signalling molecule. *Nat Rev Neurosci, 19*(4), 235-249. 10.1038/nrn.2018.19
Martin, S. F., & Chatterjee, S. (2003). Glycosphingolipid-induced cell signaling: Apoptosis. *Methods Enzymol, 363*, 284-299. 10.1016/s0076-6879(03)01058-9
Mastrorilli, V., Scopa, C., Saraulli, D., Costanzi, M., Scardigli, R., Rouault, J. P., . . .Tirone, F. (2017). Physical exercise rescues defective neural stem cells and neurogenesis in the adult subventricular zone of btg1 knockout mice. *Brain Struct Funct, 222*(6), 2855-2876. 10.1007/s00429-017-1376-4
Mayzel-Oreg, O., Omae, T., Kazemi, M., Li, F., Fisher, M., Cohen, Y., & Sotak, C. H. (2004). Microsphere-induced embolic stroke: An mri study. *Magn Reson Med, 51*(6), 1232-1238. 10.1002/mrm.20100
McBride, D. W., Klebe, D., Tang, J., & Zhang, J. H. (2015). Correcting for brain swelling's effects on infarct volume calculation after middle cerebral artery occlusion in rats. *Transl Stroke Res, 6*(4), 323-338. 10.1007/s12975-015-0400-3
McBride, D. W., & Zhang, J. H. (2017). Precision stroke animal models: The permanent mcao model should be the primary model, not transient mcao. *Transl Stroke Res*. 10.1007/s12975-017-0554-2
McGee-Russell, S. M., Brown, A. W., & Brierley, J. B. (1970). A combined light and electron microscope study of early anoxic-ischaemic cell change in rat brain. *Brain Res, 20*(2), 193-200. 10.1016/0006-8993(70)90288-x
Mergenthaler, P., Dirnagl, U., & Meisel, A. (2004). Pathophysiology of stroke: Lessons from animal models. *Metab Brain Dis, 19*(3-4), 151-167.

Merkle, F. T., Mirzadeh, Z., & Alvarez-Buylla, A. (2007). Mosaic organization of neural stem cells in the adult brain. *Science, 317*(5836), 381-384. 10.1126/science.1144914
Meschia, J. F., & Brott, T. (2018). Ischaemic stroke. *Eur J Neurol, 25*(1), 35-40. 10.1111/ene.13409
Meschia, J. F., Brushnell, C., Boden-Albala, B., Braun, L. T., Bravata, D. M., Chaturvedi, S., . . .Wilson, J. A. (2014). Guidelines for the primary prevention of stroke. *Stroke, 45*(12), 3754-3832. doi:10.1161/STR.0000000000000046
Miller, D. J., Simpson, J. R., & Silver, B. (2011). Safety of thrombolysis in acute ischemic stroke: A review of complications, risk factors, and newer technologies. *Neurohospitalist, 1*(3), 138-147. 10.1177/1941875211408731
Miyake, K., Takeo, S., & Kaijihara, H. (1993). Sustained decrease in brain regional blood flow after microsphere embolism in rats. *Stroke, 24*(3), 415-420. 10.1161/01.str.24.3.415
Moghissi, E. S., Korytkowski, M. T., DiNardo, M., Einhorn, D., Hellman, R., Hirsch, I. B., . . .Umpierrez, G. E. (2009). American association of clinical endocrinologists and american diabetes association consensus statement on inpatient glycemic control. *Endocr Pract, 15*(4), 353-369. 10.4158/ep09102.Ra
Morales-Ruiz, M., Fulton, D., Sowa, G., Languino, L. R., Fujio, Y., Walsh, K., & Sessa, W. C. (2000). Vascular endothelial growth factor-stimulated actin reorganization and migration of endothelial cells is regulated via the serine/threonine kinase akt. *Circ Res, 86*(8), 892-896. 10.1161/01.res.86.8.892
Morland, C., Andersson, K. A., Haugen, O. P., Hadzic, A., Kleppa, L., Gille, A., . . .Bergersen, L. H. (2017). Exercise induces cerebral vegf and angiogenesis via the lactate receptor hcar1. *Nat Commun, 8*, 15557. 10.1038/ncomms15557
Morland, C., Lauritzen, K. H., Puchades, M., Holm-Hansen, S., Andersson, K., Gjedde, A., . . .Bergersen, L. H. (2015). The lactate receptor, g-protein-coupled receptor 81/hydroxycarboxylic acid receptor 1: Expression and action in brain. *J Neurosci Res, 93*(7), 1045-1055. 10.1002/jnr.23593
Moskowitz, M. A., & Lo, E. H. (2003). Neurogenesis and apoptotic cell death. *Stroke, 34*(2), 324-326. 10.1161/01.str.0000054047.14853.ad
Mullen, R. J., Buck, C. R., & Smith, A. M. (1992). Neun, a neuronal specific nuclear protein in vertebrates. *Development, 116*(1), 201-211.
Mundel, T. M., & Kalluri, R. (2007). Type iv collagen-derived angiogenesis inhibitors. *Microvasc Res, 74*(2-3), 85-89. 10.1016/j.mvr.2007.05.005
Naderi, S., Alimohammadi, R., Hakimizadeh, E., Roohbakhsh, A., Shamsizadeh, A., & Allahtavakoli, M. (2018). The effect of exercise preconditioning on stroke outcome in ovariectomized mice with permanent middle cerebral artery occlusion. *Can J Physiol Pharmacol, 96*(3), 287-294. 10.1139/cjpp-2017-0157
National Institute of Neurological Disorders and Stroke rt-PA Stroke Study Group. (1995). Tissue plasminogen activator for acute ischemic stroke. *N Engl J Med, 333*(24), 1581-1587. 10.1056/nejm199512143332401
Newington, J. T., Harris, R. A., & Cumming, R. C. (2013). Reevaluating metabolism in alzheimer's disease from the perspective of the astrocyte-neuron lactate shuttle model. *J Neurodegener Dis, 2013*, 234572. 10.1155/2013/234572
Nicosia, R. F., Belser, P., Bonanno, E., & Diven, J. (1991). Regulation of angiogenesis in vitro by collagen metabolism. *In Vitro Cell Dev Biol, 27a*(12), 961-966. 10.1007/bf02631124
Ntaios, G. (2019, 06.12.2018). Ischaemic stroke. Retrieved 06.08.2019 from https://newbp.bmj.com/topics/en-gb/1078

O'Neill, L. A., & Kaltschmidt, C. (1997). Nf-kappa b: A crucial transcription factor for glial and neuronal cell function. *Trends Neurosci, 20*(6), 252-258.
Ocbina, P. J., Dizon, M. L., Shin, L., & Szele, F. G. (2006). Doublecortin is necessary for the migration of adult subventricular zone cells from neurospheres. *Mol Cell Neurosci, 33*(2), 126-135. 10.1016/j.mcn.2006.06.014
Offermanns, S. (2014). Free fatty acid (ffa) and hydroxy carboxylic acid (hca) receptors. *Annu Rev Pharmacol Toxicol, 54*, 407-434. 10.1146/annurev-pharmtox-011613-135945
Ohab, J. J., Fleming, S., Blesch, A., & Carmichael, S. T. (2006). A neurovascular niche for neurogenesis after stroke. *J Neurosci, 26*(50), 13007-13016. 10.1523/jneurosci.4323-06.2006
Osborne, K. A., Shigeno, T., Balarsky, A. M., Ford, I., McCulloch, J., Teasdale, G. M., & Graham, D. I. (1987). Quantitative assessment of early brain damage in a rat model of focal cerebral ischaemia. *J Neurol Neurosurg Psychiatry, 50*(4), 402-410. 10.1136/jnnp.50.4.402
Overberg, L. T., Lambertus, M., Andersson, K. A., Hadzic, A., Haugen, O. P., Storm-Mathisen, J., . . .Morland, C. (unpublished). *L-lactate induces neurogenesis on the ventricular-subventricular zone via the lactate receptor hcar1*.
Parent, J. M., Vexler, Z. S., Gong, C., Derugin, N., & Ferriero, D. M. (2002). Rat forebrain neurogenesis and striatal neuron replacement after focal stroke. *Ann Neurol, 52*(6), 802-813. 10.1002/ana.10393
Parmar, P. (2018). Stroke: Classification and diagnosis. *Pharmaceutical Journal, 10*. 10.1211/CP.2018.20204150
Pellerin, L., & Magistretti, P. J. (1994). Glutamate uptake into astrocytes stimulates aerobic glycolysis: A mechanism coupling neuronal activity to glucose utilization. *Proc Natl Acad Sci U S A, 91*(22), 10625-10629. 10.1073/pnas.91.22.10625
Pencea, V., Bingaman, K. D., Freedman, L. J., & Luskin, M. B. (2001). Neurogenesis in the subventricular zone and rostral migratory stream of the neonatal and adult primate forebrain. *Exp Neurol, 172*(1), 1-16. 10.1006/exnr.2001.7768
Peters, O., Back, T., Lindauer, U., Busch, C., Megow, D., Dreier, J., & Dirnagl, U. (1998). Increased formation of reactive oxygen species after permanent and reversible middle cerebral artery occlusion in the rat. *J Cereb Blood Flow Metab, 18*(2), 196-205. 10.1097/00004647-199802000-00011
Phan, T. G., Wright, P. M., Markus, R., Howells, D. W., Davis, S. M., & Donnan, G. A. (2002). Salvaging the ischaemic penumbra: More than just reperfusion? *Clin Exp Pharmacol Physiol, 29*(1-2), 1-10.
Phipps, H. W. (2016). Systematic review of traumatic brain injury animal models. *Methods Mol Biol, 1462*, 61-88. 10.1007/978-1-4939-3816-2_5
Pierre, K., & Pellerin, L. (2005). Monocarboxylate transporters in the central nervous system: Distribution, regulation and function. *J Neurochem, 94*(1), 1-14. 10.1111/j.1471-4159.2005.03168.x
Pin-Barre, C., Constans, A., Brisswalter, J., Pellegrino, C., & Laurin, J. (2017). Effects of high- versus moderate-intensity training on neuroplasticity and functional recovery after focal ischemia. *Stroke, 48*(10), 2855-2864. 10.1161/strokeaha.117.017962
Pitts, F. N., Jr., & McClure, J. N., Jr. (1967). Lactate metabolism in anxiety neurosis. *N Engl J Med, 277*(25), 1329-1336. 10.1056/nejm196712212772502
Powers, M. M., & Clark, G. (1955). An evaluation of cresyl echt violet acetate as a nissl stain. *Stain Technol, 30*(2), 83-88. 10.3109/10520295509113749
Powers, W. J., Rabinstein, A. A., Ackerson, T., Adeoye, O. M., Bambakidis, N. C., Becker, K., . . .Tirschwell, D. L. (2018). 2018 guidelines for the early management of patients with acute ischemic stroke: A guideline for healthcare professionals from the american

heart association/american stroke association. *Stroke, 49*(3), e46-e110. 10.1161/str.0000000000000158
Qu, Z., Andersen, J. L., & Zhou, S. (1997). Visualisation of capillaries in human skeletal muscle. *Histochem Cell Biol, 107*(2), 169-174. 10.1007/s004180050101
Quillinan, N., Herson, P. S., & Traystman, R. J. (2016). Neuropathophysiology of brain injury. *Anesthesiol Clin, 34*(3), 453-464. 10.1016/j.anclin.2016.04.011
Racotta, R., & Russek, M. (1977). Food and water intake of rats after intraperitoneal and subcutaneous administration of glucose, glycerol and sodium lactate. *Physiol Behav, 18*(2), 267-273. 10.1016/0031-9384(77)90132-9
Radisavljevic, Z., Avraham, H., & Avraham, S. (2000). Vascular endothelial growth factor up-regulates icam-1 expression via the phosphatidylinositol 3 oh-kinase/akt/nitric oxide pathway and modulates migration of brain microvascular endothelial cells. *J Biol Chem, 275*(27), 20770-20774. 10.1074/jbc.M002448200
Ramos-Vara, J. A. (2005). Technical aspects of immunohistochemistry. *Vet Pathol, 42*(4), 405-426. 10.1354/vp.42-4-405
Rao, M. S., & Shetty, A. K. (2004). Efficacy of doublecortin as a marker to analyse the absolute number and dendritic growth of newly generated neurons in the adult dentate gyrus. *Eur J Neurosci, 19*(2), 234-246. 10.1111/j.0953-816x.2003.03123.x
Reed, M. J., & Edelberg, J. M. (2004). Impaired angiogenesis in the aged. *Sci Aging Knowledge Environ, 2004*(7), pe7. 10.1126/sageke.2004.7.pe7
Reglodi, D., Somogyvari-Vigh, A., Maderdrut, J. L., Vigh, S., & Arimura, A. (2000). Postischemic spontaneous hyperthermia and its effects in middle cerebral artery occlusion in the rat. *Exp Neurol, 163*(2), 399-407. 10.1006/exnr.2000.7367
Renshaw, S. (2013). Immunohistochemistry and immunocytochemistry. In D. Wild (Ed.), *The immunoassay handbook (fourth edition)* (pp. 357-377). Oxford: Elsevier.
Rolim, N., Skardal, K., Hoydal, M., Sousa, M. M., Malmo, V., Kaurstad, G., . . .Wisloff, U. (2015). Aerobic interval training reduces inducible ventricular arrhythmias in diabetic mice after myocardial infarction. *Basic Res Cardiol, 110*(4), 44. 10.1007/s00395-015-0502-9
Rosene, D. L., Roy, N. J., & Davis, B. J. (1986). A cryoprotection method that facilitates cutting frozen sections of whole monkey brains for histological and histochemical processing without freezing artifact. *J Histochem Cytochem, 34*(10), 1301-1315. 10.1177/34.10.3745909
Rothwell, N. J., & Hopkins, S. J. (1995). Cytokines and the nervous system ii: Actions and mechanisms of action. *Trends Neurosci, 18*(3), 130-136.
Ruan, G. X., & Kazlauskas, A. (2012). Axl is essential for vegf-a-dependent activation of pi3k/akt. *Embo j, 31*(7), 1692-1703. 10.1038/emboj.2012.21
Ruscher, K., Isaev, N., Trendelenburg, G., Weih, M., Iurato, L., Meisel, A., & Dirnagl, U. (1998). Induction of hypoxia inducible factor 1 by oxygen glucose deprivation is attenuated by hypoxic preconditioning in rat cultured neurons. *Neurosci Lett, 254*(2), 117-120. 10.1016/s0304-3940(98)00688-0
Sacco, R. L., Kasner, S. E., Broderick, J. P., Caplan, L. R., Connors, J. J., Culebras, A., . . .Vinters, H. V. (2013). An updated definition of stroke for the 21st century: A statement for healthcare professionals from the american heart association/american stroke association. *Stroke, 44*(7), 2064-2089. 10.1161/STR.0b013e318296aeca
Sahin Kaya, S., Mahmood, A., Li, Y., Yavuz, E., & Chopp, M. (1999). Expression of nestin after traumatic brain injury in rat brain. *Brain Res, 840*(1-2), 153-157. 10.1016/s0006-8993(99)01757-6
Sajedi, G. (2019). *Effekter av laktat via laktatreseptor hcar1 ved iskemisk hjerneslag* (Master). University of Oslo, Oslo.

Saper, C. B., & Sawchenko, P. E. (2003). Magic peptides, magic antibodies: Guidelines for appropriate controls for immunohistochemistry. *J Comp Neurol, 465*(2), 161-163. 10.1002/cne.10858

Saver, J. L., Goyal, M., Bonafe, A., Diener, H. C., Levy, E. I., Pereira, V. M., . . .Jahan, R. (2015). Stent-retriever thrombectomy after intravenous t-pa vs. T-pa alone in stroke. *N Engl J Med, 372*(24), 2285-2295. 10.1056/NEJMoa1415061

Schaller, B., & Graf, R. (2004). Cerebral ischemia and reperfusion: The pathophysiologic concept as a basis for clinical therapy. *J Cereb Blood Flow Metab, 24*(4), 351-371. 10.1097/00004647-200404000-00001

Schaller, J., & Gerber, S. S. (2011). The plasmin-antiplasmin system: Structural and functional aspects. *Cell Mol Life Sci, 68*(5), 785-801. 10.1007/s00018-010-0566-5

Schenk, S., & Horowitz, J. F. (2007). Acute exercise increases triglyceride synthesis in skeletal muscle and prevents fatty acid-induced insulin resistance. *J Clin Invest, 117*(6), 1690-1698. 10.1172/jci30566

Schilling, M., Besselmann, M., Leonhard, C., Mueller, M., Ringelstein, E. B., & Kiefer, R. (2003). Microglial activation precedes and predominates over macrophage infiltration in transient focal cerebral ischemia: A study in green fluorescent protein transgenic bone marrow chimeric mice. *Exp Neurol, 183*(1), 25-33. 10.1016/s0014-4886(03)00082-7

Schindelin, J., Arganda-Carreras, I., Frise, E., Kaynig, V., Longair, M., Pietzsch, T., . . .Cardona, A. (2012). Fiji: An open-source platform for biological-image analysis. *Nat Methods, 9*(7), 676-682. 10.1038/nmeth.2019

Scholzen, T., & Gerdes, J. (2000). The ki-67 protein: From the known and the unknown. *J Cell Physiol, 182*(3), 311-322. 10.1002/(sici)1097-4652(200003)182:3<311::Aid-jcp1>3.0.Co;2-9

Schwarzkopf, T. M., Horn, T., Lang, D., & Klein, J. (2013). Blood gases and energy metabolites in mouse blood before and after cerebral ischemia: The effects of anesthetics. *Exp Biol Med (Maywood), 238*(1), 84-89. 10.1258/ebm.2012.012261

Shi, S. R., Cote, R. J., & Taylor, C. R. (2001). Antigen retrieval techniques: Current perspectives. *J Histochem Cytochem, 49*(8), 931-937. 10.1177/002215540104900801

Sommer, C. J. (2017). Ischemic stroke: Experimental models and reality. *Acta Neuropathol, 133*(2), 245-261. 10.1007/s00401-017-1667-0

Srinivasan, M., Sedmak, D., & Jewell, S. (2002). Effect of fixatives and tissue processing on the content and integrity of nucleic acids. *Am J Pathol, 161*(6), 1961-1971. 10.1016/s0002-9440(10)64472-0

Sun, M. S., Jin, H., Sun, X., Huang, S., Zhang, F. L., Guo, Z. N., & Yang, Y. (2018). Free radical damage in ischemia-reperfusion injury: An obstacle in acute ischemic stroke after revascularization therapy. *Oxid Med Cell Longev, 2018*, 3804979. 10.1155/2018/3804979

Sun, Y., Jin, K., Xie, L., Childs, J., Mao, X. O., Logvinova, A., & Greenberg, D. A. (2003). Vegf-induced neuroprotection, neurogenesis, and angiogenesis after focal cerebral ischemia. *J Clin Invest, 111*(12), 1843-1851. 10.1172/jci17977

Svensson, M., Rosvall, P., Boza-Serrano, A., Andersson, E., Lexell, J., & Deierborg, T. (2016). Forced treadmill exercise can induce stress and increase neuronal damage in a mouse model of global cerebral ischemia. *Neurobiol Stress, 5*, 8-18. 10.1016/j.ynstr.2016.09.002

Swain, R. A., Harris, A. B., Wiener, E. C., Dutka, M. V., Morris, H. D., Theien, B. E., . . .Greenough, W. T. (2003). Prolonged exercise induces angiogenesis and increases cerebral blood volume in primary motor cortex of the rat. *Neuroscience, 117*(4), 1037-1046. 10.1016/s0306-4522(02)00664-4

Swanson, R. A., Morton, M. T., Tsao-Wu, G., Savalos, R. A., Davidson, C., & Sharp, F. R. (1990). A semiautomated method for measuring brain infarct volume. *J Cereb Blood Flow Metab, 10*(2), 290-293. 10.1038/jcbfm.1990.47

Thomassen, L. (2019, 09.07.2019). Hjerneslag. Store medisinske leksikon. Retrieved 12.02.2020 from https://sml.snl.no/hjerneslag

Thored, P., Wood, J., Arvidsson, A., Cammenga, J., Kokaia, Z., & Lindvall, O. (2007). Long-term neuroblast migration along blood vessels in an area with transient angiogenesis and increased vascularization after stroke. *Stroke, 38*(11), 3032-3039. 10.1161/strokeaha.107.488445

Titford, M. (2009). Progress in the development of microscopical techniques for diagnostic pathology. *Journal of Histotechnology, 32*(1), 9-19. 10.1179/his.2009.32.1.9

Tobin, M. K., Bonds, J. A., Minshall, R. D., Pelligrino, D. A., Testai, F. D., & Lazarov, O. (2014). Neurogenesis and inflammation after ischemic stroke: What is known and where we go from here. *J Cereb Blood Flow Metab, 34*(10), 1573-1584. 10.1038/jcbfm.2014.130

Toda, T., Parylak, S. L., Linker, S. B., & Gage, F. H. (2019). The role of adult hippocampal neurogenesis in brain health and disease. *Mol Psychiatry, 24*(1), 67-87. 10.1038/s41380-018-0036-2

Tokuyasu, K. T. (1973). A technique for ultracryotomy of cell suspensions and tissues. *J Cell Biol, 57*(2), 551-565. 10.1083/jcb.57.2.551

Touzani, O., Roussel, S., & MacKenzie, E. T. (2001). The ischaemic penumbra. *Curr Opin Neurol, 14*(1), 83-88. 10.1097/00019052-200102000-00013

Traystman, R. J., Kirsch, J. R., & Koehler, R. C. (1991). Oxygen radical mechanisms of brain injury following ischemia and reperfusion. *J Appl Physiol (1985), 71*(4), 1185-1195. 10.1152/jappl.1991.71.4.1185

Tureyen, K., Vemuganti, R., Sailor, K. A., & Dempsey, R. J. (2004). Infarct volume quantification in mouse focal cerebral ischemia: A comparison of triphenyltetrazolium chloride and cresyl violet staining techniques. *J Neurosci Methods, 139*(2), 203-207. 10.1016/j.jneumeth.2004.04.029

Vafaee, M. S., Vang, K., Bergersen, L. H., & Gjedde, A. (2012). Oxygen consumption and blood flow coupling in human motor cortex during intense finger tapping: Implication for a role of lactate. *J Cereb Blood Flow Metab, 32*(10), 1859-1868. 10.1038/jcbfm.2012.89

van Praag, H., Christie, B. R., Sejnowski, T. J., & Gage, F. H. (1999). Running enhances neurogenesis, learning, and long-term potentiation in mice. *Proc Natl Acad Sci U S A, 96*(23), 13427-13431. 10.1073/pnas.96.23.13427

van Praag, H., Kempermann, G., & Gage, F. H. (1999). Running increases cell proliferation and neurogenesis in the adult mouse dentate gyrus. *Nat Neurosci, 2*(3), 266-270. 10.1038/6368

van Praag, H., Shubert, T., Zhao, C., & Gage, F. H. (2005). Exercise enhances learning and hippocampal neurogenesis in aged mice. *J Neurosci, 25*(38), 8680-8685. 10.1523/jneurosci.1731-05.2005

Wang, L., Chopp, M., Gregg, S. R., Zhang, R. L., Teng, H., Jiang, A., . . .Zhang, Z. G. (2008). Neural progenitor cells treated with epo induce angiogenesis through the production of vegf. *J Cereb Blood Flow Metab, 28*(7), 1361-1368. 10.1038/jcbfm.2008.32

Wang, R. Y., Yang, Y. R., & Yu, S. M. (2001). Protective effects of treadmill training on infarction in rats. *Brain Res, 922*(1), 140-143. 10.1016/s0006-8993(01)03154-7

Warburg, O., Wind, F., & Negelein, E. (1927). The metabolism of tumors in the body. *J Gen Physiol, 8*(6), 519-530. 10.1085/jgp.8.6.519

Weber, B., & Barros, L. F. (2015). The astrocyte: Powerhouse and recycling center. *Cold Spring Harb Perspect Biol, 7*(12). 10.1101/cshperspect.a020396

Weis, S. M., & Cheresh, D. A. (2005). Pathophysiological consequences of vegf-induced vascular permeability. *Nature, 437*(7058), 497-504. 10.1038/nature03987

Whelton, S. P., Chin, A., Xin, X., & He, J. (2002). Effect of aerobic exercise on blood pressure: A meta-analysis of randomized, controlled trials. *Ann Intern Med, 136*(7), 493-503. 10.7326/0003-4819-136-7-200204020-00006

Willey, J. Z., Moon, Y. P., Paik, M. C., Yoshita, M., Decarli, C., Sacco, R. L., . . .Wright, C. B. (2011). Lower prevalence of silent brain infarcts in the physically active: The northern manhattan study. *Neurology, 76*(24), 2112-2118. 10.1212/WNL.0b013e31821f4472

Wisloff, U., Helgerud, J., Kemi, O. J., & Ellingsen, O. (2001). Intensity-controlled treadmill running in rats: Vo(2 max) and cardiac hypertrophy. *Am J Physiol Heart Circ Physiol, 280*(3), H1301-1310. 10.1152/ajpheart.2001.280.3.H1301

Wu, H., Jiang, H., Lu, D., Qu, C., Xiong, Y., Zhou, D., . . .Mahmood, A. (2011). Induction of angiogenesis and modulation of vascular endothelial growth factor receptor-2 by simvastatin after traumatic brain injury. *Neurosurgery, 68*(5), 1363-1371; discussion 1371. 10.1227/NEU.0b013e31820c06b9

Wurmser, A. E., Palmer, T. D., & Gage, F. H. (2004). Neuroscience. Cellular interactions in the stem cell niche. *Science, 304*(5675), 1253-1255. 10.1126/science.1099344

Xing, C., Arai, K., Lo, E. H., & Hommel, M. (2012). Pathophysiologic cascades in ischemic stroke. *International journal of stroke : official journal of the International Stroke Society, 7*(5), 378-385. 10.1111/j.1747-4949.2012.00839.x

Xing, C., Hayakawa, K., Lok, J., Arai, K., & Lo, E. H. (2012). Injury and repair in the neurovascular unit. *Neurological research, 34*(4), 325-330. 10.1179/1743132812Y.0000000019

Yamashita, K., Busch, E., Wiessner, C., & Hossmann, K. A. (1997). Thread occlusion but not electrocoagulation of the middle cerebral artery causes hypothalamic damage with subsequent hyperthermia. *Neurol Med Chir (Tokyo), 37*(10), 723-727; discussion 727-729. 10.2176/nmc.37.723

Yamori, Y., Horie, R., Handa, H., Sato, M., & Fukase, M. (1976). Pathogenetic similarity of strokes in stroke-prone spontaneously hypertensive rats and humans. *Stroke, 7*(1), 46-53. 10.1161/01.str.7.1.46

Yang, G., Kitagawa, K., Matsushita, K., Mabuchi, T., Yagita, Y., Yanagihara, T., & Matsumoto, M. (1997). C57bl/6 strain is most susceptible to cerebral ischemia following bilateral common carotid occlusion among seven mouse strains: Selective neuronal death in the murine transient forebrain ischemia. *Brain Res, 752*(1-2), 209-218. 10.1016/s0006-8993(96)01453-9

Yoo, Y. M., Lee, U., & Kim, Y. J. (2005). Apoptosis and nestin expression in the cortex and cultured astrocytes following 6-ohda administration. *Neurosci Lett, 382*(1-2), 88-92. 10.1016/j.neulet.2005.02.070

Yoshimura, S., Takagi, Y., Harada, J., Teramoto, T., Thomas, S. S., Waeber, C., . . .Moskowitz, M. A. (2001). Fgf-2 regulation of neurogenesis in adult hippocampus after brain injury. *Proc Natl Acad Sci U S A, 98*(10), 5874-5879. 10.1073/pnas.101034998

Yu, Z., Lin, L., & Wang, X. (2017). Pathophysiology of ischemia-reperfusion injury and hemorrhagic transformation in the brain. In (pp. 121-124).

Yuan, Y., & Arikkath, J. (2014). Techniques in immunohistochemistry and immunocytochemistry. In H. Xiong & H. E. Gendelman (Eds.), *Current laboratory methods in neuroscience research* (pp. 387-396). New York, NY: Springer New York.

Zhang, R. L., Chopp, M., Roberts, C., Liu, X., Wei, M., Nejad-Davarani, S. P., . . .Zhang, Z. G. (2014). Stroke increases neural stem cells and angiogenesis in the neurogenic niche of the adult mouse. *PLoS One, 9*(12), e113972. 10.1371/journal.pone.0113972

Zhang, R. L., Zhang, Z. G., Zhang, L., & Chopp, M. (2001). Proliferation and differentiation of progenitor cells in the cortex and the subventricular zone in the adult rat after focal cerebral ischemia. *Neuroscience, 105*(1), 33-41. 10.1016/s0306-4522(01)00117-8

Zhang, Y., Xiong, Y., Mahmood, A., Zhang, Z. G., & Chopp, M. (2014). Angiogenesis and functional recovery after traumatic brain injury. In E. H. Lo, J. Lok, M. Ning, & M. J. Whalen (Eds.), *Vascular mechanisms in cns trauma* (pp. 141-156). New York, NY: Springer New York.

Zhang, Z., Zhang, R. L., Jiang, Q., Raman, S. B., Cantwell, L., & Chopp, M. (1997). A new rat model of thrombotic focal cerebral ischemia. *J Cereb Blood Flow Metab, 17*(2), 123-135. 10.1097/00004647-199702000-00001

Zhang, Z. G., Zhang, L., Jiang, Q., Zhang, R., Davies, K., Powers, C., . . .Chopp, M. (2000). Vegf enhances angiogenesis and promotes blood-brain barrier leakage in the ischemic brain. *J Clin Invest, 106*(7), 829-838. 10.1172/jci9369

Zhou, J., Liu, T., Guo, H., Cui, H., Li, P., Feng, D., . . .Wang, Y. (2018). Lactate potentiates angiogenesis and neurogenesis in experimental intracerebral hemorrhage. *Exp Mol Med, 50*(7), 1-12. 10.1038/s12276-018-0113-2

Åstrand, P.-O., & Rodahl, K. (1970). *Textbook of work physiology*. New York: McGraw-Hill.

Appendixes

Appendix I: Antibodies

Table 7.1. Primary antibodies for fluorescence immunohistochemistry.

Primary antibodies				
Antibody	**Host species**	**Concentration**	**Catalogue #**	**Manufacturer**
Polyclonal Collagen IV antibody	Rabbit	100 µg at 1 mg/ml	ab6586	Abcam, UK
Polyclonal Doublecortin antibody	Guinea pig	50 µg at 0.9 mg/ml	ab18723	Abcam, UK
Monoclonal Nestin antibody	Mouse	100 µg at 1 mg/ml	ab22035	Abcam, UK
Polyclonal Ki67 antibody	Rabbit	100 µg at 1 mg/ml	ab15580	Abcam, UK

Table 7.2. Secondary antibodies for fluorescence immunohistochemistry.

Secondary antibodies					
Conjugate	**Host species / Isotype**	**Species Reactivity**	**Concentration**	**Catalogue #**	**Manufacturer**
Alexa Fluor 488	Donkey / IgG	Rabbit	2 mg/ml	A21206	Invitrogen, USA
Alexa Fluor 594	Goat / IgG	Guinea pig	2 mg/ml	A11076	Invitrogen, USA
Alexa Fluor 488	Donkey / IgG	Mouse	2 mg/ml	A21202	Invitrogen, USA
Alexa Fluor 647	Goat / IgG	Rabbit	1 mg/ml	A27040	Invitrogen, USA

Appendix II: Equipment

Table 7.3. Overview of equipment and the respective manufacturers used in the experiment.

Equipment	**Manufacturer**
Applied Biosystems 2720 Thermal Cycler	Thermo Fisher Scientific, USA
Slide Scanner Axio Scan Z1	Carl Zeiss Microscopy, Germany
Brush Watercolour Round No. 0 and 3/0	Panduro Hobby, Norway
Drill, rotary	Dremel, USA
E-Gel Power Snap Electrophoresis System	Invitrogen, USA
EasyDip Slide Staining System	Simport Scientific, Canada
Exer 3/6 treadmill	Columbus Instruments, USA
Grant Boekel BBD block heater	Boekel Scientific, USA
Heraeus Fresco 21 Microcentrifuge	Thermo Fisher Scientific, USA
Heraeus Pico 17 Microcentrifuge	Thermo Fisher Scientific, USA
HM 450 Sliding Microtome	Thermo Fisher Scientific, USA
KS 34 Enclosed Cooling System	Thermo Scientific, USA
LSM 880 with Airyscan confocal microscope	Carl Zeiss Microscopy, Germany
Nikon SMZ645 stereo microscope	Nikon Instruments, USA
Paintbrush Watercolour Round No. 0 and 3/0 pine marten hair	Panduro Hobby, Norway
Parafilm M PM996	Bemis, USA
Qualitative filter paper, grade 403	VWR, USA
Superfrost Plus Adhesion Microscope Slides	Thermo Scientific, USA
Super PAP Pen	Electron Microscopy Sciences, USA
Tissue Culture Plates 24 wells, sterile	VWR, USA
VIO 50 C high-frequency generator	Erbe, Germany
Watson-Marlow 323 pump	Watson-Marlow, UK

Appendix III: Fiji macros

Macro.ijm.ijm | CollagenIV_macro_ver2.ijm

```
Macro steps part 1
run("Scale...");
run("Set Scale...", "distance=0.769225 known=1 pixel=1 unit=micron global");
//run("Channels Tool...");
Stack.setDisplayMode("composite");
run("Duplicate...", "duplicate channels=2");
Select ROI

Macro steps part 2
run("Duplicate...", "duplicate channels=2");
run("Clear Outside");
run("Enhance Contrast...", "saturated=0.3");
run("Trainable Weka Segmentation");
Train classifier and create results

Macro steps part 3
run("8-bit");
//setThreshold(26, 120);
setOption("BlackBackground", true);
run("Convert to Mask");
run("Analyze Particles...", "size=30.00-Infinity show=Outlines display include add");
```

Figure 7.1. Screenshot of macro commands used for capillary density analysis. The following macro was divided into three parts, in which each part had common procedures that were automated and performed in the order described.

Appendix IV: Result tables

Physical performance in maximal exercise-capacity test

Table 7.4. Descriptive overview of measured mean and standard deviation for mice that performed the maximal exercise-capacity test.

Week	High-intensity wild-type mice			High-intensity knockout mice			Medium-intensity wild-type mice			Medium-intensity knockout mice		
	Mean	SD	N	Mean	SD	N	Mean	SD	N	Mean	SD	N
1	25.46	1.89	16	26.11	1.71	18	26.10	1.51	16	24.95	1.43	17
3	29.88	1.73	16	31.02	1.84	18	29.80	2.20	16	29.77	2.48	17

5	33.67	2.85	16	33.50	2.29	18	31.98	2.54	16	32.25	1.69	17
7	35.04	2.95	16	33.43	1.76	18	33.45	2.58	16	33.11	2.49	17

Cerebral infarct volume

Table 7.5. Descriptive overview of calculated infarct volumes of each treatment group and genotype.

	N	**Mean**	**Std. Deviation**	**Std. Error**	**95% Confidence Interval for Mean**		**Minimum**	**Maximum**
					Lower Bound	**Upper Bound**		
Saline WT mice	12	7.93	3.42	0.98	5.75	10.10	3.19	13.42
Saline KO mice	8	8.62	3.45	1.15	5.96	11.27	3.32	14.65
Lactate WT mice	8	7.32	3.10	1.09	4.72	9.91	3.61	13.04
Lactate KO mice	8	8.27	3.24	1.14	5.56	10.97	4.91	15.14
High-intensity WT mice	8	8.59	2.51	0.88	6.49	10.69	4.85	12.25
High-intensity KO mice	10	8.08	3.33	1.05	5.69	10.46	3.37	14.02
Medium-intensity WT mice	6	8.91	3.20	1.31	5.55	12.28	4.82	14.25
Medium-intensity KO mice	7	7.85	2.17	0.82	5.84	9.86	3.63	10.64
Total	67	8.17	2.99	0.36	7.44	8.89	3.19	15.14

Table 7.6. Statistical ANOVA analysis of infarct volume.

	Sum of Squares	**df**	**Mean Square**	**F**	**Sig.**
Between Groups	13.939	7	1.991	.203	.984
Within Groups	588.382	60	9.806	-	-

Total	602.321	67		-	-

Reproducibility of volumetric infarct analysis

Table 7.7. Descriptive overview of calculated ratio and percentage of double-blinded sections (n = 79) in the test of reproducibility.

	Ipsilateral hemisphere				**Contralateral hemisphere**			
	Mean	**SD**	**Minimum**	**Maximum**	**Mean**	**SD**	**Minimum**	**Maximum**
Ratio	0.969	0.071	0.716	1.124	0.993	0.045	0.770	1.086
Percentage reproduc-ibility	96.963	7.081	71.632	112.446	99.336	4.544	77.024	108.638